Title
Mitochondrial Dynamics: The Role of Adaptations in the Mitochondrial Proteomic Profile in Different Cellular Contexts

Author
Lin, Amanda

Publication Date
2018

Peer reviewed|Thesis/dissertation

UNIVERSITY OF CALIFORNIA

Los Angeles

Mitochondrial Dynamics: The Role of Adaptations in the Mitochondrial Proteomic Profile in Different Cellular Contexts

A dissertation submitted in partial

satisfaction of the requirements for the

degree Doctor of Philosophy in

Molecular, Cellular, and Integrative Physiology

by

Amanda Lin

2018

ABSTRACT OF THE DISSERTATION

Mitochondrial Dynamics: The Role of Adaptations in the Mitochondrial Proteomic Profile in Different Cellular Contexts

by

Amanda Lin

Doctor of Philosophy in Molecular, Cellular and Integrative Physiology

University of California, Los Angeles, 2018

Professor Andrea L Hevener, Chair

Mitochondria are critical for regulating metabolism and energy expenditure. These organelles are comprised of roughly 2,000 proteins. Dysfunction of mitochondria and its components has been associated with many pathologies including cardiovascular, neurodegenerative, and metabolic diseases. While previous reports have aimed to characterize the mitochondrial proteome, the relationship between the mitochondrial proteome and function has not been experimentally established on a systematic level. This lack of understanding impedes the contextualization and translation of proteomic data to the molecular derivations of mitochondrial diseases.

To traverse this knowledge gap, we analyzed the mitochondrial proteomic profile from four different tissue types – two mitochondrial proteomes from identical genetic codons (mouse heart and mouse liver), two cardiac mitochondrial proteomes from unique genomes (mouse heart and human heart), and one well-studied metazoan model system (drosophila). By linking mitochondrial protein abundance with biochemical pathways, we were able to identify the core functionalities of these mitochondria. Using bioinformatics analyses, we identified significant enrichment of disease-associated genes and their products. Correlational analyses suggested that the mitochondrial proteome design is primarily driven by cellular environment. Taken together, these results link the mitochondrial composition with function, providing a prospective resource for mitochondrial pathophysiology and developing novel therapeutic targets in medicine.

As mitochondrial dysfunction is exacerbated by dysfunctional protein quality control and often further contributes to pathology, we addressed the mechanisms underlying the maintenance of healthy mitochondrial architecture. This requires a steady balance between protein synthesis and degradation – or turnover. It is well-documented that mitochondrial autophagy (mitophagy) is the primary mechanism to degrade dysfunctional mitochondria via lysosomes. However, as failure to contain or replenish mitochondrial proteins damaged by reactive oxygen species directly underlies many pathological phenotypes, developing therapies to target mitochondria on an individual protein level is of interest. Therefore, we designed a metabolic heavy water ($^{2}H_2O$) labeling strategy to study individual protein turnover rates in vivo. We calculated the

turnover rates for 458 proteins in mouse cardiac and hepatic mitochondria and revealed distinct tissue-specific turnover kinetics with protein half-lives spanning from hours to months. These results indicate that mitochondria are not turned over only as individual units; excess mitochondrial proteins are synthesized in the cytosol to be imported into the mitochondria when needed. Therefore, mitochondria possess a mixture of previously- and newly-synthesized proteins. Our study demonstrates the first large-scale analysis of mitochondrial protein turnover rates in vivo, with potential applications in translational research.

To further study the structure of mitochondria, we sought to investigate how alterations in mitochondrial morphology and dynamics (fission and fusion) affect metabolism and physiology. Proper mitochondrial function is required to maintain metabolic homeostasis and cellular energetic capacity and mitochondrial dysfunction has been associated with the development of insulin resistance in glucoregulatory tissues. Our laboratory has recently shown that heat shock protein 72 (HSP72) is an important molecular link between mitochondrial function, cellular metabolism, and insulin action. Indeed, HSP72 protein levels are reduced in muscle from obese and diabetic patients, and HSP72 levels are inversely associated with the degree of insulin resistance and adiposity. Findings from our laboratory show that HSP72 regulates Parkin action including mitochondrial quality control and reveal that the deletion of either HSP72 or Parkin induces mitochondrial dysfunction and skeletal muscle insulin resistance. However, the molecular phenotypes encompassing the HSP72-mitochondria-glucose homeostasis paradigm have been to date, exclusively established in male model systems. In contrast

to the obesity-insulin resistance phenotype of male HSP72 knockout (KO) mice, our findings show that female mice lacking HSP72 possess a lean phenotype with enhanced insulin sensitivity. Interestingly, loss of HSP72 promotes increased muscle ERα expression in female mice; this is a likely mediator of improved mitochondrial function and insulin action in female HSP72 KO mice fed a normal chow diet. Our studies lay the important foundation for the rational design of novel therapeutic strategies that can be used to combat metabolic-related diseases in women.

Together, our findings suggest that mitochondria and its proteomic profile are highly dynamic in composition and kinetics. These properties are dependent on not only the host organism, but also the organ milieu. In addition, our findings highlight the sex-specific role of mitochondrial dysfunction in the onset of metabolic diseases. Therefore, developing therapeutic strategies to target mitochondrial function, health, and dynamics are crucial to ameliorate complications associated with metabolic diseases, including type 2 diabetes and insulin resistance in men and women.

The dissertation of Amanda Lin is approved.

Aldons J Lusis

Karen Reue

Orian Shirihai

Julian Philip Whitelegge

Andrea L Hevener, Committee Chair

University of California, Los Angeles

2018

DEDICATION

I dedicate my dissertation to my family, friends, and mentors who have not only supported me academically through graduate career, but also in life.

TABLE OF CONTENTS

LIST OF FIGURES

ACKNOWLEDGEMENTS

I am especially indebted to my current mentor, Dr. Andrea L Hevener, for giving me the opportunity to be a member of her lab. I thank her for her scientific supervision, unwavering support, motivation and enthusiasm, and for believing in me. I would also like to express my gratitude to my previous mentor, Dr. Peipei Ping, who introduced me to the world of mitochondria.

I would like to thank the members of my doctoral committee. I wish to thank the previous and present members of our laboratory for their experimental help, scientific discussions, and critical comments. Each of the members of my Dissertation Committee has provided me extensive personal and professional guidance and taught me a great deal about both scientific research and life in general.

The mentorship I received in conjunction with the comprehensive training from the UCLA MCIP program has allowed me to mature as a young scientist and has provided me the cornerstone required to pursue a successful career in academic medicine.

BIOGRAPHICAL SKETCH

EDUCATION

Ph.D. in Molecular, Cellular, and Integrative Physiology *Expected March 2018*
University of California, Los Angeles

B.S. in Psychobiology, Minor in Cognitive Science *September 2012*
University of California, Los Angeles

WORK EXPERIENCE

Staff Research Associate I *11/2011-1/2015*
University of California, Los Angeles

Undergraduate Technician *10/2008-10/2011*
University of California, Los Angeles

SELECTED ORAL PRESENTATIONS

1. **Lin AJ**. Establishing Unidentified Functions of Mitochondrial Proteins. Proteomics of Protein Degradation & Ubiquitin Pathway Conference; 22-25 January 2012; San Diego, CA.

2. **Lin AJ**. Mitochondrial Proteome Design and Function Across Organs and Organisms. NHLBI Proteomics Center at UCLA Symposia; 20 February 2013; Stockholm, Sweden.

3. Garlid AO, **Lin AJ**. The Characterization, Design, and Function of the Mitochondrial Proteome: From Organs to Organisms. Human Proteome Organization World Congress: Mitochondria Proteomics B/D Initiative; 8 October 2014; Madrid, Spain.

PEER-REVIEWED PRESENTATIONS

1. **Lin AJ**, Zhou Z, Reddish BR, Moore TM, Cory K, Whitney K, Cohn W, Merkurjev D, Drew BG, Ribas V, Henstridge DC, Stiles L, Vergnes L, Whitelegge JP, Wanagat J, Reue K, Shirihai OS, Febrraio MA, Hevener AL. Sexual Dimorphisms in the Regulation of Metabolic Homeostasis by HSP72. Diabetes. In Preparation.

2. Moore TM, Zhou Z, **Lin AJ**, Kalajian N, Cory K, Whitney K, Ho T, Ho T, Lee J, Rucker DH, Turcotte L, Hevener AL. Exercise and mitochondrial dynamics – the role of Drp1 in metabolism and exercise. In Preparation.

3. Lau E, Huang D, Cao Q, Dincer TU, Black CM, **Lin AJ**, Lee JM, Wang D, Liem DA, Lam MP, Ping P. Spatial and temporal dynamics of the cardiac mitochondrial proteome. Expert Rev Proteomics. 2015 Apr;12(2):133-46. Epub 2015 Mar 9. PMID: 25752359. PMCID: PMC4721584.

4. Chan XC, Black CM, **Lin AJ**, Ping P, Lau E. Mitochondrial protein turnover: Methods to measure turnover rates on a large scale. J Mol Cell Cardiol. 2015 Jan;78:54-61. Epub 2014 Nov 11. PMID: 25451168. PMCID: PMC4746024.

5. Liem DA, Nsair A, Setty SP, Cadeiras M, Wang D, Maclellan R, Lotz C, **Lin AJ**, Tabaraki J, Li H, Ge J, Odeberg J, Ponten F, Larson E, Mulder J, Lundberg E, Weiss JN, Uhlen M, Ping P, Deng MC. Molecular- and organelle-based predictive paradigm underlying recovery by left ventricular assist device support. Circ Heart Fail. 2014 Mar 1;7(2):359-66. PMID: 24643888. PMCID: PMC4397259.

6. Lotz C*, **Lin AJ***, Black CM*, Zhang J*, Lau E, Deng N, Wang Y, Zong NC, Choi JH, Xu T, Liem DA, Korge P, Weiss JN, Hermjakob H, Yates JR, Apweiler R, Ping P. Characterization, Design, and Function of the Mitochondrial Proteome: From Organs to Organisms. J Proteome Res. 2014 Feb 7;13(2):433-46. Epub 2013 Dec 12. PMID: 24070373. PMCID: PMC4076470.

7. Kim T, Wang D, Kim A, Lau E, **Lin AJ**, Liem DA, Zhang J, Zong NC, Lam M, Ping P. Metabolic Labeling Reveals Proteome Dynamics of Mouse Mitochondria. Mol Cell Proteomics. 2012 Dec;11(12):1586-94. Epub 2012 Aug 21. PMID: 22915825. PMCID: PMC3518123.

8. Zhang J, **Lin A**, Powers J, Lotz C, Liem D, Lau E, Wang D, Deng N, Korge P, Zong NC, Cai H, Weiss J, Ping P. Perspectives on: SGP Symposium on Mitochondrial Physiology and Medicine: Mitochondrial proteome design: From molecular identity to pathophysiological regulation. J Gen Physiol. 2012 Jun;139(6):395-406. PMID: 22641634. PMCID: PMC3362520.

CHAPTER 1

Introduction

*Sections of this chapter are adapted from Zhang et al., Perspectives on: SGP Symposium on Mitochondrial Physiology and Medicine: Mitochondrial proteome design: From molecular identity to pathophysiological regulation, Journal of General Physiology, 139(6):395-406. http://jgp.rupress.org/content/139/6/395.long

1.1 The History of Mitochondria

The essence of mitochondria lies within their ability to generate energy, maintain metabolism, and regulate signaling cascades. As fundamental constituents of numerous rudimentary cellular processes, the molecular architecture and the proteome of the mitochondria are critical to intracellular biochemistry. The behavior of the mitochondria is subjugated to the environment of this organelle; perturbation of mitochondrial homeostasis can prompt pathophysiological conditions to arise.

The history of mitochondrial research can be traced back to Rudolf Albrecht von Kolliker in 1857 when he first described the mitochondrion. In 1890, Richard Altmann termed the mitochondria “bioblasts,” noted their ubiquitous nature, and showed exceptional foresight when he explained that these bioblasts were living inside cells and were responsible for “elementary functions.” The endosymbiotic theory was first articulated by Konstantin Mereschkowski in 1905. Although several hypotheses were put forth to explain the merger between mitochondria and cells, it was Lynn Margulis who tied the endosymbiotic theory to biochemical and cytological evidence. Mitochondria are of α-protobacterial origin, engulfed by cells through endosymbiosis about two billion years ago. The name “mitochondrion” was first introduced in 1898 by Carl Benda from the Greek words “mitos” (thread) and “chondros” (granule). The first well-preserved mitochondria were isolated by Hogeboom et al.[1] in 1948. This approach proved to be significantly advantageous to mitochondrial research for several decades, in particular, on the characterization of mitochondrial proteome biology and function which we focus

today. A key finding from the hypothesis of chemiosmosis by Mitchell[2] is an organized subproteome, i.e., the electron transport complexes, with a dedicated role, supporting the oxidation and phosphorylation function in the mitochondria. The complexity of the subproteome was further realized with the introduction of innovative methods to visualize three-dimensional structures and the role of the mitochondria in cell death signaling[2]. These discoveries inspired the research efforts to link biological pathways with their subproteome-based molecular participants in the regulation of mitochondrial function. Figure 1 summarizes the milestones of the long and fruitful history of mitochondrial research.

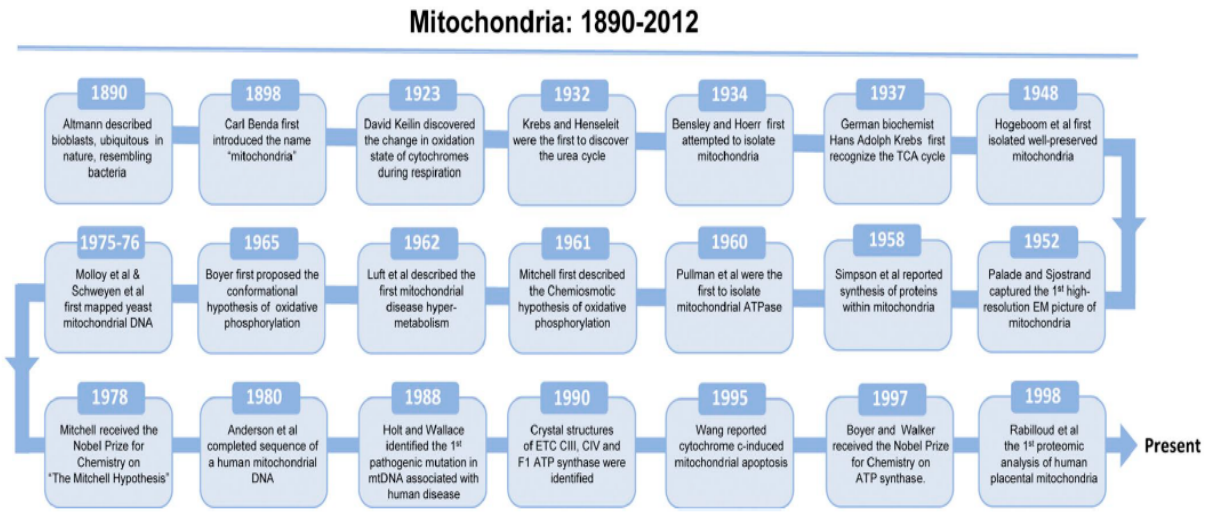

Figure 1. Milestones in mitochondrial research. Representative milestones in mitochondrial research, including mitochondrial function, structure, and mitochondrial medicine, are listed in a chronological sequence (1890–current). Our apologies to those not represented in this timeline.

The relationship between mitochondria and disease has been firmly established, with one of the first reported mitochondrial diseases by Rolf Luft and colleagues at Karolinska University in Stockholm, Sweden. A patient was presented with hypermetabolism unrelated to thyroid dysfunction. Through morphological (increased

number of mitochondria) and biochemical (loosely coupled mitochondrial oxidative phosphorylation [OXPHOS]) evidence, this group of investigators concluded that mitochondria were the source of these symptoms, marking the beginning of an era of mitochondrial medicine. Throughout the 1970s, other landmark discoveries singled out specific metabolic as well as enzymatic deficiencies, such as pyruvate dehydrogenase and carnitine palmitoyltransferase deficiencies. Over 20 years passed between the discovery of mitochondrial DNA (mtDNA) and its mapping. In 1988, for the first time, mutations in mtDNA-associated diseases were reported[3]. As the detection of mitochondrial dysfunctions became more prevalent, the identification of mitochondrial components, as well as the characterization of mitochondrial proteome dynamics, increased in relevance.

1.2 Proteins Supporting Mitochondrial Architecture and Biology

The mitochondrion is an organelle comprised of four distinct compartments—the outer mitochondrial membrane (OMM), the intermembrane space, the inner mitochondrial membrane (IMM), and the matrix— which are bordered by its unique double-membrane structure. Production and transportation of electrolytes are facilitated by proteins embedded within the membranes. Approximately 1,000 proteins have been identified by several proteomic investigations[4-9] to support mitochondrial structure and function. Figure 2 summarizes the major mitochondrial cellular processes, their subproteomes, and their involvements in metabolic diseases.

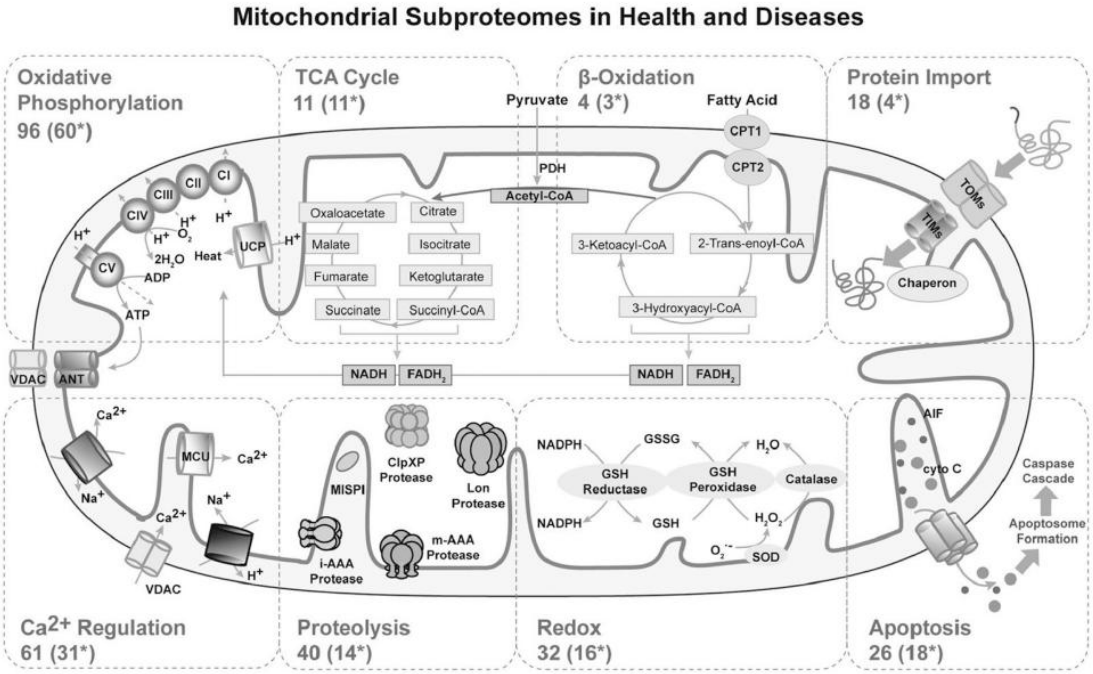

Figure 2. Schematic overview of mitochondrial subproteomes in health and disease. This figure contextualizes mitochondrial proteomes to their biological pathways and the consequences of the proteome compositions to clinical phenotypes. Mitochondrial pathways responsible for fundamental cellular functions within the cell, including OXPHOS, TCA cycle, β oxidation, apoptosis, proteolysis, redox, protein import, and calcium regulation, are detailed. Other mitochondrial functions related to specific cell types are not listed. Within each mitochondrial subproteome, the first number represents the total number of proteins associated with its function (the number of proteins was collected in our previous study; Zhang et al., 2008); the next number inside the parentheses (*) signifies the portion of the total proteins in this particular subproteome reported to be implicated in metabolic diseases.

The majority of proteins comprising the mitochondria are encoded by nuclear DNA. However, unlike their surrounding organelles, mitochondria possess their own DNA, which serves as code for the 13 proteins constituting seven proteins for complex I, one for complex III, three for complex IV, and two for complex V of the electron transport chain (ETC), also known as the respiratory complexes. In most multicellular organisms, mtDNA are inherited maternally. Because there are many copies of mtDNA and there are many mitochondria in all cell types, most mitochondrial mutations often have few detrimental effects on mitochondrial function until they reach sufficient number, a “threshold effect.” Not surprisingly, this threshold effect is lower in highly aerobic tissues such as the eye, brain, and heart[10]. Therefore, these tissues are more susceptible to

mitochondrial dysfunction. To date, proteomic approaches have been successful in characterizing the subproteome supporting OXPHOS function, including the identification of 88 proteins from the human heart[8] and 96 proteins from the mouse heart[4]. These proteins represent 90% or more of the entire OXPHOS subproteome (nuclear and mDNA combined). The remaining 10% of the OXPHOS proteins are known only by their genetic information, but are undetected by proteomic methods. They may have exceptionally low abundance or may carry unique biochemical properties (e.g., hydrophobic proteins); their protein characterization may require approaches with higher sensitivity (e.g., antibodies).

As the key energy producer of the cell, the mitochondrion is fundamental for many metabolic processes. The products of glycolysis enter the mitochondrial matrix to continue their conversion to energy in the tricarboxylic acid (TCA) cycle, which possesses a subproteome composed of 11 proteins in the mouse cardiac mitochondria[4]. Subsequently, NADH and FADH2 proceed to donate electrons to the ETC components, eventually reducing oxygen to water. An electrochemical gradient is established and maintained to harness the energy produced by the subsequent flow of protons back into the matrix to synthesize ATP from ADP and phosphate.

Calcium plays a multifaceted role in mitochondrial function. Mitochondrial calcium regulation can be denoted by influx, matrix buffering, and efflux[11, 12]. A total of 61 proteins from the mouse heart[4] has been reported to support calcium regulation in mitochondria. Mitochondria have been implicated in the induction of cell death; two

differential processes have been shown to lyse the cells: necrosis and apoptosis. The protein identities defining both the necrosis and apoptosis pathways are only partially understood. Release of apoptotic factors such as cytochrome c, Smac/Diablo, and apoptosis-induced factors into the cytosol attracts caspase-9 and apoptotic protease-activating factor 1 to form the apoptosome with ATP. The Bcl-2 family proteins are also activated during the apoptotic process. A total of 26 proteins in the mouse heart[4] has been identified to be related to apoptosis.

In parallel, mitochondria produce free radicals by leaking electrons to oxygen in the process of transferring electrons through the ETC, in particular complexes I and III. To counteract this, endogenous scavenging enzymes and antioxidants are activated to eliminate reactive oxygen species (ROS); this defense system includes superoxide dismutases, catalase, peroxidredoxin, glutathione peroxidase, and reduced glutathione. Currently, 29 proteins in the human heart are affiliated with redox functions[8], whereas 32 proteins were reported in the mouse heart.

Mitochondrial proteases participate not only in protein proteolysis[13], but they also are emerging as crucial regulators of mitochondrial function. The many types of mitochondrial proteases include the PIM1/Lon protease, the mitochondrial intermembrane space protease I and the ClpXP protease in the matrix, and the i-AAA protease and the m-AAA protease residing in the IMM. Proteases are shown to play essential roles in mitochondrial morphology maintenance, mitochondrial biogenesis, and mitochondrial metabolism regulation[14]. Mitochondrial proteases are evolutionarily

conserved from yeast to humans in support of the evolutionary prokaryotic ancestors. Disturbances of the mitochondrial proteolytic system affect mitochondrial homeostasis. Thus far, 40 proteases were reported from the mouse heart[4] in the mitochondria.

1.3 Proteomic Profiling of Mitochondria

The mitochondrial proteome is unique, complex, and dynamically regulated as it adapts to the needs of the tissues or disease states[15, 16]. Over the past decade, tremendous efforts have been made to explore mitochondrial subproteomes and their posttranslational modifications (PTMs) in both physiological and pathological environments. Indeed, mitochondrial proteomes in various organisms and tissues, including yeast[17], mouse[4-6, 9], human[8, 18], rat[7, 19, 20], and drosophila[21] have been investigated. Figure 3 deciphers the state-of-the-art experimental workflow used in mitochondrial proteomic studies, including mitochondrial isolation, purification, mass spectrometry (MS) identification, and data analyses.

Preparation of pure and functionally viable mitochondria is an important first step to achieving reliable and reproducible proteomic outputs. Hogeboom et al.[1] developed the first protocol to isolate rat liver mitochondria based on a differential centrifugation. Thereafter, isolation methods have been modified and tailored based on different tissues and species. Mitochondria could be further purified by free-flow electrophoresis or density gradient centrifugation with either percoll or other dense materials such as

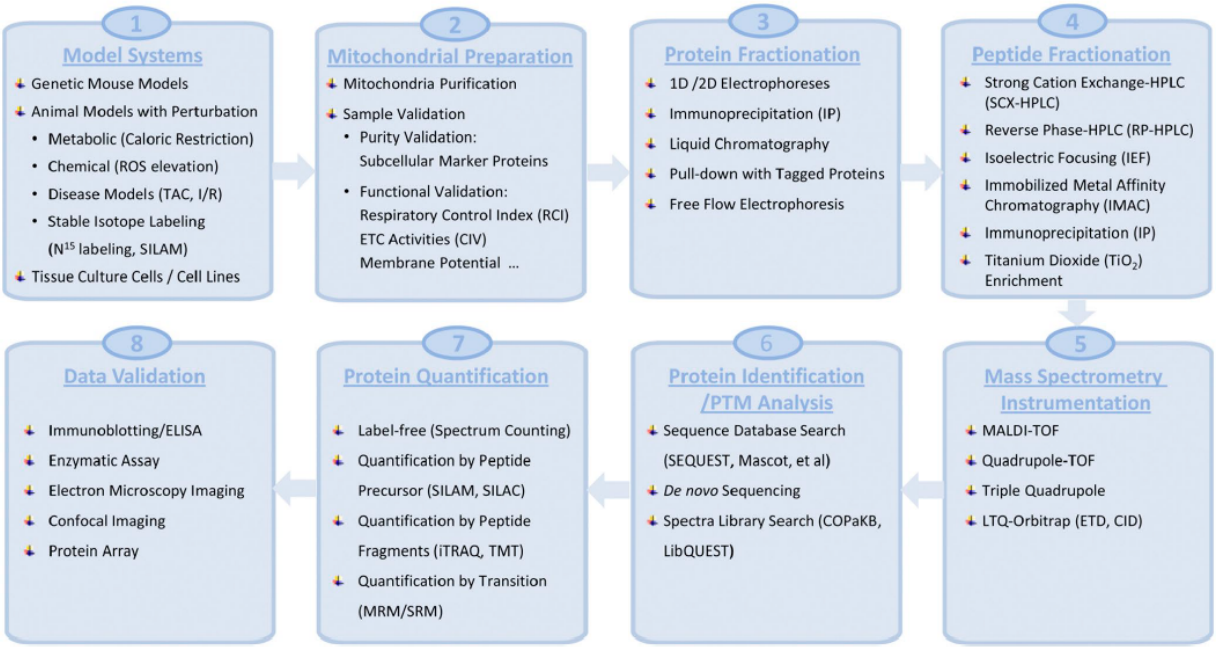

Figure 3. Current state-of-the-art technology platform to characterize mitochondrial proteomes. This figure depicts the current technology platform used to characterize mitochondrial proteomes from model systems, including mitochondrial preparation, protein/peptide fractionations, MS instrumentation, protein identification/PTM analyses, protein quantification, and data validation.

metrizamide, sucrose, and nycodenz. Mitochondrial purity and intactness could be validated by immunoblottings using specific organelle protein markers, membrane potential measurements, and respiratory control index assessments, as well as electron microscopy morphology detection[4]. If a particular mitochondrial subproteome, such as OMM, IMM, or OXPHOS, is the subject of interest, isolation of these subcompartments is desirable. Sample fractionation has been frequently applied to reduce the complexity before the sample is subjected to MS analyses. Different approaches have been used, including gel-based approaches such as one-dimensional SDS-PAGE, two-dimensional PAGE (2-DE), and blue native PAGE, as well as gel-free–based approaches such as immunoprecipitation, liquid chromatography (LC), and free-flow electrophoresis. Different separation approaches are complementary. 2-DE is preferred to separate soluble and high-abundance proteins but poorly resolves hydrophobic proteins, low-

abundance proteins, and proteins with extreme isoelectric point values. The combination of a blue native PAGE and a SDS-PAGE could be used to enrich the identification of OXPHOS protein complexes[20]. Gel-free–based shotgun proteomic analyses, combining a strong cation exchange LC and a reversed-phased LC, are beneficial for the detection of proteins with low abundance and high hydrophobicity.

An early study on mitochondrial proteomes by Rabilloud et al.[22] was conducted on human placental mitochondria using 2-DE followed by MS analyses; they reported a total of 46 proteins. Subsequently, Taylor and his collaborators[8, 18] characterized the human cardiac mitochondrial proteome using SDS-PAGE separation and multidimensional LC coupled with MS analyses, where 722 proteins were reported. Furthermore, Mootha et al.[9] characterized mitochondrial proteomes from the mouse brain, heart, liver, and kidney samples. 399 proteins were identified from proteomic studies and 428 proteins were reported from gene annotation analyses, combining for a total of 591 distinct proteins from different tissues. Among these 399 proteins, 107 proteins were conserved across tissues. Later, Kislinger et al.[6] performed a global proteomic survey of four organellar compartments (cytosol, membranes, mitochondria, and nuclei) in six mouse organs. 4,768 proteins were identified, of which 1,075 proteins were localized in the brain mitochondria, 667 in the heart mitochondria, 789 in the kidney mitochondria, 775 in the liver mitochondria, 1,072 in the lung mitochondria, and 901 in the placenta mitochondria. Among these mitochondrial proteins, only 132 proteins were conserved across tissues. Later on, studies by Zhang et al.[4] identified 940 distinct proteins from mouse cardiac mitochondria using functionally validated

mitochondria, among which 480 proteins were not identified by the aforementioned major proteomic profiling studies[6, 8, 9]. Additionally, Pagliarini et al.[5] combined MS analyses with GFP tagging, as well as machine learning, and created a mitochondrial compendium of 1,098 genes and their protein expressions across 14 different mouse tissues. By linking the characterized proteins in this inventory to known mitochondrial pathways, 19 proteins were predicted to be important for the function of ETC complex I, of which one protein (C8orf38) was further validated. Many methodological issues may contribute to these mitochondrial proteome differences as reported by their MS-based identifications. There are issues using mitochondrial samples from different tissues, including sample preparations, contaminants from abundant proteins, the overall molecular compositions of the targeted mitochondrial proteome, the dynamic ranges of protein abundance in the particular mitochondrial proteome of interest, etc. Apart from these technical factors, it is highly possible that the reported diversity in mitochondrial proteomes is a result of their tissue specificity. Despite the variability of MS-based proteomic approaches, the proteomic results from different research groups indicate the heterogeneity of mitochondrial proteomes among the rat/mouse tissues [6, 7, 16, 19]. These inter-tissue comparisons recognize that the mitochondrial proteomes are tuned to meet the metabolic and signaling requirements of their environment. For example, heart mitochondria require a constant and stable supply of ATP to maintain cardiac function, whereas the liver mitochondria are orientated toward a more biosynthetic role conducive for metabolic function. In addition, using a combination of comparative genomics and computational algorithms, the interspecies comparisons support the notion of the existence of conserved and heterogeneous proteins in the mitochondrial proteome[23].

The four subcompartments of the mitochondria are comprised of different protein contents. The matrix incorporates approximately two thirds of the mitochondrial proteins, with the IMM containing 21%, the intermembrane space occupying ~6%, and the OMM encompassing a mere 4% of the overall proteins of the mitochondrion[24]. These values are still under investigation as low-abundance proteins are difficult to detect with the current technology. Using organic acid, Da Cruz and Martinou[25] extracted the IMM fractions of hepatocytes and found 182 proteins using a 2-DE-LC-MS/MS. McDonald et al.[26] further identified 348 proteins through three separation techniques (2D-LC with ProteomeLab PF 2D Protein Fractionation System, 2-DE, and RP-HPLC). A two-step digestion with trypsin and proteinase K facilitated the detection of OMM proteins previously unidentified[24]. Another study of *Saccharomyces cerevisiae* by Zahedi et al.[27] encountered 112 OMM proteins, including integral and peripheral membrane proteins.

In parallel to protein identification, two main strategies have been applied to the quantitative mitochondrial proteomic analyses: an MS-based label-free approach and differential labeling quantitative techniques. The label-free quantification is based on either the measurement of the peptide precursor intensity ions of a protein or the number of fragmented spectra peptides of a protein. This approach has been successfully used in the comparison of mitochondrial proteome changes under physiological and pathological conditions in various animal models[7, 16]. Isotope-labeling experiments include two-dimensional difference in-gel electrophoresis (2D-

DIGE), isotope-coded affinity tag, isobaric tags for relative and absolute quantitation (iTRAQ), and stable isotopic labeling by amino acids in cell culture (SILAC), as well as stable isotopic labeling in mammals (SILAM). These approaches are more accurate, but the reagents are costly and require specialized bioinformatics tools.

In recent years, several databases of mitochondrial proteins have been created, including MitoP2[28], Mitoproteome[29], Mito-Carta[5], MitoMiner[30], as well as COPaKB, i.e., the Cardiac Organellar Protein Atlas Knowledgebase (http://www .heartproteome.org). These databases list mitochondrial proteins identified via multiple approaches, including MS/MS analyses, literature curations, and bioinformatics evaluations. COPaKB is an integrated resource of proteome biology configured to specifically focus on cardiovascular biology and medicine. Its first release includes proteomic data from large-scale proteomic surveys of cardiac mitochondrial proteins.

Defining the mitochondrial proteome is a challenge because of the dynamics of this organelle. Approximately 293 out of 940 proteins identified were found to contain mitochondrial targeting sequences[4]. In contrast, a majority of proteins do not bear the mitochondrial targeting sequences; however, they can travel to multiple subcellular localizations in parallel to their mitochondrial residency. Some proteins anchor onto the outer membrane of mitochondria with a loose attachment; they are called mitochondrial-associated proteins. Targeting sequence prediction cannot be used as a sole strategy to validate the mitochondrial localization of proteins caused by a higher false-positive prediction rate as well as multiple protein import mechanisms. Some mitochondrial

proteins are only expressed in certain developmental stages or specific species. Furthermore, some mitochondrial proteins are expressed in very low abundances and do not meet the detection threshold criteria of MS. Collectively, the above issues (the nature of mitochondrial proteins and the technological limitations) contribute to the current discrepancy of the existing mitochondrial proteome datasets.

1.4 Mitochondria in the Pathogenesis of Metabolic Dysfunction

As the central hubs of energy production and other important signaling pathways, mitochondria possess a high susceptibility for being implicated in numerous human pathological phenotypes. Dysfunction of mitochondrial proteins caused by either environmental changes or genetic mutations has been shown to be directly associated with various diseases including insulin resistance and metabolic syndrome.

The development of diabetes mellitus typically accompanies the dysfunction of insulin production and absorption by the body[31]. Using 2-DE followed by LC-MS/MS analyses, recent studies from Taurino et al.[32] observed the decreased expression of the Ndufs3 protein subunit of complex I in steptozotocin-induced type 1 diabetic rats. In combination with genetic (a decreased mRNA level) as well as biochemical (impaired catalytic activity of complex I) evidence, this group of investigators concluded that Ndufs3 is a critical contributor to the onset of diabetic encephalopathy in type 1 diabetes[32]. Through the use of iTRAQ and 2D-DIGE, subsarcolemmal mitochondria

(SSM) and interfibrillar mitochondria (IFM) were analyzed to determine whether type 1 diabetes influenced the proteomic makeup of these two mitochondrial subpopulations in the heart[31]. The proteomic makeup of IFM was affected to a greater extent than SSM, as exemplified by a decrease in fatty acid oxidation and OXPHOS proteins. Compared with diabetic SSM, the expression levels of adenine nucleotide translocator, mitochondrial phosphate carrier, mitofilin, inner membrane translocases, and mitochondrial heat shock protein 70 were decreased in diabetic IFM. The levels of mitochondrial protein import were unchanged in diabetic SSM, whereas the levels of mitochondrial protein import were substantially decreased in diabetic IFM[31, 33]. PTMs, specifically protein oxidations and deamidations, were more prevalent within IFM. Therefore, proteomic alterations were linked to the dysfunction of mitochondrial protein import such as mitochondrial heat shock protein 70. This evidence underscores the role of the mitochondrial proteomes underlying pathophysiology of diabetes, insulin resistance, and metabolic syndrome.

1.5 Sex Differences and Metabolic Regulation

Recently, the scientific community has begun taking steps to address the effect of sex on preclinical studies[34]. As such, the need to identify metabolic sex differences has become a critical issue. The effect of genetics (XX and XY in females and males, respectively) is emphasized by the actions of sex hormones including estrogens,

progesterone, and androgens which play an influential role in regulating metabolism in both males and females.

With the exception of reproductive organs, females and males have similar organ systems; however, women have a smaller muscle mass than men with greater differences in upper body than lower body muscle mass[35, 36]. The composition of these muscles is also sexually dimorphic - women tend to have a 27-35% greater Type I area relative to total fiber area as well as a greater capillary density[37]. Females are better equipped to regulate glucose homeostasis since more Type I fibers and a greater capillary density enhance tissue perfusion, providing more blood, oxygen, and metabolites to the muscles. Since Type I muscle fibers possess more mitochondria, this also increases the capacity for both glucose and lipid oxidation[37]. In addition, Type I fiber percentage and capillary density is negatively correlated with insulin resistance and type 2 diabetes mellitus (T2DM) in both lean and obese individuals[37]. Therefore, the combination of a greater proportion of Type I fibers and higher estrogen levels play a large role in how female muscles have enhanced glucose tolerance, likely contributing to improved oxidative metabolism and enhanced insulin sensitivity. However, previous literature indicates that women and men do not differ significantly in metabolic activity, suggesting that a man and woman of comparable muscle mass would have a similar endurance performance. Therefore, these studies suggest that the primary differentiating factor for energy consumption is body composition and size[38-40].

Moreover, under the same moderate intensity endurance workload, women have a lower respiratory exchange ratio (the ratio of carbon dioxide produced and oxygen used). This suggests that women have a reduced dependence on carbohydrates and preferentially oxidize lipids as a fuel source for exercise compared to men[41-46]. Having a higher glycolytic capacity and Type II fibers allows men to utilize more glucose[47, 48] in the absence of oxygen, but leads to more lactate accumulation and therefore, longer recovery times[37]. This indicates that men possess a greater ability for glycogenolysis and glycolytic flux than women, while women have increased potential for β-oxidation compared to men[47]. Sex hormones likely contribute to this difference in substrate metabolism. Furthermore, while skeletal muscle is the main tissue for glucose uptake, adipose tissue also contributes to blood glucose disposal. Lipid droplet morphology is sex-specific, with men having fewer but larger lipid droplets and women possessing a larger quantity of smaller lipid droplets[37]. Lipids are an advantageous source of fuel for prolonged exercise compared to glucose which is an ideal source of energy for short durations of intense exercise. CD36, a critical transporter of lipids to mitochondria for oxidation, is increased in both men and women after aerobic training, but is higher in women regardless of training status. Intramyocellular lipids are also elevated in female muscle with a higher percentage of these lipids in contact with mitochondria after exercise for increased oxidation potential[37]. This indicates enhanced fatty acid storage and transport[37] in women compared to men. A greater number of Type I muscle fibers and a reliance on lipids as a source of fuel suggests that women are more resistant to fatigue than men.

In addition, body fat distribution and energy substrate utilization patterns are sex-specific. Compared to males, females possess enhanced insulin sensitivity and less visceral fat. Since females also possess a greater capacity to store and clear lipids, females can utilize lipids at an increased rate, allowing for a slower time to fatigue[37, 49]. These benefits may provide females a certain metabolic flexibility to better combat cellular stressors. On the other hand, males have increased muscle mass and a higher glycolytic capacity which are beneficial for short, intense bursts of energy[37]. Together, these findings emphasize the impact of sex on the molecular mechanisms underlying metabolism.

1.6 The Sex-Specific Relationship Between Mitochondria, HSP72, and Insulin Sensitivity

Obesity is a critical health and financial burden, and a leading cause of death in the United States due to secondary complications of T2DM and cardiovascular disease[50]. Obesity is strongly associated with mitochondrial dysfunction and insulin resistance in metabolically active tissues including muscle, liver and adipose[51-53]. The severity of T2DM has been correlated with age, genetics, and sex[54]. In particular, men and women differ in their responsiveness to insulin with men more likely to develop insulin resistance than pre-menopausal women[55-57]. While there is currently no cure for T2DM, exercise and diet modification are beneficial strategies for disease management; however, the precise mechanisms underlying the health benefit of these interventions

remains incompletely understood[58, 59]. Proper mitochondrial function is required to maintain metabolic homeostasis and cellular energetic capacity. There is evidence that males and females differ in their regulation of mitochondrial processes; females have a higher mitochondrial content and antioxidant activity[60-63]. However, the mechanisms that contribute to mitochondrial dysfunction and insulin resistance in men and women remain unclear.

Recent evidence reveals that an impaired heat shock protein (HSP) response to cellular stress underlies insulin resistance[64-67] in males. A clinical target of interest is heat shock protein 72 (HSP72), a chaperone protein that facilitates the proper folding of newly translated and misfolded proteins. HSP72 expression is associated with the maintenance of insulin sensitivity since a reduction in its protein abundance promotes dysfunctional mitochondria and insulin resistance in rodents and humans alike[68, 69]. In addition, HSP72 is the most prevalent HSP induced under cellular stress including acute nutrient excess and endurance exercise[68]. As such, HSP72 expression is intimately linked to metabolic homeostasis and mitochondrial function.

Previous studies have implicated imbalances in mitochondrial fission-fusion dynamics in the onset of insulin resistance[70-73]. The equilibrium between mitochondrial fusion and fission is central to numerous aspects of physiology such as apoptosis and control of mitochondrial quality and inheritance[74]. Disrupting the balance between fusion and fission can lead to fused mitochondria that are unable to maintain bioenergetic capacity and self-regulate mitochondrial quality control[75]. Our laboratory and others have

demonstrated that chronic hyperfused and fragmented mitochondrial architecture are correlated with metabolic syndrome[70-73]. The ablation of key fusion and fission proteins, including mitofusin (Mfn) 2 and dynamin-related protein (Drp) 1, leads to insulin resistance[76-78]. Mfn2 is an outer mitochondrial membrane protein that mediates mitochondrial fusion and is a target of the E3 ubiquitin ligase Parkin, a protein involved in mitochondrial quality control[68]. Drp1, the key regulator of mitochondrial fission, is a cytosolic protein recruited to the mitochondrial outer membrane. On the membrane, Drp1 interacts with pro-fission proteins including mitochondrial fission protein 1 (Fis1) to drive the division of a mitochondrion. Drp1 expression is associated with increased mitochondrial fragmentation, resulting in inner mitochondrial membrane depolarization and decreased ATP production[73, 79]. Smaller, fragmented mitochondria and increased fission machinery were observed in the skeletal muscle of mice with genetic and diet-induced obesity[73]. These observations highlight the importance of mitochondrial fission-fusion dynamics in maintaining insulin sensitivity.

Recently our laboratory found an important function of HSP72 in skeletal muscle mitochondrial dynamics. HSP72 translocates to depolarized mitochondria and regulates the functionality of Parkin. Male HSP72 knockout (KO) mice exhibit reduced fatty acid oxidation, increased reactive oxygen species (ROS) production, and impaired insulin action[68]. This phenotype occurs as a result of whole body accumulation of dysfunctional hyperfused mitochondria and impaired Parkin action[74, 80-83]. Without HSP72, Parkin accumulates in the cytosol (impaired protein autoregulation) and fails to translocate to mitochondria to induce mitophagy. The impairments in muscle oxidative

function were paralleled by increased white adipose tissue (WAT) mass in male KO mice. In contrast, female HSP72 KO mice have decreased WAT mass and enhanced insulin sensitivity.

Since the male HSP72 KO mice are phenotypically well-characterized at a variety of ages, we studied female animals which we believe will provide important insight into both the sexually dimorphic role of HSP72 in regulating glucose homeostasis, as well as lay the foundation for potential sex-specific therapeutic interventions targeting T2DM.

1.7 The Overall Goal of Our Study

Mitochondrial function and dynamics play a crucial role in physiological cellular maintenance. Herein, we provide a framework for studying the effects of organism- and tissue-specificity of the mitochondrial proteomic profile and its associated functions (Chapter 2). We further study whether tissue-specificity can affect mitochondrial turnover (biogensis and/or degradation) rates (Chapter 3). Finally, we investigate the effect of a specific heat shock protein (HSP), HSP72, on insulin sensitivity and mitochondrial dynamics in males and females (Chapter 4). We believe that data from our studies will be essential in the development of sex-specific mitochondrial therapeutic interventions targeting diseases such as T2DM and metabolic syndrome.

1.8 References

1. Hogeboom, G.H., W.C. Schneider, and G.E. Pallade, *Cytochemical studies of mammalian tissues; isolation of intact mitochondria from rat liver; some biochemical properties of mitochondria and submicroscopic particulate material.* J Biol Chem, 1948. **172**(2): p. 619-35.

2. Ernster, L. and G. Schatz, *Mitochondria: a historical review.* J Cell Biol, 1981. **91**(3 Pt 2): p. 227s-255s.

3. Wallace, D.C., *Mitochondrial DNA mutations in disease and aging.* Environ Mol Mutagen, 2010. **51**(5): p. 440-50.

4. Zhang, J., et al., *Systematic characterization of the murine mitochondrial proteome using functionally validated cardiac mitochondria.* Proteomics, 2008. **8**(8): p. 1564-75.

5. Pagliarini, D.J., et al., *A mitochondrial protein compendium elucidates complex I disease biology.* Cell, 2008. **134**(1): p. 112-23.

6. Kislinger, T., et al., *Global survey of organ and organelle protein expression in mouse: combined proteomic and transcriptomic profiling.* Cell, 2006. **125**(1): p. 173-86.

7. Forner, F., et al., *Quantitative proteomic comparison of rat mitochondria from muscle, heart, and liver.* Mol Cell Proteomics, 2006. **5**(4): p. 608-19.

8. Taylor, S.W., et al., *Characterization of the human heart mitochondrial proteome.* Nat Biotechnol, 2003. **21**(3): p. 281-6.

9. Mootha, V.K., et al., *Integrated analysis of protein composition, tissue diversity, and gene regulation in mouse mitochondria.* Cell, 2003. **115**(5): p. 629-40.

10. DiMauro, S. and E.A. Schon, *Mitochondrial respiratory-chain diseases.* N Engl J Med, 2003. **348**(26): p. 2656-68.

11. Glancy, B. and R.S. Balaban, *Role of mitochondrial Ca2+ in the regulation of cellular energetics.* Biochemistry, 2012. **51**(14): p. 2959-73.

12. Weiss, J.N., et al., *Role of the mitochondrial permeability transition in myocardial disease.* Circ Res, 2003. **93**(4): p. 292-301.

13. Lau, E., et al., *Substrate- and isoform-specific proteome stability in normal and stressed cardiac mitochondria.* Circ Res, 2012. **110**(9): p. 1174-8.

14. Bulteau, A.L. and A. Bayot, *Mitochondrial proteases and cancer.* Biochim Biophys Acta, 2011. **1807**(6): p. 595-601.

15. Balaban, R.S., *The mitochondrial proteome: a dynamic functional program in tissues and disease states.* Environ Mol Mutagen, 2010. **51**(5): p. 352-9.

16. Johnson, D.T., et al., *Functional consequences of mitochondrial proteome heterogeneity.* Am J Physiol Cell Physiol, 2007. **292**(2): p. C698-707.

17. Sickmann, A., et al., *The proteome of Saccharomyces cerevisiae mitochondria.* Proc Natl Acad Sci U S A, 2003. **100**(23): p. 13207-12.

18. Gaucher, S.P., et al., *Expanded coverage of the human heart mitochondrial proteome using multidimensional liquid chromatography coupled with tandem mass spectrometry.* J Proteome Res, 2004. **3**(3): p. 495-505.

19. Johnson, D.T., et al., *Tissue heterogeneity of the mammalian mitochondrial proteome.* Am J Physiol Cell Physiol, 2007. **292**(2): p. C689-97.

20. Reifschneider, N.H., et al., *Defining the mitochondrial proteomes from five rat organs in a physiologically significant context using 2D blue-native/SDS-PAGE.* J Proteome Res, 2006. **5**(5): p. 1117-32.

21. Alonso, J., et al., *Characterization of the Drosophila melanogaster mitochondrial proteome.* J Proteome Res, 2005. **4**(5): p. 1636-45.

22. Rabilloud, T., et al., *Two-dimensional electrophoresis of human placental mitochondria and protein identification by mass spectrometry: toward a human mitochondrial proteome.* Electrophoresis, 1998. **19**(6): p. 1006-14.

23. Richly, E., P.F. Chinnery, and D. Leister, *Evolutionary diversification of mitochondrial proteomes: implications for human disease.* Trends Genet, 2003. **19**(7): p. 356-62.

24. Distler, A.M., J. Kerner, and C.L. Hoppel, *Proteomics of mitochondrial inner and outer membranes.* Proteomics, 2008. **8**(19): p. 4066-82.

25. Da Cruz, S. and J.C. Martinou, *Purification and proteomic analysis of the mouse liver mitochondrial inner membrane.* Methods Mol Biol, 2008. **432**: p. 101-16.

26. McDonald, T., et al., *Expanding the subproteome of the inner mitochondria using protein separation technologies: one- and two-dimensional liquid chromatography and two-dimensional gel electrophoresis.* Mol Cell Proteomics, 2006. **5**(12): p. 2392-411.

27. Zahedi, R.P., et al., *Proteomic analysis of the yeast mitochondrial outer membrane reveals accumulation of a subclass of preproteins.* Mol Biol Cell, 2006. **17**(3): p. 1436-50.

28. Elstner, M., et al., *MitoP2: an integrative tool for the analysis of the mitochondrial proteome.* Mol Biotechnol, 2008. **40**(3): p. 306-15.

29. Cotter, D., et al., *MitoProteome: mitochondrial protein sequence database and annotation system.* Nucleic Acids Res, 2004. **32**(Database issue): p. D463-7.

30. Smith, A.C. and A.J. Robinson, *MitoMiner, an integrated database for the storage and analysis of mitochondrial proteomics data.* Mol Cell Proteomics, 2009. **8**(6): p. 1324-37.

31. Baseler, W.A., et al., *Proteomic alterations of distinct mitochondrial subpopulations in the type 1 diabetic heart: contribution of protein import dysfunction.* Am J Physiol Regul Integr Comp Physiol, 2011. **300**(2): p. R186-200.

32. Taurino, F., et al., *Mitochondrial proteome analysis reveals depression of the Ndufs3 subunit and activity of complex I in diabetic rat brain.* J Proteomics, 2012. **75**(8): p. 2331-41.

33. Davidson, S.M., *A needle in a haystack: focus on "Proteomic alterations of distinct mitochondrial subpopulations in the type 1 diabetic heart".* Am J Physiol Regul Integr Comp Physiol, 2011. **300**(2): p. R183-5.

34. Clayton, J.A. and F.S. Collins, *Policy: NIH to balance sex in cell and animal studies.* Nature, 2014. **509**(7500): p. 282-3.

35. Miller, A.E., et al., *Gender differences in strength and muscle fiber characteristics.* Eur J Appl Physiol Occup Physiol, 1993. **66**(3): p. 254-62.

36. Lindle, R.S., et al., *Age and gender comparisons of muscle strength in 654 women and men aged 20-93 yr.* J Appl Physiol (1985), 1997. **83**(5): p. 1581-7.

37. Lundsgaard, A.M. and B. Kiens, *Gender differences in skeletal muscle substrate metabolism - molecular mechanisms and insulin sensitivity.* Front Endocrinol (Lausanne), 2014. **5**: p. 195.

38. Hutchinson, P.L., et al., *Relationship of cardiac size to maximal oxygen uptake and body size in men and women.* Int J Sports Med, 1991. **12**(4): p. 369-73.

39. Arciero, P.J., M.I. Goran, and E.T. Poehlman, *Resting metabolic rate is lower in women than in men.* J Appl Physiol (1985), 1993. **75**(6): p. 2514-20.

40. Klausen, B., S. Toubro, and A. Astrup, *Age and sex effects on energy expenditure.* Am J Clin Nutr, 1997. **65**(4): p. 895-907.

41. Roepstorff, C., et al., *Regulation of oxidative enzyme activity and eukaryotic elongation factor 2 in human skeletal muscle: influence of gender and exercise.* Acta Physiol Scand, 2005. **184**(3): p. 215-24.

42. Carter, S.L., et al., *Changes in skeletal muscle in males and females following endurance training.* Can J Physiol Pharmacol, 2001. **79**(5): p. 386-92.

43. Fu, M.H., et al., *Exercise, sex, menstrual cycle phase, and 17beta-estradiol influence metabolism-related genes in human skeletal muscle.* Physiol Genomics, 2009. **40**(1): p. 34-47.

44. Maher, A.C., et al., *Women have higher protein content of beta-oxidation enzymes in skeletal muscle than men.* PLoS One, 2010. **5**(8): p. e12025.

45. Thompson, J.R., et al., *Gastrocnemius mitochondrial respiration: are there any differences between men and women?* J Surg Res, 2013. **185**(1): p. 206-11.

46. Devries, M.C., *Sex-based differences in endurance exercise muscle metabolism: impact on exercise and nutritional strategies to optimize health and performance in women.* Exp Physiol, 2016. **101**(2): p. 243-9.

47. Green, H.J., I.G. Fraser, and D.A. Ranney, *Male and female differences in enzyme activities of energy metabolism in vastus lateralis muscle.* J Neurol Sci, 1984. **65**(3): p. 323-31.

48. Simoneau, J.A., et al., *Skeletal muscle histochemical and biochemical characteristics in sedentary male and female subjects.* Can J Physiol Pharmacol, 1985. **63**(1): p. 30-5.

49. Varlamov, O., C.L. Bethea, and C.T. Roberts, Jr., *Sex-specific differences in lipid and glucose metabolism.* Front Endocrinol (Lausanne), 2014. **5**: p. 241.

50. Hurt, R.T., et al., *The obesity epidemic: challenges, health initiatives, and implications for gastroenterologists.* Gastroenterol Hepatol (N Y), 2010. **6**(12): p. 780-92.

51. Cheng, Z. and F.A. Almeida, *Mitochondrial alteration in type 2 diabetes and obesity: an epigenetic link.* Cell Cycle, 2014. **13**(6): p. 890-7.

52. Vernochet, C. and C.R. Kahn, *Mitochondria, obesity and aging.* Aging (Albany NY), 2012. **4**(12): p. 859-60.

53. Ritov, V.B., et al., *Deficiency of electron transport chain in human skeletal muscle mitochondria in type 2 diabetes mellitus and obesity.* Am J Physiol Endocrinol Metab, 2010. **298**(1): p. E49-58.

54. Association, A.D., *Statistics About Diabetes.* 2014.

55. Parks, B.W., et al., *Genetic architecture of insulin resistance in the mouse.* Cell Metab, 2015. **21**(2): p. 334-347.

56. Shi, H., R.J. Seeley, and D.J. Clegg, *Sexual differences in the control of energy homeostasis.* Front Neuroendocrinol, 2009. **30**(3): p. 396-404.

57. Geer, E.B. and W. Shen, *Gender differences in insulin resistance, body composition, and energy balance.* Gend Med, 2009. **6 Suppl 1**: p. 60-75.

58. Kennedy, J.W., et al., *Acute exercise induces GLUT4 translocation in skeletal muscle of normal human subjects and subjects with type 2 diabetes.* Diabetes, 1999. **48**(5): p. 1192-7.

59. Hussey, S.E., et al., *Exercise training increases adipose tissue GLUT4 expression in patients with type 2 diabetes.* Diabetes Obes Metab, 2011. **13**(10): p. 959-62.

60. Borras, C., et al., *Direct antioxidant and protective effect of estradiol on isolated mitochondria.* Biochim Biophys Acta, 2010. **1802**(1): p. 205-11.

61. Vina, J., et al., *Why females live longer than males? Importance of the upregulation of longevity-associated genes by oestrogenic compounds.* FEBS Lett, 2005. **579**(12): p. 2541-5.

62. Vina, J., et al., *Role of mitochondrial oxidative stress to explain the different longevity between genders: protective effect of estrogens.* Free Radic Res, 2006. **40**(12): p. 1359-65.

63. Farooqui, T.F.a.A.A., *Oxidative stress in vertebrates and invertebrates : molecular aspects on cell signaling.* Wiley-Blackwell, 2011.

64. Henstridge, D.C., M. Whitham, and M.A. Febbraio, *Chaperoning to the metabolic party: The emerging therapeutic role of heat-shock proteins in obesity and type 2 diabetes.* Mol Metab, 2014. **3**(8): p. 781-93.

65. Hooper, P.L. and P.L. Hooper, *Inflammation, heat shock proteins, and type 2 diabetes.* Cell Stress Chaperones, 2009. **14**(2): p. 113-5.

66. Padmalayam, I., *The heat shock response: its role in pathogenesis of type 2 diabetes and its complications, and implications for therapeutic intervention.* Discov Med, 2014. **18**(97): p. 29-39.

67. Tiss, A., et al., *Immunohistochemical profiling of the heat shock response in obese non-diabetic subjects revealed impaired expression of heat shock proteins in the adipose tissue.* Lipids Health Dis, 2014. **13**: p. 106.

68. Henstridge, D.C., et al., *Activating HSP72 in rodent skeletal muscle increases mitochondrial number and oxidative capacity and decreases insulin resistance.* Diabetes, 2014. **63**(6): p. 1881-94.

69. Chung, J., et al., *HSP72 protects against obesity-induced insulin resistance.* Proc Natl Acad Sci U S A, 2008. **105**(5): p. 1739-44.

70. Drew, B.G., et al., *HSP72 is a mitochondrial stress sensor critical for Parkin action, oxidative metabolism, and insulin sensitivity in skeletal muscle.* Diabetes, 2014. **63**(5): p. 1488-505.

71. Joseph, A.M., et al., *Mitochondrial dysregulation in the pathogenesis of diabetes: potential for mitochondrial biogenesis-mediated interventions.* Exp Diabetes Res, 2012. **2012**: p. 642038.

72. Kim, J.A., Y. Wei, and J.R. Sowers, *Role of mitochondrial dysfunction in insulin resistance.* Circ Res, 2008. **102**(4): p. 401-14.

73. Jheng, H.F., et al., *Mitochondrial fission contributes to mitochondrial dysfunction and insulin resistance in skeletal muscle.* Mol Cell Biol, 2012. **32**(2): p. 309-19.

74. Seo, A.Y., et al., *New insights into the role of mitochondria in aging: mitochondrial dynamics and more.* J Cell Sci, 2010. **123**(Pt 15): p. 2533-42.

75. Twig, G., B. Hyde, and O.S. Shirihai, *Mitochondrial fusion, fission and autophagy as a quality control axis: the bioenergetic view.* Biochim Biophys Acta, 2008. **1777**(9): p. 1092-7.

76. Westermeier, F., et al., *Defective insulin signaling and mitochondrial dynamics in diabetic cardiomyopathy.* Biochim Biophys Acta, 2015. **1853**(5): p. 1113-8.

77. Zorzano, A., et al., *Mitofusin 2 as a driver that controls energy metabolism and insulin signaling.* Antioxid Redox Signal, 2015. **22**(12): p. 1020-31.

78. Montgomery, M.K. and N. Turner, *Mitochondrial dysfunction and insulin resistance: an update.* Endocr Connect, 2015. **4**(1): p. R1-R15.

79. Watanabe, T., et al., *Roles of mitochondrial fragmentation and reactive oxygen species in mitochondrial dysfunction and myocardial insulin resistance.* Exp Cell Res, 2014. **323**(2): p. 314-25.

80. Jin, S.M. and R.J. Youle, *PINK1- and Parkin-mediated mitophagy at a glance.* J Cell Sci, 2012. **125**(Pt 4): p. 795-9.

81. Chen, H., et al., *Mitochondrial fusion is required for mtDNA stability in skeletal muscle and tolerance of mtDNA mutations.* Cell, 2010. **141**(2): p. 280-9.

82. Joseph, A.M., et al., *Dysregulation of mitochondrial quality control processes contribute to sarcopenia in a mouse model of premature aging.* PLoS One, 2013. **8**(7): p. e69327.

83. Safdar, A., et al., *Endurance exercise rescues progeroid aging and induces systemic mitochondrial rejuvenation in mtDNA mutator mice.* Proc Natl Acad Sci U S A, 2011. **108**(10): p. 4135-40.

CHAPTER 2

Characterization, Design, and Function of the Mitochondrial Proteome:

From Organs to Organisms

*This chapter is reprinted from Lotz, Lin, Black, Zhang et al., Characterization, Design, and Function of the Mitochondrial Proteome: From Organs to Organisms, Journal of Proteome Research, 13(2):433-46. https://pubs.acs.org/doi/10.1021/pr400539j

Journal of proteome research

Article

pubs.acs.org/jpr

Characterization, Design, and Function of the Mitochondrial Proteome: From Organs to Organisms

Christopher Lotz,[†,⊥] Amanda J. Lin,[†,⊥] Caitlin M. Black,[†,⊥] Jun Zhang,[†,⊥] Edward Lau,[†] Ning Deng,[‡] Yueju Wang,[†] Nobel C. Zong,[†] Jeong H. Choi,[†] Tao Xu,[§] David A. Liem,[†] Paavo Korge,[†] James N. Weiss,[†] Henning Hermjakob,[∥] John R. Yates, III,[§] Rolf Apweiler,[∥] and Peipei Ping*[,†]

[†]Departments of Physiology and Medicine/Division of Cardiology, David Geffen School of Medicine at UCLA, 675 Charles E. Young Drive, MRL Building, Suite 1609, Los Angeles, California 90095, United States

[‡]College of Biomedical Engineering and Instrumentation, the Key Laboratory for Biomedical Engineering of Ministry of Education, Zhejiang University, #38 Zheda Rd, Hangzhou, Zhejiang, 310027, China

[§]The Scripps Research Institute, 10550 North Torrey Pines Road, La Jolla, California 92037, United States

[∥]EMBL-EBI, The Wellcome Trust Genome Campus, Hinxton, Cambridgeshire CB10 1SD, United Kingdom

Supporting Information

ABSTRACT: Mitochondria are a common energy source for organs and organisms; their diverse functions are specialized according to the unique phenotypes of their hosting environment. Perturbation of mitochondrial homeostasis accompanies significant pathological phenotypes. However, the connections between mitochondrial proteome properties and function remain to be experimentally established on a systematic level. This uncertainty impedes the contextualization and translation of proteomic data to the molecular derivations of mitochondrial diseases. We present a collection of mitochondrial features and functions from four model systems, including two cardiac mitochondrial proteomes from distinct genomes (human and mouse), two unique organ mitochondrial proteomes from identical genetic codons (mouse heart and mouse liver), as well as a relevant metazoan out-group (drosophila). The data, composed of mitochondrial protein abundance and their biochemical activities, capture the core functionalities of these mitochondria. This investigation allowed us to redefine the core mitochondrial proteome from organs and organisms, as well as the relevant contributions from genetic information and hosting milieu. Our study has identified significant enrichment of disease-associated genes and their products. Furthermore, correlational analyses suggest that mitochondrial proteome design is primarily driven by cellular environment. Taken together, these results connect proteome feature with mitochondrial function, providing a prospective resource for mitochondrial pathophysiology and developing novel therapeutic targets in medicine.

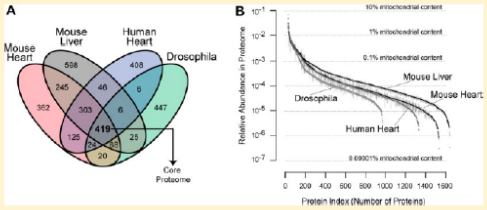

KEYWORDS: *mitochondrial proteome, mitochondrial function, heart diseases, intergenomic, intragenomic, and proteomic comparisons*

INTRODUCTION

Mitochondria are complex and intricately calibrated systems designed for the inception and perpetuation of life in a majority of eukaryotic organisms.[1−4] They are explicitly engineered to transect many aspects of cellular biology such as bioenergetics, metabolism, calcium signaling, reactive oxygen species (ROS) generation, and apoptosis. Mitochondrial dysfunctions have emerged as the underlying causes of various complex diseases including cancer, diabetes, obesity, neurodegenerative diseases, aging, and multiple forms of cardiomyopathy.[2,5−16] For instance, during heart failure, energy production decreases amid abnormal mitochondrial metabolic activity; however, on a molecular level, the mitochondrial proteome selectively alters its expression profile, including the redistribution of respiratory chain subunit abundances, as well as decreases in fatty acid oxidation proteins.[7,9,11,17−20] Therefore, advancing our knowledge of cellular functions in health and disease requires a thorough understanding of the mitochondrial proteome and its definitive relationship to biological function.

Previous studies have reported protein compositions of mitochondria in yeast[21,22] as well as in mouse,[23−26] human,[27,28] rat,[1,29−31] rabbit,[32] and drosophila[33,34] tissues. However, it is evident that there are inconsistencies and discrepancies among some of the data sets. The direct link between mitochondrial proteome biology and pathological phenotypic observations remains ambiguous, which has impeded diagnostic interpretations of large-scale proteomics data. This lack of clarity is partially due to fragmented efforts in assessing mitochondrial functionalities and proteome heterogeneity in various systems. Questions of how closely proteome parameters such as diversity and abundance conform to, or predict, biological

Received: June 7, 2013
Published: September 27, 2013

functions still remain unanswered. It is clear that an unbiased characterization of the functional proteome of mitochondria would undoubtedly further our insight into complex mitochondrial functions and mitochondrial-associated diseases. In this regard, experimental proteomics data offer an indispensable insight into organelle biology in parallel to the transcription-oriented efforts, alleviating potential issues arising from algorithms predicting mitochondrial-targeted genes and their lack of tissue specificity.

In this study, we propose a strategy that combines functional assays and protein expression measurements through label-free quantification analyses; using NSAF values[35−37] to characterize multiple aspects of mitochondrial pathways has been the only feasible and economical approach for analyzing large-scale proteomic data sets from multiple model systems. We utilized this strategy in mitochondria isolated from human hearts and compared them with data from mouse hearts because of its prevalence as a proxy for human hearts; mouse livers, used as a comparison with organ mitochondria; and drosophila, serving as both a nonmammalian metazoan out-group and an experimental model found to correlate with some human diseases.[38−40]

Our investigation reveals intergenomic and intragenomic correlations for proteome diversity, proteome abundance, and mitochondrial function. Through correlational analyses, we delineate that the molecular mechanisms of the mitochondrial proteome are primarily dictated by its cellular environment. Furthermore, the mitochondrial proteome is predominantly composed of a small number of vastly abundant proteins involved in the principal processes of cellular survival, including oxidative phosphorylation and metabolism. With our most comprehensive mitochondrial protein repertoire to date, we established a core mitochondrial proteome of 419 conserved proteins across four model systems. Additionally, we determined that fundamental mitochondrial functions are defined by the evolutionary conservation of a core mitochondrial proteome across different species, whereas organ-derived proteins, whether by novel genetic information or cell-specific translocation, reflect the diversification in the heterogeneity of mitochondrial populations. Collectively, this study provides a useful resource and network for future studies on mitochondrial biology. The definitive characteristics of mitochondrial proteomes afford great opportunities in developing targeted treatment for human disease.

■ EXPERIMENTAL PROCEDURES

Experimental procedures on human tissues were approved by the UCLA Human Subjects Protection Committee (HSPC) and the UCLA Institutional Review Boards (IRBs). The experimental procedures on animals were performed in accordance with the Animal Research Committee guidelines at UCLA and the Guide for the Care and Use of Laboratory Animals, published by the National Institutes of Health. An overview of our experimental workflow is shown in Figure S1 in the Supporting Information. A comprehensive Methods Section is available in the Supporting Information.

Tissue Sample Collection

Tissue samples were procured from each model system. Mouse heart and liver tissue samples were obtained from thirty 8−10 week old ICR strain mice. Human heart samples from the free anterior left ventricular wall were collected from individuals (average age = 49 ± 8 years, n = 5, 4 males and 1 female) previously treated with a left ventricular assist device (LVAD). These individuals exhibited normal left ventricular end diastolic dimension (LVEDD) after LVAD treatment. This improvement is featured in Figure S2 in the Supporting Information. Additionally, approximately 1000 adult wild-type *Drosophila melanogaster* (Oregon R strain) were immobilized by chilling prior to mitochondria extraction. More information regarding methods can be found in S2 in the Supporting Information.

Isolation and Purification of Functional, Viable Mitochondria from Human Heart, Mouse Heart, Mouse Liver, and Drosophila

Mitochondria were isolated from freshly collected mouse hearts, mouse livers, human hearts, and *Drosophila melanogaster* by differential centrifugation as described.[26,41,42] The freshly isolated mitochondria were subjected to a series of functional and structural validations.[26]

Assessment of Mitochondrial Function

The activities of the mitochondrial electron transport chain (ETC) complexes I (C−I) and V (C−V) were assessed in vitro by spectrophotometric measurements.[43−46] Pharmacological inhibitors were employed to determine the inhibitor-insensitive background of each complex. Pyruvate dehydrogenase (PDH) activity, proteolytic activity, and glutathione reductase activity assays were performed according to the manufacturer's instructions. Mitochondrial O_2 consumption and the susceptibility of mitochondria to calcium-induced injury were determined as described.[26,41] A detailed explanation of the assay methods is available in the Supporting Information.

Quantitative Proteomic Profiling of Mitochondrial Proteomes

SDS-PAGE, LC−MS/MS, and spectral analyses were performed as described.[26,41] Details regarding sample separation, chromatography, instrumentation settings, database searching, and protein identification criteria are detailed in the Supporting Information S4. Mitochondrial protein abundances were assessed according to normalized spectral abundance factors (NSAF);[35−37,41] this was then compared across all biological samples. The spectral counts for peptides shared among multiple proteins were divided proportionally according to the total spectral count of each protein's unique peptides, with proteins possessing a greater amount of unique spectral counts acquiring a larger portion of the shared peptide's spectral count. Figure S3 in the Supporting Information summarizes the mass spectrometry (MS) experiments.

Bioinformatics and Statistical Analyses

The molecular properties of the mitochondrial proteome, including molecular weight (MW), isoelectric point (pI), transmembrane domains, and mitochondrial target sequences, were analyzed using the UniProt Knowledgebase[26,41,47] and TargetP.[48] Biological information for individual proteins was extrapolated from gene ontology annotations (biological processes and molecular functions). Protein orthologs among human, mouse, and drosophila were identified via BioMart.[49] In addition, the involvement of mitochondrial proteins in diseases was determined by searching through the Online Mendelian Inheritance in Man (OMIM) and peer-reviewed publications on PubMed.[50] Correlational analyses were calculated using Spearman's coefficient. Finally, the IntAct database (IntAct database release 164b)[51] was used to determine the known mitochondrial protein−protein interactions among C−I, C−V, redox, and their associated partner proteins. Cytoscape 3.0

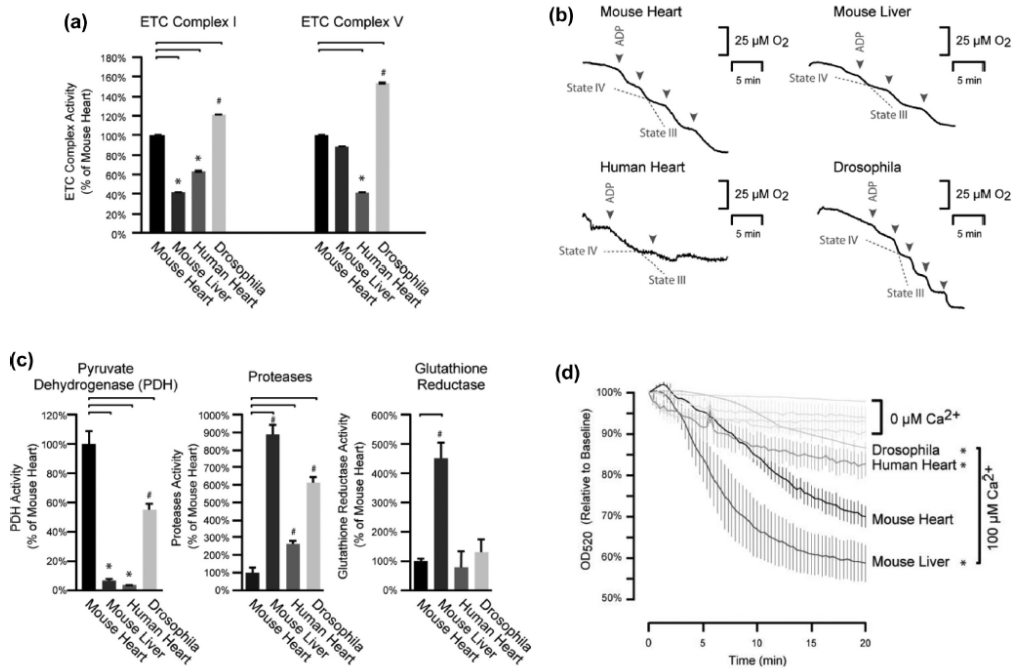

Figure 1. Mitochondrial functional characterization. (a) Electron production rate per microgram of mitochondrial proteins was analyzed to determine ETC complex activity and subsequently normalized to mouse cardiac mitochondria. Mouse liver mitochondria showed lower C−I activity and drosophila demonstrated higher C−I activity compared with the mouse heart. In addition, drosophila exhibited the highest C−V activity overall, with the lowest C−V activity in human heart mitochondria. These differences in respiratory flux and ATP generation can be attributed to cellular environment and genetic background. * or # represents $p < 0.05$ versus mouse heart; $n = 4$ per group. (b) RCI tracers are presented; they were measured as a ratio of the oxygen consumption rate by an initial O_2 concentration of 220 mmol·L^{-1}. Drosophila mitochondria were the most tightly coupled (RCI: 12.0), followed by the human heart (8.9), mouse heart (7.6), and mouse liver (7.0). A higher RCI value indicates tighter coupling of oxidation and phosphorylation processes. (c) Additional key enzymatic mitochondrial functions revealed similar intra- and intergenomic variability. Mouse liver mitochondria exhibited the highest proteolytic and glutathione reductase activities, whereas the mouse heart had the highest PDH activity, which may be explained by the altered production of reducing equivalents. * or # represents $p < 0.05$ versus mouse heart; $n = 4$ per group. (d) Calcium-induced mitochondrial swelling was measured as a reduction of optical density. Mouse liver mitochondria displayed the highest susceptibility to calcium-induced swelling. * represents $p < 0.05$ versus mouse heart with calcium overload; $n = 4$ per group.

Network Data Integration, Analysis, and Visualization software[52] was subsequently employed to depict these interactions. Swelling assay data and spectra analyses results were reported as mean ± SEM. Differences among the experimental groups were analyzed using one-way ANOVAs with posthoc contrasts utilizing the Student's t test.[53] The Mann−Whitney U test was used to determine the significance of protein abundance distribution differences. Values of $p < 0.05$ were recognized as significant.

RESULTS

Heterogeneic Programming of Mitochondrial Function across Organs and Organisms

We compiled a panel of biochemical assays to evaluate several functional parameters of intact and viable mitochondria isolated from the four model systems. To assess mitochondrial bioenergetics and other biological functions, we determined the reaction rate of the respiratory chain complexes, the respiratory control index (RCI), PDH activity, proteolytic capacity, redox regulation, and susceptibility to calcium-induced stress (Figure 1).

The activities of ETC C−I (NADH dehydrogenase) and C−V (F_1F_0 ATP synthase) were assessed. Results were normalized, by tissue weight, to mouse cardiac mitochondria for comparison (Figure 1a). Notably, mouse liver mitochondria demonstrated substantially lower C−I activity, human heart mitochondria showed the lowest C−V activity, and drosophila exhibited the highest Complex activity for C−I and C−V. These higher activities in drosophila suggest increases in both the delivery of reducing equivalents and ATP production due to the high energy turnover of insect flight muscles. In addition, the differential C−I activity levels between mouse heart and mouse liver indicate that cellular environment plays a significant role in the regulation of ETC function. Together, our data highlighted the heterogeneity of these two respiratory complexes and underscored the effect of cellular environments on functional activities.

We next examined the RCI as an indicator of coupling tightness for the respiratory circuitry. The human heart had an

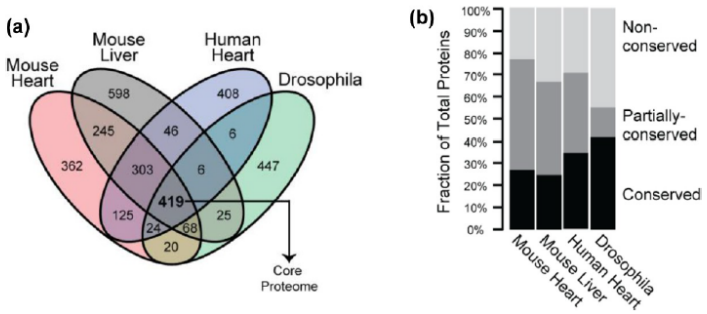

Figure 2. Mitochondrial proteome composition among four mitochondrial populations. (a) Protein orthologs were analyzed for each model systems. The 419 proteins identified in all four model systems represent the conserved core mitochondrial proteome. (b) Proportions of conserved and nonconserved proteins by protein number were denoted in each proteome. Drosophila demonstrated the highest protein count ratio of both conserved and nonconserved proteins.

RCI of 8.9, whereas mouse heart and mouse liver had RCI values of 7.6 and 7.0, respectively (Figure 1b). Drosophila mitochondria exhibited the highest RCI (12.0), demonstrating a tighter coupling of oxidation and phosphorylation processes.

To evaluate the energetic functions of mitochondria, we examined PDH, protease, and glutathione reductase activities to give a more comprehensive assessment of mitochondrial biology. We observed that mouse heart had the highest PDH activity, with significantly lower activity in mouse liver and human heart (Figure 1c). As anticipated, liver mitochondria exhibited the highest proteolytic and glutathione reductase activity. The heterogeneity of the four model systems was also confirmed by their response to calcium stress-induced injury. Liver mitochondria demonstrated a drastically higher susceptibility to calcium overload than other mitochondria (Figure 1d), likely reflecting the latter's lack of constant calcium flux as a noncontractile organ. These results accentuate the functional contributions of molecular environment and genetic background on cellular activity.

Dynamic Mitochondrial Proteome Design across Organs and Organisms

Mitochondrial Proteome Composition. To examine the molecular basis of the observed functional heterogeneity in depth, we profiled the proteome of the four mitochondrial populations. In total, we identified 1398 unique proteins from human heart mitochondria, 1620 from mouse heart mitochondria, 1733 from mouse liver mitochondria, and 1015 from drosophila mitochondria. To our knowledge, these results represent one of the most comprehensive mitochondrial protein catalogs for each of these model systems. A complete list of identified proteins is provided in Table S1 in the Supporting Information.[54] The distributions of biochemical features, including molecular weight, isoelectric point, as well as number of transmembrane domains, are shown in Figure S4 in the Supporting Information, implicating the dynamic properties of the mitochondrial proteome.

To determine how the mitochondrial proteome was partitioned among all four model systems into core proteins that preserved fundamental functions and diversified proteins that conferred specialized functions, we analyzed the number of proteins and protein orthologs shared by the four model systems. If we consider the minimal ortholog set to be common if varying numbers of homologous genes exist across organisms (Figure 2a, Table S2 in Supporting Information), 419 equivalent proteins were conserved across the model systems. Drosophila possessed the highest percentage of unique proteins (Figure 2b). Although lack of detection cannot distinguish protein absence from extremely low abundance, errors in data acquisition were minimized by comprehensive replications.

Mitochondrial Proteome Abundance. Label-free quantification analyses performed using the NSAF values of proteins, yielded the relative abundance of each protein and allowed for cross-proteome comparison among the model systems. Although the accuracy of label-free approaches may be limited by run-to-run variability and redundant peptides among proteins,[55] this technique allowed us to circumvent the challenge of synthesizing tens of thousands of stable isotope labeled peptides.[56] To ensure accurate quantification, we conducted exhaustive biological and technical replicates (from 18 replicates of the mouse heart to 29 replicates of the human heart) and developed an algorithm to proportionally allocate shared peptides to their corresponding proteins based on the percentage of unique peptides per protein. Our analysis showed that the mitochondrial proteome exhibited a high dynamic range of protein expression levels, with fractional abundance spanning more than five orders of magnitude from 10^{-1} to 10^{-6} (Figure 3a), although a vast number of proteins possessed a minimum NSAF value and are in rare abundance. For example, in mouse heart, the most abundant protein accounted for ~3% of the total mitochondrial proteome, whereas the least abundant protein accounted for ~0.00003% of its total mitochondrial proteome. These examples illustrate a 10^5-fold difference in protein abundance. Furthermore, proteins were ranked according to their abundance (Figure 3b); the top 100 most abundant proteins in each model system represented 57–83% of the mitochondrial proteome, whereas the bottom 50% only accounted for <4% of the mitochondrial protein content (Figure 3b). Conserved proteins were highly abundant, occupying 64% of mouse heart mitochondrial protein content, 52% of mouse liver mitochondria, 64% of human heart mitochondria, and 77% of drosophila mitochondria (Figure 3c). Protein abundance distributions between human heart mitochondria and mouse heart mitochondria were more similar (Spearman's ρ = 0.70) than those between mouse heart and mouse liver (ρ = 0.65), further supporting the notion that

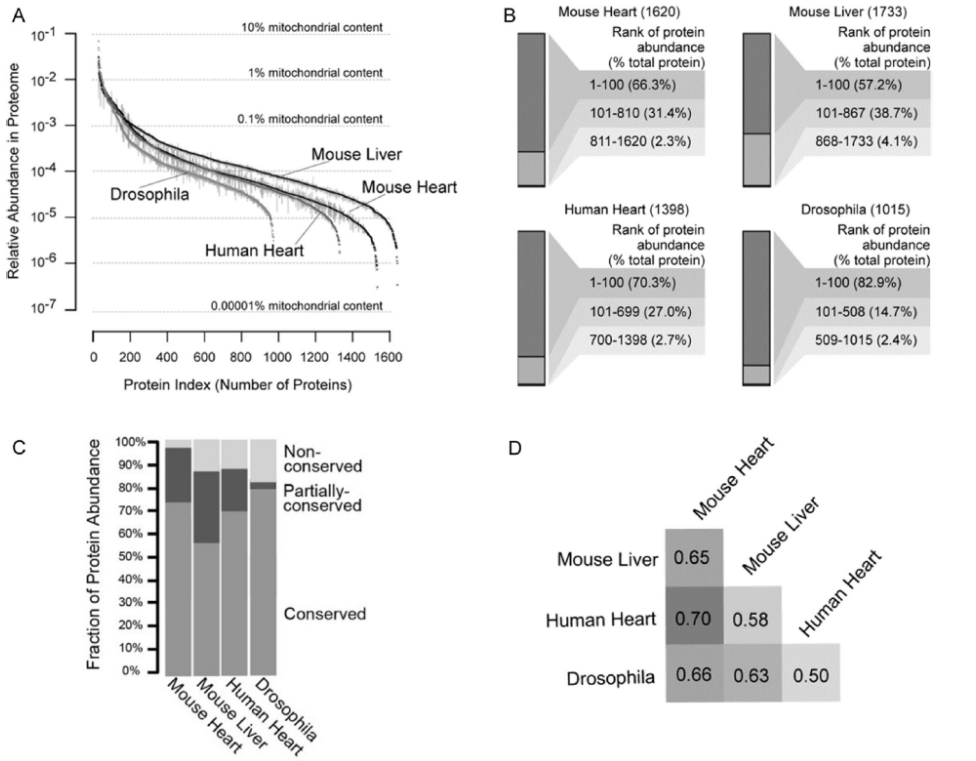

Figure 3. Mitochondrial proteome abundance. (a) Relative protein abundance was indexed based on NSAF values in descending order. The high dynamic range of protein expression levels for the mitochondrial proteome spans over five orders of magnitude. Error bar: SEM. (b) Proteins were ranked according to their abundance. The top 100 proteins in each model system are highly abundant and occupy a majority of the total mitochondrial protein content. The top 50% of each mitochondrial proteome accounts for over 95% of the total protein abundance, whereas the bottom 50% constitutes <4%. (c) The proportion of conserved, partially conserved, and unique proteins was illustrated in all four model systems. The conserved proteins are highly abundant, accounting for 72, 55, 68, and 78% of mitochondrial protein content in the mouse heart, the mouse liver, the human heart, and drosophila, respectively. Furthermore, nonconserved proteins in drosophila comprise the highest unique protein ratio among these organs and organisms, alluding to their specialized functionality. (d) Similarity in distribution of mitochondrial protein abundance was determined. Human heart and mouse heart mitochondrial protein abundance distribution levels are closely related, indicating that mitochondrial populations in the same organ of different species can demonstrate a stronger correlation than mitochondrial populations within different organs of the same organism. Moreover, mouse heart and mouse liver mitochondria had similar, but not identical distributions ($\rho = 0.65$).

abundance distribution is regulated by cellular environment (Figure 3d).

Properties of Mitochondrial Proteome and Function across Organs and Organisms

Mitochondrial Proteome and Functions. Upon categorizing proteins by biological processes, we observed that high-abundance clusters are particularly enriched in oxidative phosphorylation (OXPHOS), metabolism, transport, and signaling. Mouse liver possessed the highest abundance value for the metabolism cluster, reflecting its metabolic and biosynthetic specializations (Figure 4a). The mitochondrial proteome subpopulation abundances were analyzed for each functional category (Figure 4b). Among the conserved protein abundances, OXPHOS proteins as well as proteins associated with apoptosis and ETC complex assembly were more abundant in all mitochondrial populations. Proteins involved in TCA metabolic processes were also highly conserved. In contrast, proteins involved in signaling and proteolysis were less conserved among the four model systems. The mitochondrial proteome is therefore dominated by proteins involved in key fundamental metabolic processes.

We subsequently compared mitochondrial protein abundances and their involvement in specific functional pathways using NSAF values (Figure 4c). Mouse heart mitochondria demonstrated higher TCA cycle protein concentrations compared with mouse liver mitochondria. The differences in abundance of TCA cycle proteins among mouse heart, human heart, and drosophila were indistinguishable; this illustrates the variations in TCA activity between contractile and non-contractile tissues. Similarly, liver mitochondria contained the fewest C−I proteins. However, C−V showed no significant difference in overall protein abundance among the model

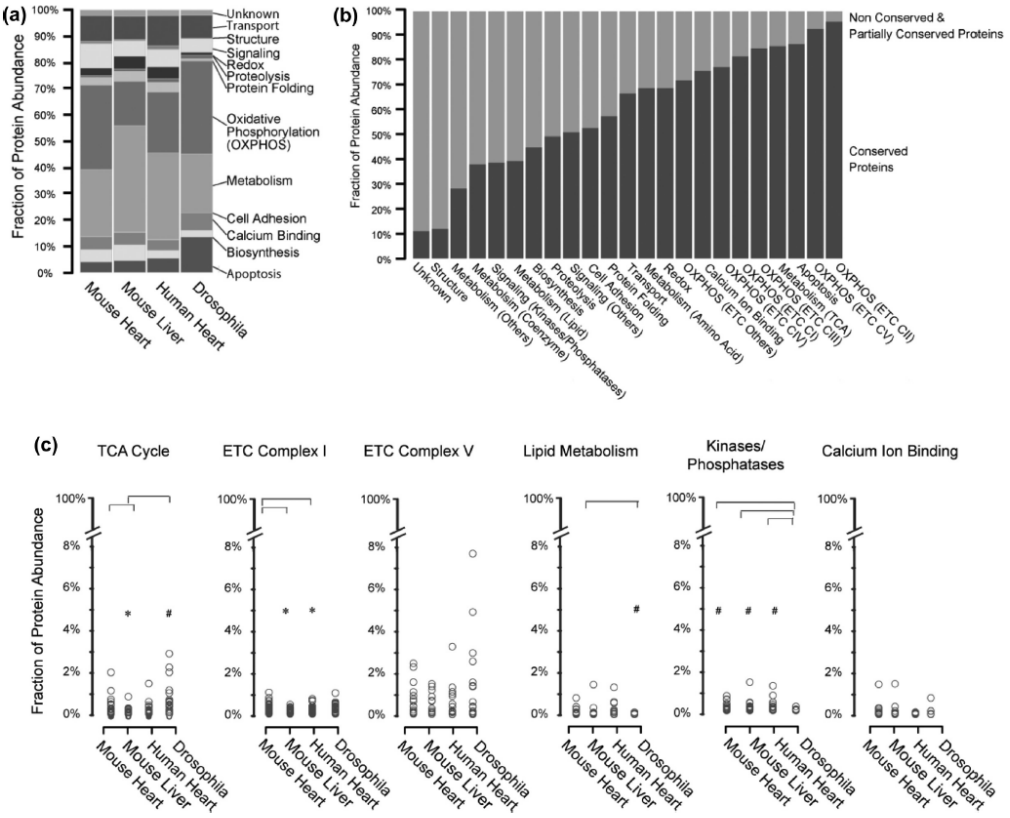

Figure 4. Correlation between the mitochondrial proteome and its functions. (a) Mitochondrial protein abundances were categorized by biological function. The high-abundance clusters are enriched in oxidative phosphorylation, metabolism, and transport-related proteins. In particular, mouse liver has the highest abundance values within the metabolism cluster, highlighting a metabolic specialization. Moreover, these conserved proteins are highly abundant, representing 81.0% of mitochondrial protein content in mouse heart, 59.5% in mouse liver, 79.7% in human heart, and 86.4% in drosophila. (b) Mitochondrial proteins were characterized by biological processes. Conserved proteins and non/partially conserved proteins in each category were quantified. Proteins involved in OXPHOS were concentrated in C−II and C−V. Conserved proteins were also found to be highly involved in apoptosis and TCA metabolism. Structural, signaling, and proteolytic processes have higher proportions of nonshared proteins. (c) Relative fraction of the proteome involved in specified functional pathways was determined. Mitochondrial proteins were further classified through bioinformatics analyses based on their involvement in specific functional pathways and then plotted by their NSAF values. $*p < 0.05$ versus mouse heart. The mouse heart, human heart, and drosophila models have high TCA cycle protein abundances, while the mouse liver shows significantly lower protein abundances, denoting the differences in TCA cycle activity between contractile and noncontractile tissues. The mouse liver mitochondria also contained the lowest abundance of C−I proteins. C−V was not found to have a significant difference in overall protein abundance among the model systems. Notably, within each Complex, differential subunit abundances spanned over three orders of magnitude. Drosophila had considerably lower lipid metabolism protein abundances in comparison with mouse liver, implicating liver mitochondria as specialized in the synthesis and degradation of lipids. In addition, drosophila mitochondria possess the lowest abundance of kinase/phosphatase proteins, suggesting that there is less phosphorylation regulation. The abundance of calcium-binding proteins was similar across the model systems; this deviates from our previous finding that shows mouse liver is more susceptible to calcium-induced swelling, indicating limitations in direct connections between proteomics data and functionality. Statistical significance was determined with a Mann−Whitney U test.

systems. In addition, it was found that within each Complex differential subunit abundances spanned over more than two orders of magnitude. The most abundant proteins within C−V are subunit β in mouse heart, mouse liver, and drosophila, but subunit α in human heart. The least abundant proteins within C−V are subunit α in mouse heart, subunit ϵ in mouse liver, and subunit β in human heart and drosophila. Moreover, we observed that proteins involved in lipid metabolism showed substantially lower abundances in drosophila when compared to mouse liver, but more than 89% of the drosophila lipid metabolism proteins were conserved among all model systems. In contrast, mouse liver possessed the highest abundance of proteins related to lipid metabolism, of which only 19% were conserved mitochondrial proteins. These results indicated that specialized pathways exist in mouse liver. Furthermore, drosophila possessed the lowest abundance of kinase/

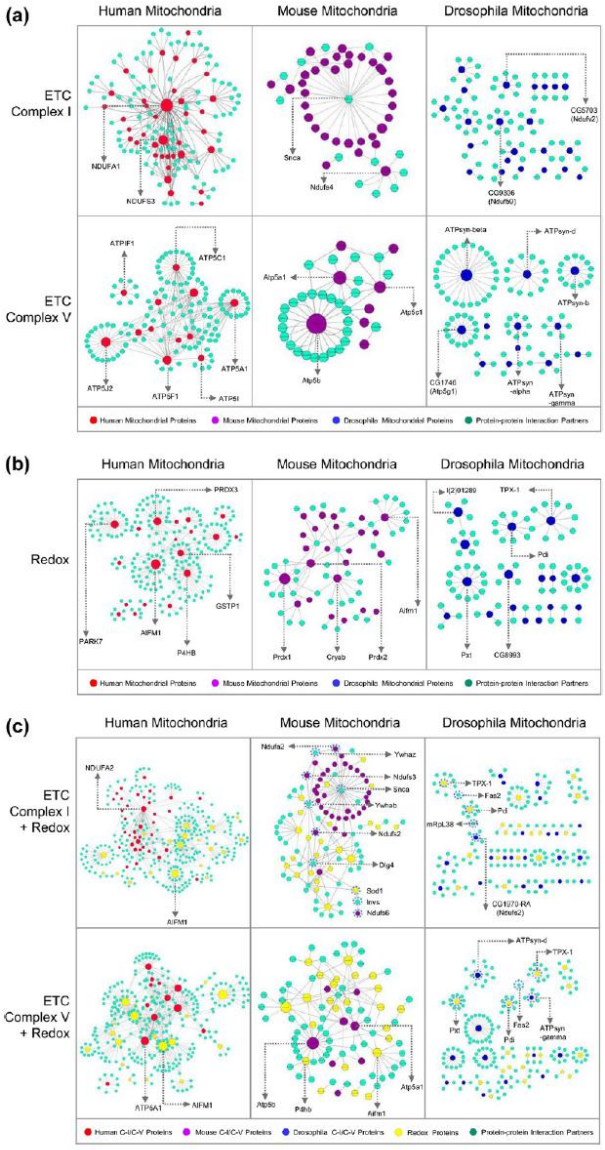

Figure 5. Mitochondrial protein−protein interactome analysis. An interactome analysis of C−I, C−V, redox, C−I + redox, and C−V + redox proteins was performed, and the protein−protein interactions are displayed. Major hubs have been labeled by gene name. The size of each mitochondrial node represents the number of connections in the protein−protein interaction network, with larger nodes indicating more interactions. (a) C−I showed NDUFA2 as the primary human mitochondrial protein with the most connections. Mouse mitochondrial proteins mainly centralized around one partner protein, α-synuclein. In contrast, drosophila proteins did not exhibit a clustered pattern. Three C−V proteins in human mitochondria, ATP5A1, ATP5B, and ATP5C1, were more interactive than other C−V proteins; however, only ATP5B was categorized as a major hub in both mouse and drosophila. (b) Analysis of redox protein−protein interactions demonstrated similar patterns to C−I with human and mouse proteins assembled around a single protein, whereas drosophila presented dispersed partnerships among its proteins. (c) Moreover, examination of C−I + redox and C−V + redox revealed little interaction between these complex proteins and redox proteins. An exception to the pattern, ATP5B (in C−V), interacted with redox protein PRDX1 in the mouse mitochondria analysis. Finally, the mouse C−I + redox interactome

dx.doi.org/10.1021/pr400539j | J. Proteome Res. 2014, 13, 433−446

Figure 5. continued

revealed an intertwining C−I and redox protein interaction network, a feature unique to the mouse mitochondrial proteome. The series of interlocking C−I and redox proteins found in the mouse C−I + redox interactome have been circled by a dotted line.

phosphatase proteins. Surprisingly, the abundance of calcium-ion binding proteins in liver mitochondria showed no significant difference across the model systems.

Mitochondrial-encoded proteins were further analyzed based on NSAF values. The ETC subunits appeared to be highly heterogeneous; in particular, mitochondrial-encoded subunits were found to be less abundant than nuclear-encoded subunits, primarily in mouse liver and human heart (under-detected). These subunits may serve as the limiting factors of complex assembly and may better explain the lower respiratory activities of C−I in mouse liver mitochondria and in C−V of human heart mitochondria.

Mitochondrial Interactome and Its Functions. Mitochondrial proteins identified in our study were queried within the IntAct database (IntAct database release 164b) for known protein−protein interactions to demonstrate associating partners among C−I, C−V, redox, and their neighboring proteins in human, mouse, and drosophila data sets. Cytoscape 3.0 Network Data Integration, Analysis, and Visualization software was then utilized to illustrate documented interactions among proteins in C−I, C−V, redox, C−I + redox, as well as C−V + redox. The resulting protein data sets focused on the differences among human, mouse, and drosophila protein connections. The size of each mitochondrial node represents the number of connections in the protein−protein interaction network, with larger nodes indicating more interactions. Interestingly, C−I proteins appeared to be centralized around NADH-ubiquinone oxidoreductase B8 subunit (NDUFA2) in human and α-synuclein in mouse (Figure 5a). In contrast, drosophila protein interactome patterns showed small scattered clusters and fragmented groupings. These results were indicative of the intergenomic protein−protein properties, which may have been influenced by the functional annotations unique to each database. Subsequently, NDUFA2 and α-synuclein were cross-analyzed for significant interactions in the mouse and human data sets, respectively. Although not a major hub, NDUFA2 was found to interact with proteins in the mouse data; however, α-synuclein was not found within the C−I human protein interactions. In the C−V interactome, subunit α (ATP5A1), β subunit (ATP5B), and subunit γ (ATP5C1) demonstrated the most protein−protein interactions (Figure 5a). Similarly, ATP5B served as the major hub in both the drosophila and the mouse network, a feature highlighting the evolutionary importance of ATP5B as a core protein. Redox proteins (Figure 5b) also portrayed a comparable pattern to C−I and C−V, with human proteins (i.e., Apoptosis Inducing Factor 1 − AIFm1) tending to serve as central hubs, whereas mouse and drosophila proteins displayed little affinity for interaction. Incorporation of both C−I + redox as well as C−V + redox revealed a lack of explicit connections between Complex proteins and redox proteins (Figure 5c). However, a single C−V protein (ATP5B) interacted with redox proteins − peroxiredoxin 1 (PRDX1), 2 (PRDX2), and 4 (PRDX4). The mouse C−I and redox protein integration serves as an important guide for the knowledge-building process regarding human protein−protein interactions. Overall, each model system showed a relatively distinct protein−protein interaction network with little overlap among the organisms for C−I, C−V, redox, C−I + redox, as well as C−V + redox proteins, indicating that the integration of protein interactions from other model systems could greatly benefit future investigations of the human interactome.

Mitochondrial Proteome and Protein Translocation. To explore the mechanisms promoting nuclear-encoded protein translocation into mitochondria, we determined the number of mitochondrial proteins with an N-terminal mitochondrial targeting sequence (MTS) using TargetP and the UniProt KnowledgeBase. Interestingly, only a small subpopulation of mitochondrial proteins possessed an MTS, ranging from 9.7% in drosophila to 19.9, 20.7, and 22.4% in mouse liver, human heart, and mouse heart, respectively (Figure 6a). Analysis of the core proteins demonstrated a similar pattern (17.4% in drosophila, 37.9% in human heart, 48.7% in mouse liver, and 49.7% in mouse heart) as exemplified in Figure 6b. Further examination illustrated that mitochondrial proteins with and without an MTS had similar functional distributions. A functional perspective demonstrated that proteins with an MTS were found to be fundamental in metabolism and biosynthesis and were localized within the general mitochondrion. Conversely, mitochondrial proteins essential in metabolism and OXPHOS without an MTS were primarily localized in nonmitochondrial domains (Figure 6c). However, the subcellular localization distribution of protein abundance showed that mitochondrial proteins with an MTS were predominantly concentrated in both the inner mitochondrial membrane (IMM) and the matrix (Figure 6d).

Mitochondrial Proteome and Disease. Mitochondrial dysfunction has been shown to be associated with the onset of disease. Literature curation using predefined terms (e.g., diabetes, obesity, muscular dystrophy, and neurodegeneration) suggested that human disease-associated genes are enriched in the conserved mitochondrial proteome, especially in conserved respiratory chain proteins (Figure 7). The diversified mitochondrial proteome contains fewer known disease associations than the conserved mitochondrial proteome but still has a higher occurrence of disease gene associations than did the whole human genome (~15%). In addition, a significant portion of the conserved respiratory proteins (~27%) and core mitochondrial proteome (~17%) plays a role in known cardiac diseases. Other conserved proteins are prime candidates for disease association as well. These data highlight the central importance of the core mitochondrial proteome to normal physiological functions.

■ DISCUSSION

In summary, we combined biochemistry assays, quantitative proteomics profiling, and interactome analysis to define four mitochondrial populations. Our analysis significantly expands the existing knowledge on the mitochondrial proteome with approximately 3350 unique proteins identified, including a core conserved mitochondrial proteome comprised of 419 proteins. These data portrayed inter- and intraspecies heterogeneities of mitochondria from both expressional and functional perspectives. Our data suggest that proteome−function correlations are subject to complex organizations with protein−protein

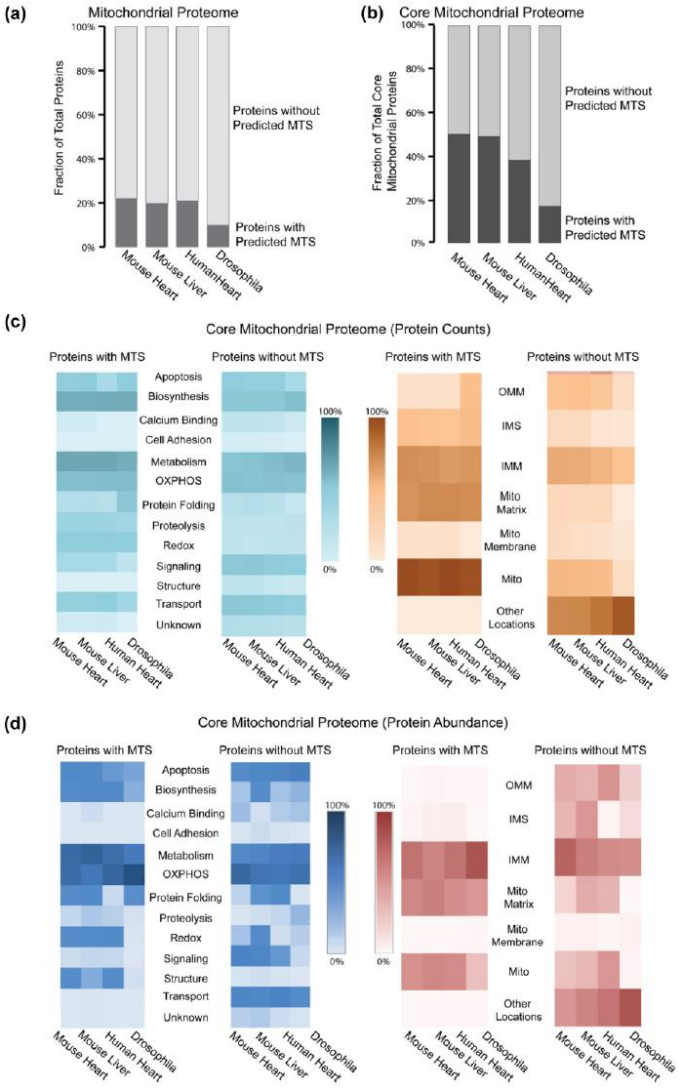

Figure 6. Distribution of proteins with mitochondrial targeting sequences in the mitochondrial proteome. (a) The number of mitochondrial proteins with an N-terminal mitochondrial targeting sequence (MTS) within the mitochondrial proteome was examined. Only a small percentage of mitochondrial proteins carried an MTS. Mitochondrial proteins with an MTS accounted for 9.7% of the total mitochondrial proteome in drosophila, 19.9% in mouse heart, 20.7% in human heart, and 22.4% in mouse liver. (b) Analysis of the core proteins demonstrated a similar pattern of mitochondrial proteins with an MTS – 17.4% in drosophila, 37.9% in human heart, 48.7% in mouse liver, and 49.7% in mouse heart. This suggests that the mitochondrial proteins without N-terminal targeting sequences are utilizing alternative methods to localize in the mitochondria. (c) Number of core mitochondrial proteins with an MTS and without an MTS was determined by their different functionalities and subcellular localizations. A majority of the mitochondrial proteins with an MTS were involved in metabolism and biosynthesis and were found throughout the mitochondrion rather than a specific mitochondrial compartment. In contrast, mitochondrial proteins without an MTS were predominantly integral in metabolism and OXPHOS and were localized in other cellular regions. (d) While the abundance of core mitochondrial proteins with an MTS and core mitochondrial proteins without an MTS were both highly involved in metabolism, OXPHOS, apoptosis, and biosynthesis, the core mitochondrial proteins with an MTS were most abundant in the outer and inner mitochondrial membrane, whereas the core mitochondrial proteins without an MTS were most abundant in the inner mitochondrial membrane, intermembrane space, matrix, and other cellular locations.

dx.doi.org/10.1021/pr400539j | *J. Proteome Res.* 2014, 13, 433−446

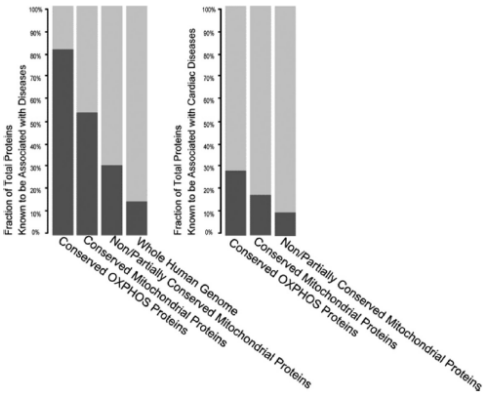

Figure 7. Pathological phenotypes of the mitochondrial proteomes. The involvement of mitochondrial proteins as well as the OXPHOS subproteome in disease phenotypes (left) and cardiac disease phenotypes (right) was determined by literature curation using predefined search terms. Human disease-associated genes are more prominent within the conserved mitochondrial proteome, and dysfunction of conserved respiratory chain proteins is particularly detrimental with 54% of these proteins implicated in disease. In contrast, only 15% of the human genome is correlated with causing disorders. Among these, 27% of conserved OXPHOS proteins and 17% of conserved mitochondrial proteins are directly associated with cardiac disease. These results illustrate the importance of the core mitochondrial proteome to physiological functions.

interactions and that concomitant molecular function assessments are essential to contextualize global proteomics data and locate decisive perturbations.

Mitochondrial Core Proteome Properties

Comparative genomics predicted that ~100 human mitochondrial genes have homologues in nine diverse eukaryotes and are mainly enriched in biological processes related to transport, metabolism, and signal transduction.[57] Indeed, a series of reports supports the existence of a highly specified, conserved, and heterogeneous mitochondrial proteome.[23,24,31,32] Our experimental data sets redefined the core mitochondrial proteome and provided additional evidence of the connection between conserved proteins and disease phenotypes. The data suggest a two-tiered architecture of the mitochondrial proteome, with the 419 conserved proteins in the core mitochondrial proteome representing essential hubs of protein networks involved in basal processes.

The Approach to Assess Protein Abundance

Existing MS approaches to assess protein abundance include label-free qualification and labeled quantification. In this particular study, we elected to quantify relative protein abundance through a label-free approach using NSAF values; this allowed us to overcome the challenge associated with synthesizing tens of thousands of stable isotope labeled peptides.[56] However, we are aware of the limitations of label-free approaches.[55] Specifically, the accuracy of such quantifications is affected by LC−MS run-to-run variability and the weight of shared peptides among different proteins. We implemented specific approaches to address these challenges. Multiple biological and technical replicates (from 18 replicates of the mouse heart to 29 replicates of the human heart) were performed to gain a reliable evaluation of protein abundance. Furthermore, an algorithm was developed to proportionally allocate shared peptides to their corresponding proteins based on the ratio of unique peptides identified among these proteins. Within the current technological capabilities, limiting factors are certainly evident; however, we believe that our approach to systematically assess relative protein abundance adequately addresses these shortcomings.

Links Between Mitochondrial Protein Composition and Function

Although the relationship between protein expression and functional differences may be affected by multiple factors, protein abundances are thought to be a selectable trait that reflects functional attributes, especially in closely related species.[58] The recent demonstration of transcript-level clustering recapitulates the phylogeny of mammalian lineages and supports the notability of expression levels in adaptation.[59] Interestingly, protein abundance, as calculated using NSAF values, varied according to their primary functions across the model systems. The two most abundant proteins in mouse heart, ADP/ATP translocase 1 and ATP synthase subunit α, are involved in the generation and transport of bioenergetics. Similarly, the most abundant proteins in human heart, ATP synthase subunit α and ATP synthase subunit β, as well as the two most abundant proteins in drosophila, ATP synthase subunit β and ADP/ATP translocase 1, are similarly involved in bioenergetics. In contrast, carbamoyl phosphate synthase 1 and 3-oxoacyl-CoA thiolase are the two most abundant proteins in mouse liver and are mainly involved in the urea cycle and β-oxidation of fatty acids, respectively. The relationship between the most abundant proteins for each model system and their respective function implies that abundance is strongly related to tissue type and mitochondrial location.

Distinct Mitochondrial Metabolic Function among the Model Systems. Previous studies have reported that mitochondrial respiratory function is heavily connected to many pathological processes, including heart failure, ischemic injury, and aging.[2,17,60] In the current study, variations in mitochondrial respiratory capacity among the examined mitochondria were observed in ETC complex activity and oxygen consumption. Mitochondria in different species/tissues dramatically differ in their ability to consume oxygen and make ATP. The higher C−I, C−V, and oxygen consumption activity seen in drosophila and mouse heart tissue, respectively, indicates that these model systems have a high NADH delivery and ATP generation rate. Consistent with our functional data, we found that C−I subunits in mouse heart are significantly more abundant compared with mouse liver and human heart. However, C−V showed no significant differences in protein abundance, signifying the existence of potential regulatory mechanisms such as post-translational modifications and complex assembly, other than protein expression level. C−I activity and respiratory rates of liver mitochondria are not particularly reflected in the overall complex subunit abundance but instead correlate with those of the mitochondrial-encoded subunits (Figure 4d). Similarly, lower C−V activity in human heart mitochondria is consistent with the lower abundance of mitochondrial-encoded C−V proteins. These results suggest that complex assembly may be significantly restricted by the abundance of mitochondrial-encoded proteins. Furthermore, our data emphasize that mitochondria in different species/tissues are specialized for diverse metabolic duties. The

metabolism functional group not only contains the most proteins but also possesses the most nonconserved and conserved proteins.

Evolved Mitochondrial Phosphorylation Events among the Model Systems. Phosphorylation signaling regulated by kinases and phosphatases plays a critical role in regulating biological processes in all living organisms. However, identifying the entire phosphoproteome is a daunting task. Due to its unique evolutionary origin and enriched functionality, mitochondrial phosphoproteome studies have begun to draw increasing attention.[43,61−64] Gnad et al.[63] compared the phosphoproteomes of different organisms and found that serine/threonine phosphorylation in prokaryotes has occurred relatively recently in evolution. Another study carried out by Beltrao and colleagues[65] showed that kinase−substrate interactions change more slowly than transcription factor−promoter interactions and that protein kinases are an important source of phenotypic diversity. Accordingly, we observed that the distribution of kinase/phosphatase in drosophila is scarce in terms of number and abundance of proteins compared with other model systems. These findings are consistent with the notion that phosphorylation rapidly expanded in higher metazoan lineages as a general mechanism for increased cellular signaling and complexity.[63]

Differential Mitochondrial Calcium Regulation among the Model Systems. Functional assays on calcium-induced swelling show that liver mitochondria are the most susceptible to calcium damage. This agrees with previous data[66] showing that rat liver mitochondria have larger uptake of calcium than heart mitochondria and is probably a reflection of the heart being an excitable organ under constant calcium flux. At face value, one might reasonably posit that liver mitochondria, being in a nonexcitable tissue, would contain fewer calcium binding proteins. On the contrary, there was no significant difference in the total expression of calcium-binding proteins between liver mitochondria and other mitochondria. Although we cannot differentiate the effect of differing affinities of calcium influx, efflux, and buffering proteins across organisms, this nevertheless indicates that protein calcium regulation mechanisms besides protein expression levels should be taken into account. An attempt to correlate individual protein abundance with functional differences proved more promising, as we observed that liver has a relatively high abundance of calcium uniporters (MCUs) but almost no mitochondrial sodium/calcium exchanger (NCX), which taken together would suggest increased calcium influx and decreased efflux. A recently published study suggests that the activity and abundance of the mitochondrial calcium uniporter varies greatly between tissues of different species; mouse heart and drosophila flight muscle showed low mitochondrial calcium uniporter activity in comparison with that of mouse liver, kidney, and brown fat.[67] This result is consistent with the higher susceptibility of liver mitochondria to calcium overload compared with mitochondria from mouse heart, human heart, and drosophila. In our opinion, these examples demonstrate the limitations of reducing proteomics data to simplistic functional categories and the values of functional assays in augmenting proteomics data.

Broadening the Mitochondrial Interactome

There is a need to bridge the translational divide by determining the protein−protein interactions within the interactomes of nonhuman organisms as well as highlighting similar structures in the human interactome. While animal models and computational insights remain indispensable, the success of translational discoveries is fostered by our understanding of protein connectivity in human cellular networks.

Each of the model systems characterized in our investigation demonstrated a distinct protein−protein interaction pattern; ostensibly these molecular interactions may be limited by the present knowledge of the scientific community as well as the IntAct database. A more accurate and comprehensive data set collecting multiple model systems has yet to be available due to investigator-specific foci of research, targeting a specific organ, tissue, disease, or pathway. An integrated framework addressing protein interactions from different organs, tissues, diseases, and pathways may elucidate mechanistic insights that play a fundamental role in targeting disease origins in humans, as many diseases affect protein partnerships in multiple organ systems. Proteins whose interactions have not been extensively studied in humans such as α-synuclein may act as future areas of research in translational medicine.

Although it was evident that a distinguished pattern arose in each model system, one major mouse hub emerged among the C−I protein−protein interactions. Although not a Complex protein, α-synuclein was found to be central for C−I mitochondrial proteins in mouse; this differed greatly in the human C−I interactome, as it was not seen to interact with human C−I proteins. As a protein heavily involved in signaling, α-synuclein has been studied extensively in humans and is a key protein associated with Parkinson's and other neurodegenerative diseases.[68] The interaction of α-synuclein with multiple C−I proteins in the mouse may implicate its important regulatory role in energy metabolism and therefore be relevant to human molecular pathways.

In addition, examination of C−I + redox and C−V + redox protein networks revealed little interaction between C−I and redox proteins as well as C−V and redox proteins, with the exception of ATP5B in C−V. This evolutionarily conserved C−V protein serves as a major hub in human, mouse, and drosophila. However, in the mouse interactome, ATP5B interacts with several peroxiredoxin (redox) proteins. PRDX1 and ATP5B have emerged as key proteins in this C−V + redox protein interaction network. As seen in previous studies, the centrality of both proteins predisposes them to be highly associated with the onset of disease. The intermingled network of connections between C−I and redox proteins in the mouse interactome serves as a proponent for the necessity of analyzing human protein−protein interactions that have yet to be investigated. Investigation of proteins highly involved in C−I, C−V, and redox in nonhuman organisms could facilitate the identification of new target proteins for translational medicine and scientific research.

Mitochondrial-Targeted Protein Localization

Mitochondrial targeting sequences facilitate the translocation of mitochondrial proteins to their designated location. In this study, we identified mitochondrial proteins with an N-terminal MTS, specifically focusing on the core conserved proteins. Our results suggest that many mitochondrial proteins without an MTS are utilizing alternative ways of translocating into the mitochondria, although a sophisticated method of predicting proteins possessing internal mitochondrial targeting sequences has yet to be developed. We postulate that these proteins lacking an MTS may have been imported through various mechanisms or attracted by biochemical signals (i.e., cardiolipin, $\Delta\Psi$, motifs, positively charged amino acids

residues, etc.). These results indicate that some mitochondrial proteins may either share multiple cellular localizations or only transiently reside in the mitochondria. Identification of currently unknown sequence patterns may aid in the clarification of this issue and provide clinical relevance to the field of medicine.[69]

Involvement of Mitochondrial Proteins in Diseases

As the center of metabolism and energy production, mitochondrial protein dysfunction, caused by either genetic or environmental alterations, has been shown to be directly associated with diseases, specifically cardiomyopathies, neurodegenerative disorders, and diabetes.[11,60,70,71] Through literature curation, we found that the 419 conserved mitochondrial core proteins are heavily involved in disease phenotypes (~54%). In particular, ~82% of conserved OXPHOS proteins are related to the development of disease. These data highlight the evolutionary prominence of these proteins.

The involvement of mitochondrial proteins in cardiovascular diseases, including ischemic injury, heart failure, and congenital heart disease, has also been analyzed. Corroborating prior studies, the dysfunction of a significant portion of core mitochondrial proteins (>17%) and conserved OXPHOS proteins (>27%), compared with shared and nonconserved proteins among the model systems, plays a role in cardiac diseases. In addition, OXPHOS proteins implicated in these pathologies have high abundance values and can be considered a requirement for normal physiological OXPHOS function. A mutation of one gene-encoded OXPHOS protein might show multiple clinical symptoms, whereas the mutation of various OXPHOS proteome genes may cause the same disease; our data mark the OXPHOS system as an injury-prone subproteome.

In summary, we conducted a comprehensive analysis to integrate information from biochemical, proteomic, and genomic data sets to characterize mitochondrial biology from a multifaceted perspective. Among the published reports describing the mitochondrial proteome, our current analysis uniquely and significantly expands the mitochondrial proteome pools, highlighting a core mitochondrial proteome from four model systems. These analyses simultaneously portray the inter- and intraspecies heterogeneity of mitochondria from both expressional and functional perspectives. Our study of the proteome−function correlation confirms previous observations of mitochondrial biology and contributes new evidence of the expediency of diagnosing mitochondrial disease through proteomic parameters. This investigation bridges the knowledge gap between molecular compositions and their accompanying functions, which ultimately aids in the translation of mitochondrial proteomics data to a contextualized understanding of complex mitochondrial biology as well as allows for the acquisition of a prospective source for not only the diagnosis of mitochondrial pathologies but also the procurement of mitochondrial therapeutic targets.

■ ASSOCIATED CONTENT

Supporting Information

Materials, isolation, and purification of functionally viable mitochondria from mouse heart, mouse liver, human heart, and drosophila; assessment of mitochondrial function; proteomic profiling of mitochondria from mouse heart, mouse liver, human heart, and drosophila; mitochondrial proteome and properties; approach to assess protein abundance; schematic diagram of experimental workflow; functionally-enabled recovery of the individuals; summary of mass spectrometry experiments; biochemical features of mitochondrial proteins; proteins identified from mitochondria across organs and organisms; and mitochondrial proteome annotation and inter/intra-genomic comparison across organs and organisms. Additional supporting raw data can be found at http://149.142.212.48/ (user name: pinglab; password: proteomics). This material is available free of charge via the Internet at http://pubs.acs.org.

■ AUTHOR INFORMATION

Corresponding Author

*Tel: 310-267-5624. Fax: 310-267-5623. E-mail: pping@mednet.ucla.edu.

Author Contributions

⊥C.L., A.J.L., C.M.B., and J.Z. contributed equally to this study.

Notes

The authors declare no competing financial interest.

■ ACKNOWLEDGMENTS

We thank the members of our laboratory for their helpful discussions. We are supported by the NHLBI Proteomics Center Award (HHSN268201000035C) to Dr. Peipei Ping; NIH Award HL-63901 to Dr. Peipei Ping; and AHA predoctoral fellowship 12PRE11610024 to Edward Lau.

■ REFERENCES

(1) Johnson, D. T.; Harris, R. A.; Blair, P. V.; Balaban, R. S. Functional consequences of mitochondrial proteome heterogeneity. *Am. J. Physiol.: Cell Physiol.* **2007**, *292*, C698−707.

(2) Balaban, R. S. Regulation of oxidative phosphorylation in the mammalian cell. *Am. J. Physiol.* **1990**, 377−389.

(3) Shao, D.; Oka, S.; Brady, C. D.; Haendeler, J.; Eaton, P.; Sadoshima, J. Redox modification of cell signaling in the cardiovascular system. *J. Mol. Cell. Cardiol.* **2012**, *52*, 550−558.

(4) Zhang, J.; Lin, A.; Powers, J.; Lam, M. P.; Lotz, C.; Liem, D.; Lau, E.; Wang, D.; Deng, N.; Korge, P.; Zong, N. C.; Cai, H.; Weiss, J.; Ping, P. Perspectives on: Sgp symposium on mitochondrial physiology and medicine: Mitochondrial proteome design: From molecular identity to pathophysiological regulation. *J. Gen. Physiol.* **2012**, *139*, 395−406.

(5) Gucek, M.; Murphy, E. What can we learn about cardioprotection from the cardiac mitochondrial proteome? *Cardiovasc. Res.* **2010**, *88*, 211−218.

(6) Balaban, R. S. The mitochondrial proteome: A dynamic functional program in tissues and disease states. *Environ. Mol. Mutagen.* **2010**, *51*, 352−359.

(7) Hollander, J. M.; Baseler, W. A.; Dabkowski, E. R. Proteomic remodeling of mitochondria in heart failure. *Congestive Heart Failure* **2011**, *17*, 262−268.

(8) Karamanlidis, G.; Bautista-Hernandez, V.; Fynn-Thompson, F.; Del Nido, P.; Tian, R. Impaired mitochondrial biogenesis precedes heart failure in right ventricular hypertrophy in congenital heart disease. *Circ.: Heart Failure* **2011**, *4*, 707−713.

(9) Neubauer, S. The failing heart−an engine out of fuel. *N. Engl. J. Med.* **2007**, *356*, 1140−1151.

(10) Rosca, M.; Popescu, B. A.; Beladan, C. C.; Calin, A.; Muraru, D.; Popa, E. C.; Lancellotti, P.; Enache, R.; Coman, I. M.; Jurcut, R.; Ghionea, M.; Ginghina, C. Left atrial dysfunction as a correlate of heart failure symptoms in hypertrophic cardiomyopathy. *J. Am. Soc. Echocardiography* **2010**, *23*, 1090−1098.

(11) Wallace, D. C. Mitochondrial DNA mutations in disease and aging. *Environ. Mol. Mutagen.* **2010**, 440−450.

(12) Yoshioka, J.; Chutkow, W. A.; Lee, S.; Kim, J. B.; Yan, J.; Tian, R.; Lindsey, M. L.; Feener, E. P.; Seidman, C. E.; Seidman, J. G.; Lee, R. T. Deletion of thioredoxin-interacting protein in mice impairs mitochondrial function but protects the myocardium from ischemia-reperfusion injury. *J. Clin. Invest.* **2012**, *122*, 267−279.
(13) Rodriguez, K. A.; Wywial, E.; Perez, V. I.; Lambert, A. J.; Edrey, Y. H.; Lewis, K. N.; Grimes, K.; Lindsey, M. L.; Brand, M. D.; Buffenstein, R. Walking the oxidative stress tightrope: A perspective from the naked mole-rat, the longest-living rodent. *Curr. Pharm. Des.* **2011**, *17*, 2290−2307.
(14) Ago, T.; Liu, T.; Zhai, P.; Chen, W.; Li, H.; Molkentin, J. D.; Vatner, S. F.; Sadoshima, J. A redox-dependent pathway for regulating class ii hdacs and cardiac hypertrophy. *Cell* **2008**, *133*, 978−993.
(15) Chen, E. I.; Hewel, J.; Krueger, J. S.; Tiraby, C.; Weber, M. R.; Kralli, A.; Becker, K.; Yates, J. R., 3rd; Felding-Habermann, B. Adaptation of energy metabolism in breast cancer brain metastases. *Cancer Res.* **2007**, *67*, 1472−1486.
(16) Calvo, S. E.; Mootha, V. K. The mitochondrial proteome and human disease. *Annu. Rev. Genomics Hum. Genet.* **2010**, *11*, 25−44.
(17) Rosca, M. G.; Hoppel, C. L. Mitochondria in heart failure. *Cardiovasc. Res.* **2010**, *88*, 40−50.
(18) Lindsey, M. L.; Goshorn, D. K.; Comte-Walters, S.; Hendrick, J. W.; Hapke, E.; Zile, M. R.; Schey, K. A multidimensional proteomic approach to identify hypertrophy-associated proteins. *Proteomics* **2006**, *6*, 2225−2235.
(19) Wu, F.; Zhang, J.; Beard, D. A. Experimentally observed phenomena on cardiac energetics in heart failure emerge from simulations of cardiac metabolism. *Proc. Natl. Acad. Sci. U. S. A.* **2009**, *106*, 7143−7148.
(20) Zhang, J.; Merkle, H.; Hendrich, K.; Garwood, M.; From, A. H.; Ugurbil, K.; Bache, R. J. Bioenergetic abnormalities associated with severe left ventricular hypertrophy. *J. Clin. Invest.* **1993**, *92*, 993−1003.
(21) Pflieger, D.; Le Caer, J. P.; Lemaire, C.; Bernard, B. A.; Dujardin, G.; Rossier, J. Systematic identification of mitochondrial proteins by lc-ms/ms. *Anal. Chem.* **2002**, *74*, 2400−2406.
(22) Sickmann, A.; Reinders, J.; Wagner, Y.; Joppich, C.; Zahedi, R.; Meyer, H. E.; Schonfisch, B.; Perschil, I.; Chacinska, A.; Guiard, B.; Rehling, P.; Pfanner, N.; Meisinger, C. The proteome of saccharomyces cerevisiae mitochondria. *Proc. Natl. Acad. Sci. U. S. A.* **2003**, *100*, 13207−13212.
(23) Kislinger, T.; Cox, B.; Kannan, A.; Chung, C.; Hu, P.; Ignatchenko, A.; Scott, M. S.; Gramolini, A. O.; Morris, Q.; Hallett, M. T.; Rossant, J.; Hughes, T. R.; Frey, B.; Emili, A. Global survey of organ and organelle protein expression in mouse: Combined proteomic and transcriptomic profiling. *Cell* **2006**, *125*, 173−186.
(24) Mootha, V. K.; Bunkenborg, J.; Olsen, J. V.; Hjerrild, M.; Wisniewski, J. R.; Stahl, E.; Bolouri, M. S.; Ray, H. N.; Sihag, S.; Kamal, M.; Patterson, N.; Lander, E. S.; Mann, M. Integrated analysis of protein composition, tissue diversity, and gene regulation in mouse mitochondria. *Cell* **2003**, *115*, 629−640.
(25) Pagliarini, D. J.; Calvo, S. E.; Chang, B.; Sheth, S. A.; Vafai, S. B.; Ong, S. E.; Walford, G. A.; Sugiana, C.; Boneh, A.; Chen, W. K.; Hill, D. E.; Vidal, M.; Evans, J. G.; Thorburn, D. R.; Carr, S. A.; Mootha, V. K. A mitochondrial protein compendium elucidates complex i disease biology. *Cell* **2008**, *134*, 112−123.
(26) Zhang, J.; Li, X.; Mueller, M.; Wang, Y.; Zong, C.; Deng, N.; Vondriska, T. M.; Liem, D. A.; Yang, J. I.; Korge, P.; Honda, H.; Weiss, J. N.; Apweiler, R.; Ping, P. Systematic characterization of the murine mitochondrial proteome using functionally validated cardiac mitochondria. *Proteomics* **2008**, *8*, 1564−1575.
(27) Gaucher, S. P.; Taylor, S. W.; Fahy, E.; Zhang, B.; Warnock, D. E.; Ghosh, S. S.; Gibson, B. W. Expanded coverage of the human heart mitochondrial proteome using multidimensional liquid chromatography coupled with tandem mass spectrometry. *J. Proteome Res.* **2004**, *3*, 495−505.
(28) Taylor, S. W.; Fahy, E.; Zhang, B.; Glenn, G. M.; Warnock, D. E.; Wiley, S.; Murphy, A. N.; Gaucher, S. P.; Capaldi, R. A.; Gibson, B. W.; Ghosh, S. S. Characterization of the human heart mitochondrial proteome. *Nat. Biotechnol.* **2003**, *21*, 281−286.
(29) Reifschneider, N. H.; Goto, S.; Nakamoto, H.; Takahashi, R.; Sugawa, M.; Dencher, N. A.; Krause, F. Defining the mitochondrial proteomes from five rat organs in a physiologically significant context using 2d blue-native/sds-page. *J. Proteome Res.* **2006**, *5*, 1117−1132.
(30) Forner, F.; Foster, L. J.; Campanaro, S.; Valle, G.; Mann, M. Quantitative proteomic comparison of rat mitochondria from muscle, heart, and liver. *Mol. Cell. Proteomics* **2006**, *5*, 608−619.
(31) Phillips, D.; Covian, R.; Aponte, A. M.; Glancy, B.; Taylor, J. F.; Chess, D.; Balaban, R. S. Regulation of oxidative phosphorylation complex activity: Effects of tissue-specific metabolic stress within an allometric series and acute changes in workload. *Am. J. Physiol.: Regul., Integr. Comp. Physiol.* **2012**, *302*, R1034−1048.
(32) White M. Y., Brown D. A., Sheng S., Cole R. N., O'Rourke B., Van Eyk J. E. Parallel proteomics to improve coverage and confidence in the partially annotated oryctolagus cuniculus mitochondrial proteome. *Mol. Cell. Proteomics* **2011**;*10*:M110 004291
(33) Alonso, J.; Rodriguez, J. M.; Baena-Lopez, L. A.; Santaren, J. F. Characterization of the drosophila melanogaster mitochondrial proteome. *J. Proteome Res.* **2005**, *4*, 1636−1645.
(34) Brunner, E.; Ahrens, C. H.; Mohanty, S.; Baetschmann, H.; Loevenich, S.; Potthast, F.; Deutsch, E. W.; Panse, C.; de Lichtenberg, U.; Rinner, O.; Lee, H.; Pedrioli, P. G.; Malmstrom, J.; Koehler, K.; Schrimpf, S.; Krijgsveld, J.; Kregenow, F.; Heck, A. J.; Hafen, E.; Schlapbach, R.; Aebersold, R. A high-quality catalog of the drosophila melanogaster proteome. *Nat. Biotechnol.* **2007**, *25*, 576−583.
(35) Liu, H.; Sadygov, R. G.; Yates, J. R., 3rd. A model for random sampling and estimation of relative protein abundance in shotgun proteomics. *Anal. Chem.* **2004**, *76*, 4193−4201.
(36) Paoletti, A. C.; Parmely, T. J.; Tomomori-Sato, C.; Sato, S.; Zhu, D.; Conaway, R. C.; Conaway, J. W.; Florens, L.; Washburn, M. P. Quantitative proteomic analysis of distinct mammalian mediator complexes using normalized spectral abundance factors. *Proc. Natl. Acad. Sci. U. S. A.* **2006**, *103*, 18928−18933.
(37) Mosley, A. L.; Florens, L.; Wen, Z.; Washburn, M. P. A label free quantitative proteomic analysis of the saccharomyces cerevisiae nucleus. *J. Proteomics* **2009**, *72*, 110−120.
(38) Bier, E.; Bodmer, R. Drosophila, an emerging model for cardiac disease. *Gene* **2004**, *342*, 1−11.
(39) Taghli-Lamallem, O.; Akasaka, T.; Hogg, G.; Nudel, U.; Yaffe, D.; Chamberlain, J. S.; Ocorr, K.; Bodmer, R. Dystrophin deficiency in drosophila reduces lifespan and causes a dilated cardiomyopathy phenotype. *Aging Cell* **2008**, *7*, 237−249.
(40) Mukhida, K.; Kobayashi, N. R.; Mendez, I. A novel role for parkin in trauma-induced central nervous system secondary injury. *Med. Hypotheses.* **2005**, *64*, 1120−1123.
(41) Zhang, J.; Liem, D. A.; Mueller, M.; Wang, Y.; Zong, C.; Deng, N.; Vondriska, T. M.; Korge, P.; Drews, O.; Maclellan, W. R.; Honda, H.; Weiss, J. N.; Apweiler, R.; Ping, P. Altered proteome biology of cardiac mitochondria under stress conditions. *J. Proteome Res.* **2008**, *7*, 2204−2214.
(42) Lau, E.; Wang, D.; Zhang, J.; Yu, H.; Lam, M. P.; Liang, X.; Zong, N.; Kim, T. Y.; Ping, P. Substrate- and isoform-specific proteome stability in normal and stressed cardiac mitochondria. *Circ. Res.* **2012**, *110*, 1174−1178.
(43) Deng, N.; Zhang, J.; Zong, C.; Wang, Y.; Lu, H.; Yang, P.; Wang, W.; Young, G. W.; Wang, Y.; Korge, P.; Lotz, C.; Doran, P.; Liem, D. A.; Apweiler, R.; Weiss, J. N.; Duan, H.; Ping, P. Phosphoproteome analysis reveals regulatory sites in major pathways of cardiac mitochondria. *Mol. Cell. Proteomics* **2011**, *10*, M110.000117.
(44) Kirby, D. M.; Thorburn, D. R.; Turnbull, D. M.; Taylor, R. W. Biochemical assays of respiratory chain complex activity. *Methods Cell Biol.* **2007**, *80*, 93−119.
(45) Kramarova, T. V.; Shabalina, I. G.; Andersson, U.; Westerberg, R.; Carlberg, I.; Houstek, J.; Nedergaard, J.; Cannon, B. Mitochondrial atp synthase levels in brown adipose tissue are governed by the c-fo subunit p1 isoform. *FASEB J.* **2008**, *22*, 55−63.
(46) Wittig, I.; Braun, H. P.; Schagger, H. Blue native page. *Nat Protoc.* **2006**, *1*, 418−428.

(47) Magrane, M.; Consortium, U. Uniprot knowledgebase: A hub of integrated protein data. *Database* **2011**, *2011*, bar009.
(48) Emanuelsson, O.; Nielsen, H.; Brunak, S.; von Heijne, G. Predicting subcellular localization of proteins based on their n-terminal amino acid sequence. *J. Mol. Biol.* **2000**, *300*, 1005−1016.
(49) Kasprzyk, A. Biomart: Driving a paradigm change in biological data management. *Database* **2011**, *2011*, bar049.
(50) Auston, I.; Cahn, M. A.; Selden, C. R. *Literature Search Methods for the Development of Clinical Practice Guidelines*; Report No. PB92-221175; National Library of Medicine: Bethesda, MD, 1992.
(51) Kerrien, S.; Aranda, B.; Breuza, L.; Bridge, A.; Broackes-Carter, F.; Chen, C.; Duesbury, M.; Dumousseau, M.; Feuermann, M.; Hinz, U.; Jandrasits, C.; Jimenez, R. C.; Khadake, J.; Mahadevan, U.; Masson, P.; Pedruzzi, I.; Pfeiffenberger, E.; Porras, P.; Raghunath, A.; Roechert, B.; Orchard, S.; Hermjakob, H. The intact molecular interaction database in 2012. *Nucleic Acids Res.* **2012**, *40*, D841−846.
(52) Saito, R.; Smoot, M. E.; Ono, K.; Ruscheinski, J.; Wang, P. L.; Lotia, S.; Pico, A. R.; Bader, G. D.; Ideker, T. A travel guide to cytoscape plugins. *Nat. Methods* **2012**, *9*, 1069−1076.
(53) Wallenstein, S.; Zucker, C. L.; Fleiss, J. L. Some statistical methods useful in circulation research. *Circ. Res.* **1980**, *47*, 1−9.
(54) Zong, N. C.; Li, H.; Li, H.; Lam, M. P.; Jimenez, R. C.; Kim, C. S.; Deng, N.; Kim, A. K.; Choi, J. H.; Zelaya, I.; Liem, D.; Meyer, D.; Odeberg, J.; Fang, C.; Lu, H. J.; Xu, T.; Weiss, J.; Duan, H.; Uhlen, M.; Yates, J. R., III; Apweiler, R.; Ge, J.; Hermjakob, H.; Ping, P. Integration of cardiac proteome biology and medicine by a specialized knowledgebase. *Circ. Res.* **2013**, *113* (9), 1043−1053.
(55) Wilm, M. Quantitative proteomics in biological research. *Proteomics* **2009**, *9*, 4590−4605.
(56) Neilson, K. A.; Ali, N. A.; Muralidharan, S.; Mirzaei, M.; Mariani, M.; Assadourian, G.; Lee, A.; van Sluyter, S. C.; Haynes, P. A. Less label, more free: Approaches in label-free quantitative mass spectrometry. *Proteomics* **2011**, *11*, 535−553.
(57) Richly, E.; Chinnery, P. F.; Leister, D. Evolutionary diversification of mitochondrial proteomes: Implications for human disease. *Trends Genet.* **2003**, *19*, 356−362.
(58) Agnetti, G.; Husberg, C.; Van Eyk, J. E. Divide and conquer: The application of organelle proteomics to heart failure. *Circ. Res.* **2011**, *108*, 512−526.
(59) Brawand, D.; Soumillon, M.; Necsulea, A.; Julien, P.; Csardi, G.; Harrigan, P.; Weier, M.; Liechti, A.; Aximu-Petri, A.; Kircher, M.; Albert, F. W.; Zeller, U.; Khaitovich, P.; Grutzner, F.; Bergmann, S.; Nielsen, R.; Paabo, S.; Kaessmann, H. The evolution of gene expression levels in mammalian organs. *Nature* **2011**, *478*, 343−348.
(60) Fosslien, E. Mitochondrial medicine - cardiomyopathy caused by defective oxidative phosphorylation. *Ann. Clin. Lab. Sci.* **2003**, *33*, 371−395.
(61) Lee, J.; Xu, Y.; Chen, Y.; Sprung, R.; Kim, S. C.; Xie, S.; Zhao, Y. Mitochondrial phosphoproteome revealed by an improved imac method and ms/ms/ms. *Mol. Cell. Proteomics* **2007**, *6*, 669−676.
(62) Reinders, J.; Wagner, K.; Zahedi, R. P.; Stojanovski, D.; Eyrich, B.; van der Laan, M.; Rehling, P.; Sickmann, A.; Pfanner, N.; Meisinger, C. Profiling phosphoproteins of yeast mitochondria reveals a role of phosphorylation in assembly of the atp synthase. *Mol. Cell. Proteomics* **2007**, *6*, 1896−1906.
(63) Gnad, F.; Forner, F.; Zielinska, D. F.; Birney, E.; Gunawardena, J.; Mann, M. Evolutionary constraints of phosphorylation in eukaryotes, prokaryotes, and mitochondria. *Mol. Cell. Proteomics* **2010**, *9*, 2642−2653.
(64) Lam, M. P.; Lau, E.; Scruggs, S. B.; Wang, D.; Kim, T. Y.; Liem, D. A.; Zhang, J.; Ryan, C. M.; Faull, K. F.; Ping, P. Site-specific quantitative analysis of cardiac mitochondrial protein phosphorylation. *J. Proteomics* **2013**, *81*, 15−23.
(65) Beltrao, P.; Trinidad, J. C.; Fiedler, D.; Roguev, A.; Lim, W. A.; Shokat, K. M.; Burlingame, A. L.; Krogan, N. J. Evolution of phosphoregulation: Comparison of phosphorylation patterns across yeast species. *PLoS Biol.* **2009**, *7*, e1000134.
(66) Favaron, M.; Bernardi, P. Tissue-specific modulation of the mitochondrial calcium uniporter by magnesium ions. *FEBS Lett.* **1985**, *183*, 260−264.
(67) Fieni, F.; Lee, S. B.; Jan, Y. N.; Kirichok, Y. Activity of the mitochondrial calcium uniporter varies greatly between tissues. *Nat. Commun.* **2012**, *3*, 1317.
(68) O'Connor, K.; Magne, J.; Rosca, M.; Pierard, L. A.; Lancellotti, P. Impact of aortic valve stenosis on left atrial phasic function. *Am. J. Cardiol.* **2010**, *106*, 1157−1162.
(69) Yamada, Y.; Harashima, H. Mitochondrial drug delivery systems for macromolecule and their therapeutic application to mitochondrial diseases. *Adv. Drug Delivery Rev.* **2008**, *60*, 1439−1462.
(70) Cwerman-Thibault, H.; Sahel, J. A.; Corral-Debrinski, M. Mitochondrial medicine: To a new era of gene therapy for mitochondrial DNA mutations. *J. Inherited Metab. Dis.* **2011**, *34*, 327−344.
(71) Lesnefsky, E. J.; Hoppel, C. L. Ischemia-reperfusion injury in the aged heart: Role of mitochondria. *Arch. Biochem. Biophys.* **2003**, *420*, 287−297.

Supporting Information

S1. Materials.

Hepes, percoll, β-nicotinamide adenine dinucleotide, reduced dipotassium salt (NADH), nicotinamide adenine dinucleotide phosphate sodium salt (NADP), nitro blue tetrazolium (NTB), antimycin A, diphenyleneiodonium, sodium succinate, iodoacetamide, phenazine methasulfate, 3,3'-diaminobenzidine (DAB), cytochrome c, phosphoenolpyruvate, n-dodecyl-β-D-maltopyranoside (DDM), rotenone, pyruvate kinase, lactate dehydrogenase, 3-nitropropionic acid, potassium cyanide (KCN), oligomycin, protease fluorescent detection kit, and all other chemicals were purchased from Sigma-Aldrich (St Louis, MO).

S2. Isolation and Purification of Functionally Viable Mitochondria from Mouse Heart, Mouse Liver, Human Heart, and Drosophila.

Mitochondria were isolated from freshly collected mouse hearts (8-10 week old, ICR strain), mouse livers (8-10 week old, ICR strain), or human hearts as described[1, 2]. Briefly, the samples were homogenized in isolation buffer (250mM sucrose, 1mM EGTA, 20mM Hepes, pH 7.5) and crude mitochondria were obtained by differential centrifugation, which were further purified by resuspension in 19% percoll isolation solution, followed by its addition onto two layers of 30% and 60% percoll (v/v). After centrifugation at 10,000g for 15 minutes, purified mitochondria were collected and washed (3x) with isolation buffer without EGTA. Drosophila mitochondria were also isolated by differential centrifugation[3]. Approximately 1,000 adult wild-type Drosophila Melanogaster were immobilized by chilling, then pressed 5-6 times with a pre-chilled pestle in a mortar containing isolation buffer. The homogenate was then centrifuged at 500g for 5 minutes followed by filtering through a layer of surgical gauze and further centrifugation at 500g for 5 minutes. The resulting supernatant was subjected to another centrifugation at 9,000g for 30 minutes. The mitochondrial-enriched fraction acquired from the pellet was then subjected to the percoll purification step as described above. All procedures were

performed at 4°C. Freshly isolated mitochondria from human hearts, mouse hearts, mouse livers and drosophila were validated via functional and structural analyses[1].

S3. Assessment of Mitochondrial Function.

Mitochondrial electron transport chain (ETC) complex activity assay.

The activities of ETC CI and CV were assessed as previously described[4-7]. Briefly, for the CI activity assay, 15µg mitochondrial lysate was mixed with 100µl of CI reaction buffer (10mM Tris-HCl, pH 7.4, 0.2mg/ml NADH, 2mg/ml NBT, 2µM antimycin A and 2mM KCN) at room temperature. The absorbance at 550nm was measured at multiple time points to yield a time lapse curve. The ETC CV activity (F1-F0 ATPase) was measured by mixing mitochondrial lysate with reaction buffer (50mM Hepes/KOH, pH 8.0, 5mM $MgCl_2$, 350µM NADH, 5mM phosphoenolpyruvate, 4µM rotenone, 4mM KCN, 7units/ml pyruvate kinase, 15units/ml lactate dehydrogenase, and 5mM ATP) and monitoring the decrease of NADH absorbance (340nm). Background activities were assayed with the specific inhibitors diphenyleneiodonium (10µM) for CI and oligomycin (5µM) for CV. The enzymatic activities were normalized to that of the mouse heart.

Mitochondrial O_2 consumption measurement.

Mitochondrial O_2 consumption was measured continuously by recording the pO_2 in the buffer using a fiber optic oxygen sensor inserted through a hole in the cuvette cover during the addition of ADP[1].

Mitochondrial pyruvate dehydrogenase (PDH) activity assay.

ELISA-based PDH activity was assayed with a kit (Abcam, Cambridge, MA) according to the manufacturer's instructions. Briefly, the PDH enzyme was immunocaptured within the wells of the microplate which contained 100µg of mitochondrial proteins. PDH activity was determined by monitoring the reduction of NAD^+ to NADH, coupled with the conversion of a reporter dye to a colored reaction product (absorbance at 450nm). Mouse heart activity served as the standard for the other model systems.

Mitochondrial proteolytic activity assay.

The proteolytic activity of mitochondria was estimated using the Protease Fluorescent Detection Kit from Sigma-Aldrich[8]. Briefly, 100μg of isolated mitochondrial lysate were incubated with 100mM ATP and 10μl of FITC-labeled casein substrates for 2 hours at 37°C in the dark. Undigested proteins were precipitated by incubation with 150μl 0.6N trifluroacetic acid at 37°C for 30min, followed by centrifugation at 10,000g for 10min. To detect the digested peptides, 10μl of the supernatant was diluted with 200μl 500mM Tris, pH 8.5, and fluorescence was read at 485/527nm. We used the enzymatic activities of the mouse heart to normalize the activity of the mouse liver, human heart, and drosophila.

Mitochondrial glutathione reductase activity assay.

Using a kit from Bioversion (Milpitas, California), glutathione reductase (GR) activities were assessed *in vitro*. Briefly, using oxidized glutathione (GSSG) as a substrate, GR activity was determined spectrophotometrically by measuring the conversion of GSSG to glutathione (GSH), which was monitored by the absorbance at 450nm. The enzymatic activities of the model systems were standardized to the activity of the mouse heart.

Mitochondrial calcium-induced swelling assay.

The susceptibility of mitochondria to calcium-induced injury was measured spectrophotometrically as a reduction in absorbance at 520nm attributed to the swelling of the isolated mitochondria[1, 2].

S4. Proteomic Profiling of Mitochondria from Mouse Heart, Mouse Liver, Human Heart, and Drosophila.

SDS-PAGE, LC-MS/MS and spectral analyses were performed as previously described[1, 2]. Purified mitochondria (200μg) were lysed in isolation buffer supplemented with 0.5% DDM and proteins were displayed via standard SDS-PAGE. After Commassie G-250 staining, SDS-PAGE gels were sliced into strips which were subjected to reduction with DTT, alkylation with iodoacetamide and in-gel trypsin digestion. Resulting peptides were analyzed with MS/MS instruments (LTQ and LTQ-Orbitrap,

ThermoFisher, Waltham, MA) integrated with capillary reverse-phase chromatography (75µm id x 10cm, BioBasic C18 5µm particle size, New Objectives, Woburn, MA). Mass spectra were collected in data dependent mode with 5 MS/MS scans following 1 survey MS scan.

Raw spectral data were converted to ms2 format with RawXtract (V1.9.9.2) under default settings, which then analyzed with the ProLuCID algorithm (V1.3.3)[9] using the UniProt Databases[10] as references. The search parameters for LTQ datasets were set as follows: partial tryptic digestion allowing two missed cleavages, fixed modification on cysteine with carbamidomethylation (+57.02146 Da) and differential modification on methionine with oxidation (+15.9949 Da), with tolerances for mass measurement deviations at 1.5 AMU (peptide) and 1.0 AMU (fragment). The tolerance for peptide precursor measured by the LTQ-Orbitrap was set at 50 ppm. Missed cleavages were unlimited and protein cleavage chemistry utilized trypsin (KR). Mass spectra derived from the human heart were analyzed with UniProt human database (06-15-2012 download – 262,274 proteins), drosophila datasets were analyzed with UniProt drosophila database (07-16-2011 download – 37,596 proteins) and murine dataset were analyzed with UniProt mouse database (01-19-2012 download – 93,312 proteins) as references, respectively. Protein analysis proceeded with 2 steps. First, DTASelect (V2.0)[11] was used reverse sequence database to implement a negative control. Secondly, these preliminary results used ProteinInferencer, which was applied to the output to calculate protein and peptide confidence based the peptide confidence from all the experiments, ensuring a Global False Positive Rate of <1% in the final protein list (Xu et al. manuscript in preparation). Proteins with at least two peptide identifications were retained.

Mitochondrial protein abundances were assessed by normalized spectral abundance factors (NSAF)[2, 12-14]. For each identified protein, the total peptide spectral count was divided by its length in order to generate the spectral abundance factor (SAF). The NSAF of each protein was calculated by dividing its SAF value by the total SAF of all proteins within a proteome; this was then compared across all biological samples. The spectral counts for peptides shared by multiple proteins were divided into each of these proteins according to the ratio of spectral counts on their unique peptides, with proteins

possessing a greater amount of unique spectral counts acquiring a larger portion of the shared peptide's spectral count.

S5. Mitochondrial Proteome and Properties

We subsequently compared mitochondrial protein abundances and their involvement in specific functional pathways via bioinformatics analyses using NSAF values (Figure 4C). Mouse heart mitochondria demonstrated higher TCA cycle protein concentrations compared to mouse liver mitochondria, demonstrating an intrinsically higher energy-conversion capacity. The difference in TCA cycle protein abundance among the mouse heart, human heart, and drosophila were indistinguishable; this illustrates the variations in TCA activity between contractile and non-contractile tissues. Liver mitochondria contained the fewest C-I proteins. However, C-V showed no significant difference in overall protein abundance. Within each complex, differential subunit abundances spanned over three orders of magnitude. For example, subunit alpha in the human heart and subunit beta in the mouse heart, mouse liver and drosophila constitute the most abundant proteins within C-V. The least abundant proteins within C-V are ATP synthase subunit alpha in mouse heart, ATPase subunit epsilon in mouse liver, and ATP synthase subunit beta located in both human heart and drosophila. Moreover, we observed that proteins involved in lipid metabolism showed substantially lower abundance in drosophila compared to mouse liver, but more than 89% of the drosophila lipid metabolism proteins were conserved among all the model systems. This finding may allude to the minimum number of proteins fundamental for lipid metabolism. Furthermore, drosophila possessed the lowest abundance of kinase/phosphatase proteins, evidence of less specialized phosphorylation signaling in drosophila. Surprisingly, the abundance of calcium-ion binding proteins in liver mitochondria showed no significant difference across the model systems; this deviates from our calcium-induced swelling observations that mouse liver mitochondria are more susceptible to swelling under the same calcium concentration compared to other mitochondria.

S6. The Approach to Assess Protein Abundance.

Existing MS approaches to assess protein abundance include label-free qualification and labeled quantification. In this particular study, we elected to quantify relative protein abundance through a label-free approach using NSAF values; this allowed us to overcome the challenge associated with synthesizing tens of thousands of stable isotope labeled peptides[55]. However, we are aware of the limitations of label-free approaches[56]. Specifically, the accuracy of such quantifications is affected by LC-MS run-to-run variability and the weight of shared peptides among different proteins. We implemented specific approaches to address these challenges. Multiple biological and technical replicates (from 18 replicates of the mouse heart to 29 replicates of the human heart) were performed to gain a reliable evaluation of protein abundance. Furthermore, an algorithm was developed to proportionally allocate shared peptides to their corresponding proteins based on the ratio of unique peptides identified among these proteins. Within the current technological capabilities, limiting factors are certainly evident; however, we believe that our approach to systematically assess relative protein abundance adequately addresses these shortcomings.

Supporting Information Figure Legends

Figure S1. Schematic diagram of experimental workflow. We combined a series of functional assays with simultaneous proteomic assessments followed by the integration of the proteome with different analyses of functionality to determine the correlation and variations across mitochondrial populations.

Figure S2. Functionally-enabled recovery of the individuals. This figure depicts the cardiac parameter of the individuals. The left ventricular end diastolic dimension (LVEDD) of the 5 individuals was reversed back to normal values after implantation of a ventricular assist device, as highlighted in the figure.

Figure S3. Summary of mass spectrometry experiments. This table summarizes the total biological replicates as well as technical replicates including LC-MS/MS runs upon using LTQ and Orbitrap on the various mitochondrial samples of the human heart, mouse heart, mouse liver and drosophila.

Figure S4. Biochemical features of mitochondrial proteins. A depiction of the allocation of biochemical features among the mouse heart, mouse liver, human heart, and drosophila is presented. Details regarding the molecular weight, isoelectric point, as well as number of transmembrane domains are listed, implicating the dynamic characteristics of the mitochondrial proteomes among the model systems. The molecular weights portray a skewed disposition, either indicating that the lower-molecular-weight proteins predominantly cover a vast proportion of the mitochondrial proteome, or that residue from lower recovery of higher-molecular-weight proteins is present in the polyacrylamide gels. The isoelectric point distribution of the mitochondrial proteins parallels a normalized distribution, with proteins of higher alkalinity (pIs≥8) found to be more highly abundant. Ranges from ~16-23% of mitochondrial proteins identified with a transmembrane domain indicate that the extraction technique was effective in facilitating the classification of membrane proteins.

Supporting Information Table Legends

Table S1. Proteins identified from mitochondria across organs and organisms. This table contains four individual spreadsheets listing mitochondrial proteins identified from mouse heart, mouse liver, human heart, and drosophila, respectively. Each spreadsheet lists the protein identification parameters, including representative protein UniProt ID#, protein gene name, protein name, peptide sequences, best XCorr, a total number of unique peptides assigned to the protein, sequence coverage (%), average NSAF value, standard error of the mean, and all UniProt protein ID# s in this group.

Table S2. Mitochondrial proteome annotation and inter/intra-genomic comparison across organs and organisms. This table contains the following information listed sequentially: conservation among the model systems (presence denoted by *), UniProt entry ID, UniProt entry name, gene name,

protein name, and biological functions of the protein (Swiss Prot and Gene Ontology) for the mouse heart (blue), mouse liver (green), human heart (peach), and drosophila (purple), respectively. Additional information as to whether the protein has been found to be associated with disease (presence denoted by +) and/or cardiac disease (presence denoted by x) in the last two columns is also provided.

***Excerpts of Supporting Information Tables S1 and S2 are shown. Complete Supporting Information Tables S1 and S2 can be found at: https://pubs.acs.org/doi/suppl/10.1021/pr400539j/suppl_file/pr400539j_si_001.pdf**

Table S1A: Proteins Identified from Mouse Heart Mitochondria

Representative Protein UniProt ID#	Representative Protein Gene Name	Representative Protein Name	Peptide Sequence	Best Xcorr	# of Unique Peptide	Sequence Coverage (%)	Average NSAF	SEM	All UniProt Protein ID# in the Group	Occurances
A1BN54	Actn1 Actn1a	Alpha actinin 1a (Alpha-actinin-1)	ACLISM(15.9949)GYNMGEAEFAR	3.8706	10	27.28	0.000095	0.000042	A1BN54	2
			ALDFIASK	1.8026						
			ILAGDKNYITEDELR	2.9652						
			KAGTQIENIEEDFRDGLK	3.9914						
			LASDLLEWIR	3.5539						
			LIDYGK	1.7377						
			LLETIDQLYLEYAK	4.0875						
			TINEVENQILTR	3.0101						
			VGWEQLLTTIAR	4.4918						
			VLAVNQENEQLM(15.9949)EDYEK	5.763						
A2A4Q0	Rpl27 RP23-328K2.2-004	60S ribosomal protein L27	YSVDIPLDK	2.3709	1	10.34	0.000046	0.000000	G3UWF4;P61358; A2A4Q0	1
A2A547	Rpl19 RP23-309H19.6-002	60S ribosomal protein L19	ILMEHIHK	2.2311	3	13.40	0.000068	0.000036	A2A547;P84099	2
			KVWLDPNETNEIANANSR	2.9565						
			VWLDPNETNEIANANSR	6.3365						
			RACQVALDEIKAELEK	3.3046						
A2ACG7	Rpn2 RP23-163J20.6-002	Dolichyl-diphosphooligosaccharide--protein glycosyltransferase subunit 2	EETVLATVQALQTASHLSQQADLR	3.7116	10	26.50	0.000050	0.000026	Q3U505;A2ACG7; Q9DBG6	3
			FPEEEAPSTVLSQSLFTPK	5.6758						
			LGKEETVLATVQALQTASHLSQQADLR	5.0465						
			LQVSNVLSQPLAQAAVK	5.9779						
			NFESLSEAFSVASAAAALSQNR	7.1955						
			NIVEEIEDLVAR	4.8101						
			NPILWNVADVVIK	3.3517						
			TPFSLVGNVFELNFK	6.351						
			YHVPVVVVPEGSTSDTQEQAILR	7.3313						
			YLAVLGTVTFLAGNR	2.7588						
A2A6Q8	Myl4 RP23-38H19.3-7	Myosin light chain 4 (Fragment)	ALGQNPTNAEVLR	3.7019	12	63.02	0.000278	0.000244	Q9CZ19;A2A6Q8	2
			EQGTYEDFVEGLR	3.3053						
			ETAKPAAAPAPAASAAPEPLKDSAFDPK	4.266						
			HVLATLGEK	2.2637						
			IDFSADQIEEFK	4.5937						
			KETAKPAAAPAPAASAAPEPLK	5.3808						
			KETAKPAAAPAPAASAAPEPLKDSAFDPK	4.9842						
			NKEQGTYEDFVEGLR	5.6192						
			PAAAPAPAASAAPEPLKDSAFDPK	3.5605						
			TLDFEM(15.9949)FLPILQHISR	5.9804						
			TLDFEMFLPILQHISR	4.4659						
			VFDKESNGTVM(15.9949)GAELR	4.3663						
A2ACH6	Sgcd RP23-43C21.1-3	Delta-sarcoglycan	LEGDSEFLQPLYAK	3.8244	2	15.63	0.000035	0.000000	A2ACH6;P82347	1
			LLFSADDSEVVVGAER	3.6615						
A2ADF7	Slc25a34 Gm1369	Solute carrier family 25 member 34	ADGLWGLQK	1.8491	13	36.48	0.000047	0.000011	A2ADF7	7
			GFVSSVAAVAR	4.5043						
			GLAAGLLYQGLMNGVR	2.8663						
			GLGPAYLR	2.1473						
			GQLYGGLADCLVK	2.6801						
			LGPHTILSM(15.9949)FFWDELR	6.3921						
			LGPHTILSM(15.9949)FFWDELRK	2.8951						
			LGPHTILSMFFWDELR	5.1161						
			LGPHTILSMFFWDELRK	4.5672						
			LQLQGELQAPGTYPR	5.7845						
			LQLQGELQAPGTYPRPYR	3.3418						
			LYNQPVDR	2.1421						
			VTVGSAAQLATFTSAK	5.6454						
A2AFK4	Gtpbp5 mCG_6724 RP24-74N4.1-3	GTP binding protein 5, isoform CRA_a (Protein Gtpbp5)	ELHDAHIEAELEQGR	5.1389	4	19.01	0.000023	0.000002	A2AFK4	3
			GGATLYIQVPVGTLVK	2.7996						
			IVADLSNLGDEYVAALGGAGGK	7.6637						
			LGQEAIGLSALTGENLEQLLLHLK	5.1251						
A2AIL4	Ndufaf6	NADH dehydrogenase (ubiquinone) complex I, assembly factor 6	AFNVELAQVK	3.0811	14	44.14	0.000060	0.000012	A2AIL4	8
			AFNVELAQVKDSVSEK	5.3439						
			DLHADHAASHIGK	3.8025						
			DVVYDIASQAHLHLK	5.0299						
			DYESYLCSLLFPAECQR	3.5065						
			IIDEREKNLDDKAYR	2.3247						
			NLDDKAYR	2.1447						
			NM(15.9949)LLPLSLYIQSWR	5.0788						
			NMLLPLSLYIQSWR	4.2224						
			SVAAASGPGIPGSHLYCLELLR	2.5909						
			SVPAEAFPAFLQTVSLEDYLK	5.2763						
			SVPAEAFPAFLQTVSLEDYLKK	4.5087						
			VAAASGPGIPGSHLYCLELLR	3.2683						
			VDFDIFHPSLQQK	4.1865						
P58774	Tpm2	Tropomyosin beta chain	AISEELDNALNDITSL	4.6868	2	10.21	0.000054	0.000005	P58774; A2AIM4	2
			TIDDLEDEVYAQK	4.5188						
F6WF36	Map7d1	MAP7 domain-containing protein 1	SLQLSAWESSIVDR	3.2896	3	7.36	0.000005	0.000000	F6WF36; A2AJI1	1
			TAEGLLPFAEAEAFLK	3.4552						
			YLAAKKAVWLEKEEKAKALREKQLQER	3.5404						
A2AKD7	Snta1 RP23-192L3.1-1	Alpha-1-syntrophin	GSVPYDAELSFALR	4.1054	2	6.01	0.000013	0.000000	Q61234;A2AKD7	1
			YLEICAADGQDAVFLR	3.5584						
A2AKI5	Itgav RP23-111F12.3-5	Integrin alpha-V light chain	FGSAIAPLGDLDQDGFNDIAIAAPYGGEDKK	5.7078	4	7.24	0.000011	0.000000	A2AKI5;P43406	1
			FSVHQQSEM(15.9949)DTSVK	3.8245						
			IQSSNSFDNVSPVVSYK	4.0118						
			LTPITIFM(15.9949)EYR	2.4533						
A2AMM0	Murc	Muscle-related coiled-coil protein (Muscle-restricted coiled-coil protein)	VASVVDSVQASQK	4.4157	2	8.56	0.000015	0.000000	A2AMM0	1
			VVIFQEDIPCPASLSVVK	3.0309						
A2APT9	Klhdc7a	Kelch domain-containing protein 7A	ADSRPVPCPAALADAPSPGPGPEPLVTGAASR	3.804	3	10.61	0.000006	0.000000	A2APT9	2
			DEAANTAGGGASEAASPQPVASPSAPGFSR	5.1017						
			GTLLPAVLTLPVPDVPQTPV	4.1653						
A2APY7	Ndufaf5	NADH dehydrogenase [ubiquinone] 1 alpha subcomplex assembly factor 5	AGFNTLTVDTDEIQVNYPGMFELMEDLK	3.9056	19	58.31	0.000123	0.000024	A2APY7	14

			ALEQIHYVLKPDGVFVGAMFGGDTLYELR	2.7211						
			ALNIFDRELK	1.954						
			CSLQLAETER	3.3874						
			CSLQLAETEREGGFSPHISPFTAVNDLGHLLGR	7.4196						
			DFPLALDIGCGR	3.6647						
			DTM(15.9949)LAAAAVYR	3.8277						
			DTMLAAAAVYR	3.0071						
			EGGFSPHISPFTAVNDLGHLLGR	6.882						
			GSATVSFGELAK	4.1612						
			GYIAQHLDKETVGK	4.5208						
			HISPFTAVNDLGHLLGR	2.9354						
			IADRVYDIAR	2.587						
			IFQTDIAEHALK	4.1761						
			ISPFTAVNDLGHLLGR	5.3785						
			LNDVMSHEK	1.7102						
			LNDVMSHEKK	2.2849						
			NEDGSIPATFQIYHMIGWK	3.4555						
			TAVNDLGHLLGR	3.5667						
A2AQ17	Ndufaf1 RP23-22A15.6-001	Complex I intermediate-associated protein 30, mitochondrial	(42.0106)IPRGAFERKLSYDWSQFNTLYLR	3.9879	22	50.00	0.000093	0.000011	A2AQ17;Q9CWX2	14
			AIRDEAIEHFR	3.5779						
			AIRDEAIEHFRR	3.6775						
			DVQGPLVLDK	2.8494						
			EKEDLDKWIVTSDK	4.6464						
			EVALDAPSPDR	2.8541						
			EVALDAPSPDRTPEVSFDK	7.5073						
			FFFSNQGR	2.7255						
			GGPYWQEVK	2.2922						
			GPDGRPLQEVIM(15.9949)EQAR	4.4198						
			GPDGRPLQEVIMEQAR	4.6784						
			KLSYDWSQFNTLYLR	5.201						
			LKDEIVAHLR	3.3655						
			LSYDWSQFNTLYLR	5.4231						
			NQM(15.9949)YSYFM(15.9949)FTR	3.3901						
			PLQEVIMEQAR	4.5602						
			RLKDEIVAHLR	3.7347						
			SALLYGTLSSEPPQDGDSR	5.8743						
			TEEGLQGHDHK	3.0718						
			TEEGLQGHDHKEVALDAPSPDR	4.5573						
			TPEVSFDK	1.8825						
			VRDVQGPLVLDK	4.14						
A2AQ53	Fbn1 RP23-368I1.1-1	Fibrillin-1	GTQCEDINECEVFPGVCK	3.398	4	2.44	0.000009	0.000005	A2AQ53	2
			PNM(15.9949)CTCPSGQISPSCGSR	4.874						
			TGCTDINECEIGAHNCGR	5.2417						
			TNVDQTM(15.9949)CLDINECER	5.6124						
A2ASQ1	Agrn Agrn	Agrin [Cleaved into: Agrin N-terminal 110 kDa subunit; Agrin C-terminal 110 kDa subunit	DQCPETCQFNSVCLSR	4.305	7	5.74	0.000116	0.000113	A2ASQ1	3
			EPLYVGGAPDFSK	2.5223						
			FDTGSGPAVLTSLVPVEPGR	5.3087						
			GM(15.9949)LCGFGAVCEPSVEDPGR	3.6751						
			LYVGGLPEEQVATVLDR	3.199						
			M(15.9949)LDINNGQLELSDWQR	3.6479						
			SIESTLDDLFR	3.4309						
A2ASS6	Ttn	Titin (EC 2.7.11.1) (Connectin)	AANIVGEGEPR	2.4068	100	5.14	0.000001	0.000001	A2ASS6	8
			AENEVGIGEPSLPSRPVVAK	3.3382						
			AENIIGLGLPDTTIPIECQEK	5.4777						
			AEPTPSPQFPFADM(15.9949)PPPDTYK	3.8056						
			AGDNIKVEIPVLGRPK	2.9319						
			AGDSIVLSAISILGKPLPK	2.987						
			AGTKIELPATVTGKPEPK	2.6658						
			ALPQEAAIETTAISSSM(15.9949)VIK	5.312						
			APCSVSVLDTPGPPINFVFEDIRK	4.8921						
			APPIEPAPTPIAAPVTAPVVGK	4.5047						
			ATNQGGSVSGTASLEVEVPAK	3.4322						
			AVNAVGVSEPSEISENVVAK	5.8719						
			AVNVAGVGEPGEVTDVIEM(15.9949)K	6.2625						
			DAAIIDVTSSFTSLVLDNVNR	3.992						
			DATLQDM(15.9949)GTYVVM(15.9949)VGAAR	3.5416						
			DCGFPDEGEYVVTAGQDK	5.5227						
			DDQTLESGDKYDIIADGK	4.2567						
			DEVEPPRISMDPKYR	2.9325						
			DIRPSDIAQITSTPTSSM(15.9949)LTVK	3.6763						
			DKRVDLIHDLPR	2.5997						
			DPFEPPDAPDKPIVEDVTSNSM(15.9949)LVK	3.3949						
			DSPNIQTSFLDNIATLNIFK	3.8274						
			DVTAEDSASIM(15.9949)VK	4.3974						
			DVVM(15.9949)TDTSITEEQAGPGEPAAPFFISK	4.3465						
			PVVQK							
			EFM(15.9949)EVEEGTDVNIVAK	3.6753						
			EIRPGGNYK	1.5573						
			ELPLIFITPLSDVK	5.3387						
			EPTHVEESHSQQTTLEYGYK	5.2786						
			EPVVYDTHVNK	2.6748						
			EQQEVVFNCEVNTEGAK	3.5786						
			ETAM(15.9949)LSWDVPENDGGAPVK	2.64						
			FIQPEEPELEPEPEEIPVQEPEPEK	2.7685						
			FQDEGEYTCLASNEYGK	5.5326						
			HLVDTISEEGDTVHLTSSISNAK	4.3551						
			HRFIADGKDR	2.4369						
			IDSIISQDSAWYTATAINK	6.335						
			IEPLEVALGHLAKFTCEIQGAPNVRFQWFK	3.3944						
			IHAENLYGISDPLVSDSM(15.9949)K	4.97						
			ILIIQNAQLEDAGSYNCR	7.2414						
			IM(15.9949)AENAAGISAPSATSPFYK	6.3743						
			INVTDSLDLTTLSIK	2.3251						
			IPVVLPEDEGIYTAFASNIK	6.0008						
			ISAINDAGVGEPAVIPNVEIVEK	4.8175						
			KDSGYYSLTAENSSGSDTQK	4.762						
			KVEERRIIPPK	2.8955						
			LDDQANFNVSLTNHR	3.0034						
			LDQAGEVLYQACNAITAILTVK	5.7454						
			LDQTGGVDFQAANVK	4.2347						

			LEDAGEVQLTAK	3.5799						
			LIVEELPVR	2.2737						
			LLWTVVSEDIQACR	2.6636						
			LYVEPAAPFSAPTYM(15.9949)PTPEAVSR	4.0559						
			M(15.9949)EFTVTSLDENQEYEFR	5.7981						
			M(15.9949)INEFGYCSLDYGAAYSR	7.1787						
			NAVGVSMPR	1.7007						
			NTAGAISAPSESTGTIICKDEYEAPTIVLDPTIK	3.7515						
			QFTIGGLLEATEYEFR	4.9562						
			QQKPFFKKKLTSLRLK	2.1082						
			RIEPLEVALGHLAK	3.3451						
			SDIGQYTCDCGTDQTSGK	7.4586						
			SLDAVITNLTQGEEYLFR	4.1129						
			SLSGQYSCTATNPIGSASSGAK	5.2037						
			SLSLQYSTK	1.6356						
			TFVEDQEFHISSFEER	4.3909						
			TIVSTAQISETR	3.3186						
			TLETTISGLTAGEEYVFR	3.3373						
			TSAQLFVTGIR	1.9042						
			VAAENAAGVGEPSEPSVFYR	4.1642						
			VAAENAIGQSDYTEIGDSVLAK	7.496						
			VAAENM(15.9949)YGVGEPVQAAPIIAK	4.5859						
			VCAVNAAGVGPFSEPSDFYK	4.7819						
			VDGLLEGLTYVFR	2.2359						
			VEVFDVPGPVLDLKPVVTNR	3.454						
			VFAENAAGLSLPSETSPLVR	5.4464						
			VFAENLAGLSNPSPSSDPIK	4.3047						
			VKLDQAGEVLYQACNAITTAILTVK	6.1126						
			VLAENEIGIGEPCETTEPVK	4.1741						
			VLAENEYGIGLPAETAESVK	3.2298						
			VLASNEYGIGLPAETAEPVK	5.8061						
			VLAVNEAGESDPAHVPEPVLVK	3.2677						
			VLDRPGPPEGPVAISGVTAEK	5.437						
			VLDTPGPVADLK	2.4666						
			VM(15.9949)AENEFGVGVPTETSDAVK	6.1541						
			VM(15.9949)AENEYGVGEPTETTEPVR	6.0122						
			VM(15.9949)DFVTDLEFTVPDLVQGK	5.5422						
			VNAESTENNSLLTIK	2.4212						
			VNVENTATSTILNINECVR	4.2912						
			VREPREPTHVEESHSQQTTLEYGYKEHISTTK	2.7624						
			VSAENAAGLSEPSPPSAYQK	4.8352						
			VSAENAAGVGEPSPATVYYK	4.1359						
			VSAENENGEGTPSEIVVVAK	5.644						
			VSVESTAVNTTLVVYDCQK	5.2323						
			VTAVNEYGPGVPTDIPKPVLASDPLSEPDPPR	5.501						
			VTEATITGLIQGEEYSFR	5.3928						
			VYAINAAGVGPASLPSDPVTAR	6.8308						
			WEPPLDDGGSEIINYTLEK	4.2807						
			YDIIADGK	1.9654						
			YGVGEPLESEPVLAVDPYGPPDPPKNPEVTTITK	3.5671						
			YTLTIQNVLSAASM(15.9949)TFVVK	5.3209						
			YTVVAGGNM(15.9949)STANLFVEGR	3.5824						
A2AST1	Ccdc141 CAMDI mCG_142258 RP23-82M15.2-1	Coiled-coil protein associated with myosin II and DISC1 (MCG142258, isoform CRA_a) (Protein Ccdc141)	IDSLLELLQDR	3.2958	4	3.72	0.000127	0.000120	A2AST1	2
			NELELNEVALLPLK	2.8879						
			NLQQQLEALELESR	3.2126						
			TLQYQIQQVDTYAEK	3.399						
A2AT91	Plcb4 RP23-7A19.1-1	Protein Plcb4 (Fragment)	AM(15.9949)GIETSDIADVPSDTSK	2.5844	2	3.40	0.000005	0.000000	A2AT91;Q91UZ1	1
			YCEDLFGDLLLK	3.3166						
A2AVJ7	Rrbp1 RP23-77A2.2-002	Ribosome-binding protein 1	DALNQATSQVESK	3.2254	14	12.36	0.000017	0.000005	A2AVJ7;Q99PL5	3
			EAEETQNSLQAECDQYR	5.1581						
			IPEHDLDPNVTIILK	2.5628						
			LKELESQVSCLEK	3.3228						
			LLATEQEDAAVAK	4.2938						
			LQQENSILR	2.5404						
			LREAEETQNSLQAECDQYR	4.278						
			LTAEFEEAQR	3.5594						
			QLLLESQSQLDEAK	4.1095						
			SHVEDGDVAGSPAVPPAEQDPM(15.9949)K	2.937						
			SHVEDGDVAGSPAVPPAEQDPMK	3.0372						
			TLQEQLENGPNTQLAR	5.2511						
			TLVSTVGSM(15.9949)VFSEGEAQR	3.2649						
			VEPAVSSIVNSIQVLASK	7.0906						
A2BFF8	Dync1i2 RP23-299A2.1-6	Cytoplasmic dynein 1 intermediate chain 2	EAAVSVQEESDLEK	4.2972	2	7.69	0.000009	0.000000	A2BFF9;Q3TPJ8;O88487;A2BFF5;A2BFF8	1
			ETQTPVTAQPKEDEEEEDDVATPKPPVEPEEEK	5.7359						
A3KGU7	Spna2 RP23-443G7.6-004	Spectrin alpha chain, non-erythrocytic 1	ADVVESWIGEK	3.4686	50	31.81	0.000021	0.000019	A3KGU7	3
			AGTFQAFEQFGQQLLAHGHYASPEIK	6.0287						
			ALINADELANDVAGAEALLDR	8.8887						
			CTELNQAWTSLGK	3.4467						
			DLASVQALLR	3.1637						
			DLNSQADSLM(15.9949)TSSAFDTSQVK	8.3066						
			DLSSVQTLLTK	3.9061						
			DLTGVQNLR	1.9035						
			DVDEIEAWISEK	3.5362						
			DVTGAEALLER	3.4842						
			EAALTNEEVGADLEQVEVLQK	7.4566						
			EAFLNTEDKGDSLDSVEALIK	5.9005						
			EAIVTSEELGQDLEHVEVLQK	6.8705						
			EANELQQWITEK	3.8503						
			EEEAWINEKMTLVASEDYGDTLAAIQGLLK	4.1256						
			EKEPIVGSTDYGKDEDSAEALLK	3.8878						
			ELPTAFDYVEFTR	4.0549						
			ELVLALYDYQEK	2.6958						
			GNAM(15.9949)VEEGHFAAEDVK	2.7706						
			HQAFEAELSANQSR	4.8892						

Table S2. Mitochondrial Proteome Annotation and Inter & Intra-Genomic Comparisons Across Organs and Organisms

Note #1: Mitochondrial core proteins are marked with * in Column 1

Note #2: Diseased associated mitochondrial proteins are marked with # in Column 18

Note #3: Cardiac diseased associated mitochondrial proteins are marked with x in Column 19

Core Protein	Mouse Heart				Mouse Liver				Human Heart				Drosophila				Disease Associated Mito Proteins	Cardiac Disease-Associated Mito Proteins
	Representative Protein UniProt ID	Gene Name	Representative Protein Name	Functional Cluster	Representative Protein UniProt ID	Gene Name	Representative Protein Name	Functional Cluster	Representative Protein UniProt ID#	Gene Name	Representative Protein Name	Functional Cluster	Representative Protein UniProt ID#	Gene Name	Representative Protein Name	Functional Cluster		
*	P23242	Gja1 Cxn-43	Gap junction alpha-1 protein (Connexin 43) (Cx43) (Gap junction 43 kDa heart protein)	Apoptosis	P28230	Gjb1	Gap junction beta-1 protein (Connexin-32) (Cx32)	Apoptosis	B4DGM6	null	Gap junction protein	Apoptosis	E1JJF3	inx2 prp33 CG4590	Innexin inx2 (Innexin-2) (Gap junction protein prp33)	Apoptosis		
*	Q61696	Hspa1a Hsp70-3 Hsp70A1	Heat shock 70 kDa protein 1A (Heat shock 70 kDa protein 3) (HSP70.3) (Hsp68)	Apoptosis	Q61696	Hspa1a	Heat shock 70 kDa protein 1A (Heat shock 70 kDa protein 3) (HSP70.3) (Hsp68)	Apoptosis	A8K5I0	HSPA1A HSPA1; HSPA1B	Heat shock 70 kDa protein 1A/1B	Apoptosis	P11147	Hsc70-4 Hsc4 CG4264	Heat shock 70 kDa protein cognate 4 (Heat shock 70 kDa protein 88E)	Apoptosis		
*	Q61696	Hspa1a Hsp70-3 Hsp70A1	Heat shock 70 kDa protein 1A (Heat shock 70 kDa protein 3) (HSP70.3) (Hsp68)	Apoptosis	Q61696	Hspa1a	Heat shock 70 kDa protein 1A (Heat shock 70 kDa protein 3) (HSP70.3) (Hsp68)	Apoptosis	P34931	HSPA1L	Heat shock 70 kDa protein 1-like	Apoptosis	P11147	Hsc70-4 Hsc4 CG4264	Heat shock 70 kDa protein cognate 4 (Heat shock 70 kDa protein 88E)	Apoptosis		
*	P16627	Hspa1l Hsc70t	Heat shock 70 kDa protein 1-like (Heat shock 70 kDa protein 1L) (Heat shock 70 kDa-like protein 1)	Apoptosis	P16627	Hspa1l	Heat shock 70 kDa protein 1-like (Heat shock 70 kDa protein 1L) (Heat shock 70 kDa-like protein 1)	Apoptosis	P34931	HSPA1L	Heat shock 70 kDa protein 1-like	Apoptosis	P11147	Hsc70-4 Hsc4 CG4264	Heat shock 70 kDa protein cognate 4 (Heat shock 70 kDa protein 88E)	Apoptosis	+	
*	P63017	Hspa8 Hsc70 Hsc73	Heat shock cognate 71 kDa protein (Heat shock 70 kDa protein 8)	Apoptosis	P63017	Hspa8	Heat shock cognate 71 kDa protein (Heat shock 70 kDa protein 8)	Apoptosis	P11142	HSPA8 HSC70 HSP73 HSPA10	Heat shock cognate 71 kDa protein (Heat shock 70 kDa protein 8)	Apoptosis	P11147	Hsc70-4 Hsc4 CG4264	Heat shock 70 kDa protein cognate 4 (Heat shock 70 kDa protein 88E)	Apoptosis	+	x
*	P17742	Ppia	trans isomerase A (PPIase A) (EC 5.2.1.8) (Cyclophilin A) (Cyclosporin A-binding protein) (Rotamase A)	Apoptosis	P17742	Ppia	trans isomerase A (PPIase A) (EC 5.2.1.8) (Cyclophilin A) (Cyclosporin A-binding protein)	Apoptosis	A8K220	PPIA	Peptidyl-prolyl cis-trans isomerase	Apoptosis	P25007	Cyp1 Cyp-1 CG9916	trans isomerase (PPIase) (EC 5.2.1.8) (Cyclophilin) (Cyclosporin A-binding protein)	Apoptosis		x
*	P63101	Ywhaz	14-3-3 protein zeta/delta (Protein kinase C inhibitor protein 1)	Apoptosis	P63101	Ywhaz	14-3-3 protein zeta/delta (Protein kinase C inhibitor protein 1)	Apoptosis	B7Z2E6	YWHAZ	14-3-3 protein zeta/delta	Apoptosis	P29310	14-3-3zeta	14-3-3 protein zeta (14-3-3-like protein)	Apoptosis		
*	P08228	Sod1	Superoxide dismutase [Cu-Zn] (EC 1.15.1.1)	Apoptosis	P08228	Sod1	Superoxide dismutase [Cu-Zn] (EC 1.15.1.1)	Apoptosis	P00441	SOD1	Superoxide dismutase [Cu-Zn] (EC 1.15.1.1) (Superoxide dismutase 1) (hSod1)	Apoptosis	P61851	Sod CG11793	Superoxide dismutase [Cu-Zn] (EC 1.15.1.1)	Apoptosis	+	x
*	P09671	Sod2 Sod-2	Superoxide dismutase [Mn], mitochondrial (EC 1.15.1.1)	Apoptosis	P09671	Sod2	Superoxide dismutase [Mn], mitochondrial (EC 1.15.1.1)	Apoptosis	F5H4R2	SOD2	Superoxide dismutase [Mn], mitochondrial	Apoptosis	Q00637	Sod2 CG8905	Superoxide dismutase [Mn], mitochondrial (EC 1.15.1.1)	Apoptosis	+	x
*	Q3V132	Slc25a31 Aac4 Ant4 Sfec	ADP/ATP translocase 4 (ADP,ATP carrier protein 4)	Apoptosis	Q3V132	Slc25a31	ADP/ATP translocase 4 (ADP,ATP carrier protein 4)	Apoptosis	Q9H0C2	SLC25A31 AAC4 ANT4 SFEC	ADP/ATP translocase 4 (ADP,ATP carrier protein 4)	Apoptosis	Q26365-2	sesB A/A-T CG16944	ADP,ATP carrier protein (ADP/ATP translocase)	Apoptosis		
*	P51881	Slc25a5 Ant2	ADP/ATP translocase 2 (ADP,ATP carrier protein 2)	Apoptosis	P51881	Slc25a5	ADP/ATP translocase 2 (ADP,ATP carrier protein 2)	Apoptosis	P05141	SLC25A5 ANT2	ADP/ATP translocase 2 (ADP,ATP carrier protein 2)	Apoptosis	Q26365-2	sesB A/A-T CG16944	ADP,ATP carrier protein (ADP/ATP translocase)	Apoptosis	+	
*	O08600	Endog	Endonuclease G, mitochondrial (Endo G) (EC 3.1.30.-)	Apoptosis	O08600	Endog	Endonuclease G, mitochondrial (Endo G) (EC 3.1.30.-)	Apoptosis	E5KNL5	ENDOG	Endonuclease G, mitochondrial (Endo G) (EC 3.1.30.-)	Apoptosis	Q7JXB9	EndoG CG8862 Dmel_CG8862	Endonuclease G (LD35517p)	Apoptosis	+	

*	Q60931	Vdac3	Voltage-dependent anion-selective channel protein 3 (VDAC-3) (mVDAC3)	Apoptosis	Q60931	Vdac3	Voltage-dependent anion-selective channel protein 3 (VDAC-3) (mVDAC3)	Apoptosis	Q9Y277	VDAC3	Voltage-dependent anion-selective channel protein 3 (VDAC-3) (hVDAC3)	Apoptosis	Q94920	porin POR-1 VDAC CG6647	Voltage-dependent anion-selective channel (DmVDAC)	Apoptosis		
*	Q60930	Vdac2 Vdac6	Voltage-dependent anion-selective channel protein 2 (VDAC-2) (mVDAC2)	Apoptosis	Q60930	Vdac2	Voltage-dependent anion-selective channel protein 2 (VDAC-2) (mVDAC2)	Apoptosis	B4DKM5	VDAC2	Voltage-dependent anion-selective channel protein 2	Apoptosis	Q94920	porin POR-1 VDAC CG6647	Voltage-dependent anion-selective channel (DmVDAC)	Apoptosis		
*	Q791T5	Mtch1	Mitochondrial carrier homolog 1 (Mitochondrial carrier-like protein 1)	Apoptosis	Q791T5	Mtch1	Mitochondrial carrier homolog 1 (Mitochondrial carrier-like protein 1)	Apoptosis	A4FVA6	MTCH1	MTCH1 protein (Fragment)	Apoptosis	Q9V3Y4	Mtch Mtch-RB CG6851 Dmel_CG6851	[illegible] (Mitochondrial carrier homolog) (Mitochondrial carrier homolog 1, isoform A) (Mitochondrial	Apoptosis		
*	Q91YM4	Tbrg4 Kiaa0948	Protein TBRG4 (Transforming growth factor beta regulator 4)	Apoptosis	Q91YM4	Tbrg4	Protein TBRG4 (Transforming growth factor beta regulator 4)	Apoptosis	Q969Z0	TBRG4 CPR2 FASTKD4 KIAA0948	Protein TBRG4 (Cell cycle progression restoration protein 2) (Cell cycle progression protein 2)	Apoptosis	Q9VD14	CG13850 Dmel_CG13850	CG13850 (GH07286p)	Apoptosis		
*	Q9JIY5	Htra2 Omi Prss25	[illegible] HTRA2, mitochondrial (EC 3.4.21.108) (High temperature requirement protein A2) (HtrA2)	Apoptosis	Q9JIY5	Htra2	[illegible] HTRA2, mitochondrial (EC 3.4.21.108) (High temperature requirement protein A2) (HtrA2)	Apoptosis	O43464	null	[illegible] highly similar to Homo sapiens protease, serine, 25 (PRSS25), nuclear gene encodingmitocho	Apoptosis	Q9VFJ3	HtrA2 Omi/HtrA2 CG8464	[illegible] HTRA2, mitochondrial (EC 3.4.21.108) (High temperature requirement protein A2)	Apoptosis	+	
*	Q9Z0X1	Aifm1 Aif Pdcd8	Apoptosis-inducing factor 1, mitochondrial (EC 1.-.-.-) (Programmed cell death protein 8)	Apoptosis	Q9Z0X1	Aifm1	Apoptosis-inducing factor 1, mitochondrial (EC 1.-.-.-) (Programmed cell death protein 8)	Apoptosis	O95831	AIFM1 AIF PDCD8	Apoptosis-inducing factor 1, mitochondrial (EC 1.-.-.-) (Programmed cell death protein 8)	Apoptosis	Q9VQ79-1	AIF CG7263	Putative apoptosis-inducing factor 1, mitochondrial (DmAIF) (EC 1.-.-.-)	Apoptosis	+	
*	Q9D0M3	Cyc1	Cytochrome c1, heme protein, mitochondrial (Complex III subunit 4) (Cytochrome b-c1 complex subunit 4)	Apoptosis	Q9D0M3	Cyc1	Cytochrome c1, heme protein, mitochondrial (Complex III subunit 4) (Cytochrome b-c1 complex subunit 4)	Apoptosis	Q8TBT6	null	Cytochrome c1, heme protein, mitochondrial (Cytochrome b-c1 complex subunit 4)	Apoptosis	Q9VRL0	CG4769 Dmel_CG4769	CG4769 (GM14501p)	Apoptosis	+	
*	Q9D6U8	Fam162a E2ig5	Protein FAM162A (E2-induced gene 5 protein homolog)	Apoptosis	Q9D6U8	Fam162a	Protein FAM162A (E2-induced gene 5 protein homolog) (Growth and transformation-dependent protein) (HGTD-P)	Apoptosis	F8W7Q4	FAM162A	Protein FAM162A	Apoptosis	Q9VW12	CG9231	UPF0389 protein CG9231	Apoptosis		
*	Q91VC9	Ghitm Mics1	Growth hormone-inducible transmembrane protein (Mitochondrial morphology and cristae structure 1) (MICS1)	Apoptosis	Q91VC9	Ghitm	Growth hormone-inducible transmembrane protein (Mitochondrial morphology and cristae structure 1)	Apoptosis	Q5VT94	GHITM	Growth hormone-inducible transmembrane protein (Mitochondrial morphology and cristae structure 1)	Apoptosis	Q9VZ34	CG2076 Dmel_CG2076	CG2076 (RH72958p)	Apoptosis		
*	Q8VCM5	Mul1 Gide	Mitochondrial ubiquitin ligase activator of NFKB 1 (EC 6.3.2.-) (E3 ubiquitin-protein ligase MUL1)	Apoptosis	Q8VCM5	Mul1	Mitochondrial ubiquitin ligase activator of NFKB 1	Apoptosis	Q969V5	MUL1 C1orf166 GIDE MAPL MULAN RNF218	Mitochondrial ubiquitin ligase activator of NFKB 1 (EC 6.3.2.-) (E3 SUMO-protein ligase MUL1)	apoptosis	Q9VZI9	Mul1 CG1134 Dmel_CG1134	AT15655p (CG1134)	Apoptosis		
*	P11352	Gpx1	Glutathione peroxidase 1 (GPx-1) (GSHPx-1) (EC 1.11.1.9) (Cellular glutathione peroxidase)	Apoptosis	P11352	Gpx1	Glutathione peroxidase 1 (GPx-1) (GSHPx-1) (EC 1.11.1.9) (Cellular glutathione peroxidase)	Apoptosis	Q6NSD4	GPX1	Glutathione peroxidase	Apoptosis	Q9VZQ8	PHGPx PHGPx-RA CG12013	Glutathione peroxidase	Apoptosis	+	x
*	Q9DCT2	Ndufs3	NADH dehydrogenase [ubiquinone] iron-sulfur protein 3, mitochondrial (EC 1.6.5.3)	Apoptosis	Q9DCT2	Ndufs3	NADH dehydrogenase [ubiquinone] iron-sulfur protein 3, mitochondrial (EC 1.6.5.3) (EC 1.6.99.3)	Apoptosis	B4DFM8	NDUFS3	NADH dehydrogenase [ubiquinone] iron-sulfur protein 3, mitochondrial (Uncharacterized protein)	Apoptosis	Q9VZU4	CG12079 Dmel_CG12079	CG12079 (EC 1.6.5.3) (EC 1.6.99.3) (LD25561p) (RH59487p)	Apoptosis	+	
*	Q9ER88	Dap3 Mrps29	28S ribosomal protein S29, mitochondrial (MRP-S29) (S29mt) (Death-associated protein 3) (DAP-3)	Apoptosis	Q9ER88	Dap3	28S ribosomal protein S29, mitochondrial (MRP-S29) (S29mt) (Death-associated protein 3) (DAP-3)	Apoptosis	E7EM60	DA	ribosomal protein 29, mitochondrial	Apoptosis	Q9W253	mRpS29 CG3633 Dmel_CG3633	LD41023p (Mitochondrial ribosomal protein S29)	Apoptosis	+	
*	Q9ERS2	Ndufa13 Grim19	NADH dehydrogenase [ubiquinone] 1 alpha subcomplex subunit 13	Apoptosis	Q9ERS2	Ndufa13	NADH dehydrogenase [ubiquinone] 1 alpha subcomplex subunit 13 (Cell death regulatory protein GRIM-19)	Apoptosis	Q9P0J0	NDUFA13 GRIM19	NADH dehydrogenase [ubiquinone] 1 alpha subcomplex subunit 13	Apoptosis	Q9W402	CG3446 Dmel_CG3446	CG3446 (EC 1.6.99.3) (RE14725p)	Apoptosis	+	x
	Q9JLR9	Higd1a Hig1	HIG1 domain family member 1A, mitochondrial (Hypoxia-inducible gene 1 protein)	Apoptosis	Q9JLR9	Higd1a	HIG1 domain family member 1A, mitochondrial (Hypoxia-inducible gene 1 protein)	Apoptosis	Q9Y241	HIGD1A HIG1 HSPC010	HIG1 domain family member 1A, mitochondrial (Hypoxia-inducible gene 1 protein)	Apoptosis						

	Q9JIQ3	Diablo Smac	Diablo homolog, mitochondrial (Direct IAP-binding protein with low pI)	Apoptosis	Q542V8	Diablo	Diablo homolog, mitochondrial	Apoptosis	Q502X2	DIABLO hCG_1782202	Diablo homolog (Drosophila) (HCG1782202, isoform CRA_d)	Apoptosis					+	
	Q9D1I2	null	Bcl10-interacting CARD protein (BinCARD)	Apoptosis	Q9D1I2	null	Bcl10-interacting CARD protein (BinCARD)	Apoptosis	Q96LW7	C9orf89	Bcl10-interacting CARD protein (BinCARD)	Apoptosis						
	Q9D0S9	Hint2	Histidine triad nucleotide-binding protein 2, mitochondrial (HINT-2) (EC 3.-.-.-) (HINT-3)	Apoptosis	Q9D0S9	Hint2	Histidine triad nucleotide-binding protein 2, mitochondrial (HINT-2) (EC 3.-.-.-) (HINT-3)	Apoptosis	Q9BX68	HINT2	Histidine triad nucleotide-binding protein 2, mitochondrial (HINT-2) (EC 3.-.-.-) (HINT-3) (HIT-17kDa)	Apoptosis					+	
	Q9CQ92	Fis1 Ttc11	Mitochondrial fission 1 protein (FIS1 homolog) (Tetratricopeptide repeat protein 11) (TPR repeat protein 11)	Apoptosis	Q9CQ92	Fis1	Mitochondrial fission 1 protein (FIS1 homolog) (Tetratricopeptide repeat protein 11) (TPR repeat protein 11)	Apoptosis	Q9Y3D6	FIS1 TTC11 CGI-135	Mitochondrial fission 1 protein (FIS1 homolog) (hFis1) (Tetratricopeptide repeat protein 11) (TPR repeat	Apoptosis					+	
	Q99KR7	Ppif	Peptidyl-prolyl cis-trans isomerase F, mitochondrial (PPIase F) (EC 5.2.1.8) (Cyclophilin D)	Apoptosis	Q99KR7	Ppif	Peptidyl-prolyl cis-trans isomerase F, mitochondrial (PPIase F) (Cyclophilin F) (Rotamase F)	Apoptosis	P23284	PPIB CYPB	Peptidyl-prolyl cis-trans isomerase B (PPIase B) (EC 5.2.1.8)	Apoptosis					+	
	Q91ZX7	Lrp1 A2mr	Prolow-density lipoprotein receptor-related protein 1 (LRP-1) (Alpha-2-macroglobulin receptor) (A2MR)	Apoptosis	Q91ZX7	Lrp1	Prolow-density lipoprotein receptor-related protein 1 (LRP-1) (Alpha-2-macroglobulin receptor) (A2MR)	Apoptosis	Q07954	LRP1 A2MR APR	Prolow-density lipoprotein receptor-related protein 1 (LRP-1)	Apoptosis					+	
	Q8BG51	Rhot1 Arht1	Mitochondrial Rho GTPase 1 (MIRO-1) (EC 3.6.5.-) (Ras homolog gene family member T1)	Apoptosis	Q8BG51	Rhot1	Mitochondrial Rho GTPase 1 (MIRO-1) (EC 3.6.5.-) (Ras homolog gene family member T1)	apoptosis	Q8IXI2	RHOT1 ARHT1	Mitochondrial Rho GTPase 1 (MIRO-1) (hMiro-1) (EC 3.6.5.-) (Rac-GTP-binding protein-like protein)	Apoptosis						
	Q61171	Prdx2 Tdpx1 Tpx	Peroxiredoxin-2 (EC 1.11.1.15) (Thiol-specific antioxidant protein) (TSA) (Thioredoxin peroxidase 1)	Apoptosis	Q61171	Prdx2	(EC 1.11.1.15) (Thiol-specific antioxidant protein) (TSA) (Thioredoxin peroxidase 1)	Apoptosis	B4DF70	null	cDNA FLJ60461, highly similar to Peroxiredoxin-2 (EC 1.11.1.15)	Apoptosis					+	x
	Q5XJY4	Parl Psarl	associated rhomboid-like protein, mitochondrial (EC 3.4.21.105) (Mitochondrial	Apoptosis	Q5XJY4	Parl	Presenilins-associated rhomboid-like protein, mitochondrial (EC 3.4.21.105)	Apoptosis	F8WCQ4	PARL	P-beta	Apoptosis					+	
	Q542V8	Diablo	39S ribosomal protein L28, mitochondrial (L28mt) (MRP-L28)	Apoptosis	Q542V8	Diablo	Diablo homolog, mitochondrial	Apoptosis	Q502X2	DIABLO hCG_1782202	(Drosophila) (HCG1782202, isoform CRA_d) (cDNA FLJ10537 fis, clone NT2RP2001119,	Apoptosis					+	
	Q3UJU9	Fam82a2 Fam82c	Regulator of microtubule dynamics protein 3 (RMD-3) (mRMD-3) (Protein FAM82A2) (Protein FAM82C)	Apoptosis	Q3UJU9	Fam82a2	Regulator of microtubule dynamics protein 3 (RMD-3) (mRMD-3) (Protein FAM82A2) (Protein FAM82C)	Apoptosis	H0YMB1	FAM82A2	Regulator of microtubule dynamics protein 3 (Fragment)	Apoptosis						
	P59017	Bcl2l13 Mil1	Bcl-2-like protein 13 (Bcl2-L-13) (Bcl-rambo) (Protein Mil1)	Apoptosis	P59017	Bcl2l13	Bcl-2-like protein 13 (Bcl2-L-13) (Bcl-rambo) (Protein Mil1)	Apoptosis	Q9BXK5	BCL2L13 MIL1 CD003	Bcl-2-like protein 13 (Bcl2-L-13) (Bcl-rambo) (Protein Mil1)	Apoptosis					+	
	P58281	Opa1	Dynamin-like 120 kDa protein, mitochondrial (EC 3.6.5.5) (Large GTP-binding protein) (LargeG) (Optic atrophy protein 1	Apoptosis	P58281	Opa1	Dynamin-like 120 kDa protein, mitochondrial (EC 3.6.5.5) (Large GTP-binding protein) (LargeG) (Optic atrophy protein 1	Apoptosis	H7C3G2	OPA1	Dynamin-like 120 kDa protein, mitochondrial (Fragment)	Apoptosis					+	
	P27773	Pdia3 Erp Erp60 Grp58	Protein disulfide-isomerase A3 (EC 5.3.4.1) (58 kDa glucose-regulated protein)	Apoptosis	P27773	Pdia3	Protein disulfide-isomerase A3 (EC 5.3.4.1) (58 kDa glucose-regulated protein)	Apoptosis	P30101	PDIA3 ERPS7 ERP60 GRP58	Protein disulfide-isomerase A3 (EC 5.3.4.1) (58 kDa glucose-regulated protein)	Apoptosis					+	
	P08226	Apoe	Apolipoprotein E (Apo-E)	Apoptosis	P08226	Apoe	Apolipoprotein E (Apo-E)	Apoptosis	P02649	APOE	Apolipoprotein E (Apo-E)	Apoptosis					+	x

References

(1) Zhang, J.; Li, X.; Mueller, M.; Wang, Y.; Zong, C.; Deng, N.; Vondriska, T. M.; Liem, D. A.; Yang, J. I.; Korge, P.; Honda, H.; Weiss, J. N.; Apweiler, R.; Ping, P., Systematic characterization of the murine mitochondrial proteome using functionally validated cardiac mitochondria. *Proteomics.* **2008,** 8, (8), 1564-75.

(2) Zhang, J.; Liem, D. A.; Mueller, M.; Wang, Y.; Zong, C.; Deng, N.; Vondriska, T. M.; Korge, P.; Drews, O.; Maclellan, W. R.; Honda, H.; Weiss, J. N.; Apweiler, R.; Ping, P., Altered proteome biology of cardiac mitochondria under stress conditions. *J Proteome Res.* **2008,** 7, (6), 2204-14.

(3) Miwa, S.; St-Pierre, J.; Partridge, L.; Brand, M. D., Superoxide and hydrogen peroxide production by Drosophila mitochondria. *Free Radic Biol Med.* **2003,** 35, (8), 938-48.

(4) Deng, N.; Zhang, J.; Zong, C.; Wang, Y.; Lu, H.; Yang, P.; Wang, W.; Young, G. W.; Korge, P.; Lotz, C.; Doran, P.; Liem, D. A.; Apweiler, R.; Weiss, J. N.; Duan, H.; Ping, P., Phosphoproteome analysis reveals regulatory sites in major pathways of cardiac mitochondria. *Mol Cell Proteomics.* **2011,** 10, (2), M110 000117.

(5) Kirby, D. M.; Thorburn, D. R.; Turnbull, D. M.; Taylor, R. W., Biochemical assays of respiratory chain complex activity. *Methods Cell Biol.* **2007,** 80, 93-119.

(6) Wittig, I.; Braun, H. P.; Schagger, H., Blue native PAGE. *Nat Protoc.* **2006,** 1, (1), 418-28.

(7) Kramarova, T. V.; Shabalina, I. G.; Andersson, U.; Westerberg, R.; Carlberg, I.; Houstek, J.; Nedergaard, J.; Cannon, B., Mitochondrial ATP synthase levels in brown adipose tissue are governed by the c-Fo subunit P1 isoform. *FASEB J.* **2008,** 22, (1), 55-63.

(8) Twining, S. S., Fluorescein isothiocyanate-labeled casein assay for proteolytic enzymes. *Anal Biochem.* **1984,** 143, (1), 30-4.

(9) Xu, T.; Wong, C. C.; Kashina, A.; Yates, J. R., 3rd, Identification of N-terminally arginylated proteins and peptides by mass spectrometry. *Nat Protoc.* **2009,** 4, (3), 325-32.

(10) Wu, C. H.; Apweiler, R.; Bairoch, A.; Natale, D. A.; Barker, W. C.; Boeckmann, B.; Ferro, S.; Gasteiger, E.; Huang, H.; Lopez, R.; Magrane, M.; Martin, M. J.; Mazumder, R.; O'Donovan, C.; Redaschi, N.; Suzek, B., The Universal Protein Resource (UniProt): an expanding universe of protein information. *Nucleic Acids Res.* **2006,** 34, (Database issue), D187-91.

(11) Cociorva, D.; D, L. T.; Yates, J. R., Validation of tandem mass spectrometry database search results using DTASelect. *Curr Protoc Bioinformatics.* **2007,** Chapter 13, Unit 13 4.

(12) Paoletti, A. C.; Parmely, T. J.; Tomomori-Sato, C.; Sato, S.; Zhu, D.; Conaway, R. C.; Conaway, J. W.; Florens, L.; Washburn, M. P., Quantitative proteomic analysis of distinct mammalian Mediator complexes using normalized spectral abundance factors. *Proc Natl Acad Sci U S A.* **2006,** 103, (50), 18928-33.

(13) Mosley, A. L.; Florens, L.; Wen, Z.; Washburn, M. P., A label free quantitative proteomic analysis of the Saccharomyces cerevisiae nucleus. *J Proteomics.* **2009,** 72, (1), 110-20.

(14) Liu, H.; Sadygov, R. G.; Yates, J. R., 3rd, A model for random sampling and estimation of relative protein abundance in shotgun proteomics. *Anal Chem.* **2004,** 76, (14), 4193-201.

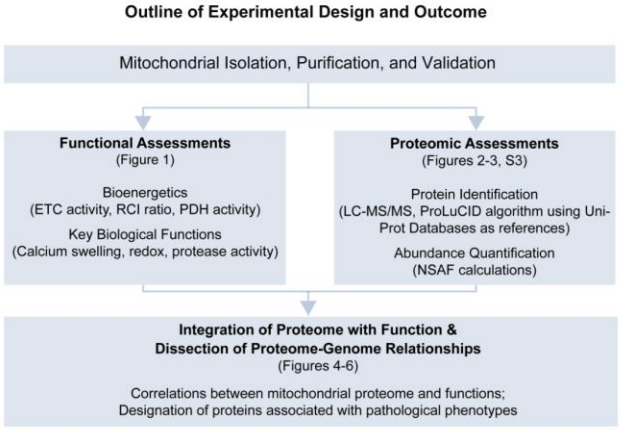

Supplemental Figure S1

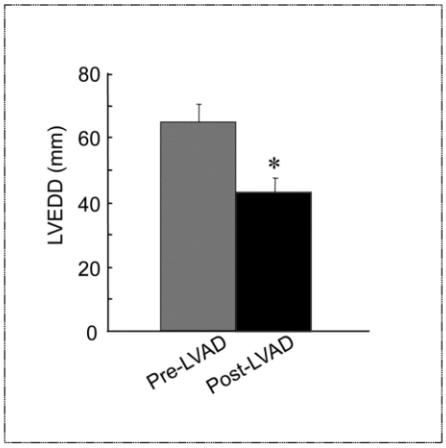

Supplemental Figure S2

	Human Heart		Mouse Heart		Mouse Liver		Drosophila	
Instrument	Orbitrap	LTQ	Orbitrap	LTQ	Orbitrap	LTQ	Orbitrap	LTQ
Biological Replicates	5	6	4	9	4	4	3	4
Technical Replicates	11	18	9	9	13	13	9	12
Total LC-MS/MS Runs	29		18		26		21	
Total Raw MS Files	850		669		1183		701	

Supplemental Figure S3

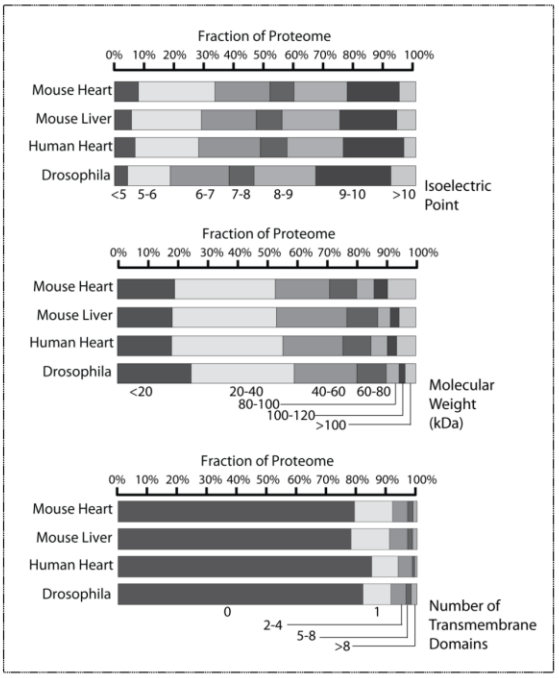

Supplemental Figure S4

CHAPTER 3

Metabolic Labeling Reveals Proteome Dynamics of Mouse Mitochondria

*This chapter is reprinted from Kim, et al., Metabolic Labeling Reveals Proteome Dynamics of Mouse Mitochondria, Molecular & Cellular Proteomics, 11(12):1586-94. http://www.mcponline.org/content/11/12/1586.long

MCP MOLECULAR & CELLULAR PROTEOMICS ASBMB

Metabolic Labeling Reveals Proteome Dynamics of Mouse Mitochondria*[S]

Tae-Young Kim‡§, Ding Wang‡§, Allen K. Kim‡§, Edward Lau‡§, Amanda J. Lin§, David A. Liem§, Jun Zhang§, Nobel C. Zong§, Maggie P. Y. Lam§, and Peipei Ping§¶

Mitochondrial dysfunction is associated with many human diseases. Mitochondrial damage is exacerbated by inadequate protein quality control and often further contributes to pathogenesis. The maintenance of mitochondrial functions requires a delicate balance of continuous protein synthesis and degradation, *i.e.* protein turnover. To understand mitochondrial protein dynamics *in vivo*, we designed a metabolic heavy water (^2H_2O) labeling strategy customized to examine individual protein turnover in the mitochondria in a systematic fashion. Mice were fed with ^2H_2O at a minimal level (<5% body water) without physiological impacts. Mitochondrial proteins were analyzed from 9 mice at each of the 13 time points between 0 and 90 days (d) of labeling. A novel multiparameter fitting approach computationally determined the normalized peak areas of peptide mass isotopomers at initial and steady-state time points and permitted the protein half-life to be determined without plateau-level ^2H incorporation. We characterized the turnover rates of 458 proteins in mouse cardiac and hepatic mitochondria and found median turnover rates of 0.0402 d^{-1} and 0.163 d^{-1}, respectively, corresponding to median half-lives of 17.2 d and 4.26 d. Mitochondria in the heart and those in the liver exhibited distinct turnover kinetics, with limited synchronization within functional clusters. We observed considerable interprotein differences in turnover rates in both organs, with half-lives spanning from hours to months (~60 d). Our proteomics platform demonstrates the first large-scale analysis of mitochondrial protein turnover rates *in vivo*, with potential applications in translational research. ***Molecular & Cellular Proteomics 11: 10.1074/mcp.M012.021162, 1586–1594, 2012.***

Mitochondrial dysfunctions are observed in disorders such as neurodegeneration, cardiovascular diseases, and aging (1–3). It is postulated that the failure to contain or replenish mitochondrial proteins damaged by reactive oxygen species directly underlies many pathological phenotypes (4). The development of effective treatments for these diseases therefore relies on understanding the molecular basis of protein dynamics. Outstanding questions are how the processes of mitochondrial proteome dynamics are regulated in different systems, and how their perturbations could progress to pathological remodeling of the organelle. Thus far, quantitative proteomics efforts have been predominated by steady-state measurements, which often provide fragmentary snapshots of the proteome that are difficult to comprehend in the context of other cellular events.

To further understand mitochondrial dynamics *in vivo*, we examined the turnover rates of individual heart and liver mitochondrial proteins on a proteome scale. Both the liver and the heart contain large numbers of mitochondria, but cardiac and hepatic mitochondria differ in their protein composition, oxygen consumption, substrate utilization, and disease manifestation. However, these differences are often interpreted only by protein compositions and steady-state abundance, without the consideration of protein kinetics in the temporal dimension. Abnormal protein kinetics may indicate dysfunctions in protein quality control, the accumulation of damaged proteins, misfolding, or other proteinopathies. Protein dynamics itself is an important intrinsic property of the proteome, the disruption of which could be causal of cellular etiologies.

At minimum, a kinetic definition of the proteome requires knowledge of the rate at which individual proteins are being replaced. Isotope tracers are particularly useful for tracking such continual renewal of the proteome in living systems, because they allow differentiation between preexisting and newly synthesized proteins (5). Among the available stable isotope precursors, heavy water (^2H_2O) labeling offers several advantages with respect to safety, labeling kinetics, and cost (6, 7). First, ^2H_2O administration to animals and humans at low enrichment levels is safe for months or even years (8). Second, maintaining constant ^2H enrichment levels in body water following the initial intake of ^2H_2O is easily achieved, because administrated ^2H_2O rapidly equilibrates over all tissues but decays slowly (9, 10). Third, ^2H_2O labeling is more cost effective than other stable isotope labeling methods. Importantly, ^2H_2O intake induces universal ^2H incorporation into biomolecules. Systematic insights into protein turnover *in vivo* could therefore be correlated to that of nucleic acids, carbohydrates, or lipids, enabling broad applications for this

From the §Departments of Physiology and Medicine, David Geffen School of Medicine, UCLA, Los Angeles, CA 90095, USA

Received, June 11, 2012, and in revised form, August 15, 2012
Published, MCP Papers in Press, August 21, 2012, DOI 10.1074/mcp.M112.021162

technology in studying mammalian systems, including humans.

A variety of methodologies have been developed to analyze the extent of ^2H incorporation in proteins following ^2H_2O labeling, including GC-MS measurements of hydrolyzed target proteins (11–14) and peptide analysis in MALDI-TOF MS (15) and LC-MS (16, 17). More recently, Price *et al.* described an approach for measuring protein turnover by calculating the theoretical number of ^2H-labeling sites on a peptide sequence (18) and reported the turnover rates of ~100 human plasma proteins. Here we describe another novel strategy to determine protein turnover rates on a proteomic scale using ^2H_2O labeling. By computing the parameters needed to deduce fractional protein synthesis using software we developed, we were able to obtain protein half-life data without relying on the asymptotic isotopic abundance of peptide ions. Our approach also has the unique benefit of automating all steps of isotopomer quantification and postcollection data analysis, and it does not require knowledge of the exact precursor enrichment or labeling sites of peptides. We observed diverse kinetics from 458 liver and heart mitochondrial proteins that inform essential characteristics of mitochondrial dynamics and intragenomic differences between the two organs.

EXPERIMENTAL PROCEDURES

^2H_2O Labeling of Mice and Tissue Collection—All animal experiments were conducted in accordance with the National Research Council's Guide for the Care and Use of Laboratory Animals and approved by the University of California, Los Angeles. Male Hsd:ICR (CD-1) outbred mice (8 to 10 weeks of age) (Harlan Laboratories, Indianapolis, IN) were housed upon arrival in a 12:12 h light-dark cycle with controlled temperature and humidity and free access to standard lab chow and natural water. No significant change was observed in the body weights of mice (~40 g) during the labeling period. ^2H_2O labeling was initiated by two intraperitoneal (IP) injections of 99.9% saline ^2H_2O (Cambridge Isotope Laboratories, Andover, MA) spaced 4 h apart; then mice were allowed free access to 8% ^2H_2O to maintain a steady-state labeling level at ~4.5% in body water (Fig. 1*A*). Heart, liver, and blood were harvested at 13 time points (0, 0.5, 1, 2, 4, 7, 12, 17, 22, 27, 32, 37, and 90 d) from the second IP injection (t = 0). At each time point, three groups of three mice each were euthanized. All three groups from each time point were used to determine the extent of ^2H labeling in body water; one group was used to calculate protein turnover rates.

GC-MS Analysis of Serum Water—^2H labeling in body water was measured via GC-MS after exchange with acetone as described elsewhere (13). Serum was centrifuged for 20 min at 4,000 rpm at 4 °C, and 20 μl of serum or ^2H_2O standard for calibration curve was reacted with 2 μl of 10 N NaOH and 4 μl of 5% (v/v) acetone in acetonitrile (ACN). After overnight incubation at ambient temperature, acetone was extracted by adding 500 μl of chloroform and 0.5 g of anhydrous sodium sulfate, and 300 μl of the extracted solution was aliquoted and analyzed on a GC[1] mass spectrometer (Agilent 6890/5975) with an Agilent J&W DB17-MS capillary column (30 m × 0.25 mm × 0.25 μm). The column temperature gradient was as follows: 60 °C initial, 20 °C/min increase to 100 °C, 50 °C/min increase to 220 °C, and 1 min hold. The mass spectrometer operated in the electron impact mode (70 eV) and selective ion monitoring at m/z 58 and 59, with a 10 ms dwell time.

Isolation of Cardiac and Hepatic Mitochondria—Mitochondria were isolated by means of ultracentrifugation as described elsewhere (19). Hearts and livers were excised from euthanized mice, homogenized in the homogenization buffer (250 mmol/l sucrose, 10 mmol/l HEPES, 10 mmol/l Tris-HCl, 1 mmol/l EGTA, protease inhibitors (Roche Complete, 1×), phosphatase inhibitors (Sigma Phosphatase Inhibitor Mixture II and III, 1×), and 10 mmol/l of dithiothreitol (Sigma), pH 7.4), and then centrifuged at 800 relative centrifugal force (rcf) at 4 °C for 7 min. The supernatant was centrifuged at 4,000 rcf at 4 °C for 20 min. The pellets were washed, centrifuged again, resuspended in 19% (v/v) Percoll (Sigma) in the homogenization buffer, overlaid on 30% and 60% Percoll, and ultracentrifuged at 12,000 rcf at 4 °C for 20 min to remove microsomes. Purified mitochondria were collected from the 30%/60% Percoll interface, washed twice, centrifuged at 4,000 rcf at 4 °C for 20 min, and then lysed by sonication in 10 mmol/l Tris-HCl, pH 7.4.

Electrophoresis and In-gel Digestion of Proteins—Mitochondrial proteins were separated via SDS-PAGE; 200 μg of proteins were denatured at 70 °C in Laemmli sample buffer for 5 min and then separated on a 12% Tris-glycine acrylamide gel with 6% stacking gel, at 80 V, at ambient temperature for ~19 h. The gel was Coomassie-stained and cut into 21 fractions. Each fraction was digested with 30:1 (w/w) sequencing-grade trypsin (Promega, Madison, WI) following reduction and alkylation by dithiothreitol and iodoacetamide (Sigma), respectively.

LC-MS and MS/MS—Peptide identification and mass isotopomer quantification were performed on an LTQ Orbitrap XL mass spectrometer (ThermoFisher Scientific, San Jose, CA), coupled to a nanoACQUITY UPLC system (Waters, Manchester, UK). The trapping (30 mm) and analytical (200 mm) columns for peptide separation were packed in IntegraFrit columns (New Objective, Woburn, MA) (360-μm outer diameter, 75-μm inner diameter) using Jupiter Proteo C_{12} resin (Phenomenex, Torrance, CA) (90-Å pore, 4-μm particle). The binary buffer system consisted of 0.1% formic acid in 2% and 80% ACN for buffers A and B, respectively. The separation gradient was made by changing buffer B as follows: 0 min, 2%; 0.1 min, 5%; 70 min, 40%; 90 min, 98%; 100 min, 98%; and 105 min, 2%, with subsequent equilibrium at 2% for 5 min. Mass spectra were obtained in profile mode for MS survey scan in the Orbitrap at a resolution of 7,500 and in centroid mode for MS/MS scan in the LTQ. The top five intense peaks in the MS scan were subjected to collision-induced dissociation with an isolation window of 3 Th and a dynamic exclusion of 25 s.

Database Search for Protein Identification—The raw data were processed uisng BioWorks, version 3.3.1 SP1 (ThermoFisher Scientific), and searched using SEQUEST, version 3.3.1 (ThermoFisher Scientific), against the UniProt mouse database (July 27, 2011; 55,744 entries). Search parameters included fixed cysteine carbamidomethylation and variable methionine oxidation, trypsin enzymatic specificity, and two missed cleavages. The mass tolerances for the precursor and the product ions were 100 ppm and 1 Th, respectively. The minimum redundancy set of proteins was acquired with Scaffold, version 3.3.3 (Proteome Software, Portland, OR). At least two peptides and 99.0% protein confidence were required for protein identification, and the global false discovery rate was 0.1%. Peptides shared by multiple proteins or protein isoforms were excluded from downstream turnover rate calculations.

Quantification of Mass Isotopomers—^2H in body water is metabolically incorporated into the C–H bonds of free nonessential amino acids by multiple enzymes (11). Unlike labile N–H or O–H bonds, the C–H bonds are stable, and the incorporated ^2H in nonessential amino

[1] The abbreviations used are: GC, gas chromatography; IP, intraperitoneal; rcf, relative centrifugal force; XIC, extracted ion chromatogram; HBB-B2, hemoglobin subunit beta-2.

acids do not back-exchange during sample processing. Additionally, H in the α-carbon of essential amino acids is reversibly accessible to ^2H via transamination. The ^2H-labeled amino acids are integrated into newly synthesized protein via t-RNAs and, with each cycle of turnover, into proteins until their ^2H content reaches steady-state equilibrium with surrounding ^2H_2O. The rate of protein turnover is determined by tracking the time evolution of mass isotopomer distributions (Fig. 1*B*). To accommodate the determination of the protein turnover rate on a proteomic scale, in-house software was developed in Java that contained two modules, one for quantifying the peptide ion mass isotopomer distribution (IsotoQuan) and the other for curve fitting to determine the rate constants of protein turnover (RateQuan). RAW files were converted into mzML format using ProteoWizard (version 2.2.2913) for input. IsotoQuan extracts the extracted ion chromatogram (XIC) for each identified peptide ion using retention time and a mass isolation window of ±100 ppm. Then, the peak area under the XIC is integrated to determine the normalized abundances of all mass isotopomers corresponding to a peptide ion. At any given time point t, the normalized peak area for a designated mass isotopomer, $A_i(t)$, is determined by dividing the peak area I of the mass isotopomer i (*i.e.* $I_i(t)$, over the summation of peak areas from all mass isotopomers ($\sum_{j=0}^{N} I_j(t)$).

$$A_i(t) = I_i(t) / \sum_{j=0}^{N} I_j(t) \quad \text{(Eq. 1)}$$

where I_j is the peak area of the mass isotopomer m_j (j = 0, 1, 2, . . ., N).

Calculation of Protein Turnover Rates—To determine the protein turnover rate, the normalized peak intensities at t = 0, $A(0)$, and at full enrichment, $A(\infty)$, were defined from the time-series data of each mass isotopomer via nonlinear fitting into a first-order kinetics equation.

$$A(t) = A(0) + \{A(\infty) - A(0)\}(1 - e^{-kt}) \quad \text{(Eq. 2)}$$

where k is the rate constant, which describes the rate at which proteins are newly synthesized to replace the existing pool; assuming equilibrium, it equals the rate at which proteins are degraded. Subsequently, the time-series data of all mass isotopomers from a protein were transformed into fraction synthesis, $f(t)$, which is the fraction of total protein newly synthesized through turnover, by rearranging Equation 2.

$$f(t) = \{A(t) - A(0)\} / \{A(\infty) - A(0)\} = 1 - e^{-kt} \quad \text{(Eq. 3)}$$

RateQuan excluded data from the curve fitting with an R^2 value less than 0.7 or containing fewer than five time points from the calculation of fractional synthesis. The chosen R^2 value of 0.7 was adjudged empirically to balance high accuracy and precision in the measurement of the kinetic data. As $A(0)$ and $A(\infty)$ are theoretically bound between 0 and 1, only experimental values between −0.1 and 1.1, in consideration of experimental errors, were included in fractional synthesis calculation. Finally, fractional syntheses from all of the mass isotopomers corresponding to a particular protein were fitted to the first-order kinetics equation (Equation 3) to determine k for protein turnover.

Statistical Analyses—Uncertainties in rate constants were estimated using the Monte Carlo method. The distribution of the relative abundance was approximated using the absolute value of the residues. At each measured time point, a single point was synthetically generated using random numbers from a Gaussian distribution with the same width as the distribution of the absolute values of the residuals and a mean of the model value. New rate constants were determined for the 10,000 synthetic datasets, and the distribution of rates was observed to converge approximately to a Gaussian distribution. The width of this distribution (1σ) was reported as the standard error of the rate constant. (In principle, there is little difference between the standard error estimations of the Monte Carlo and nonlinear curve fitting methods. For comparison, the histograms of the errors in the rate constants for cardiac proteins are given in supplemental Fig. S4.) Quantile-quantile plots clearly suggest that degradation rates of proteins within an organ are not normally distributed. The significance of differences between groups was thus assessed via the rank-based, nonparametric Mann-Whitney *U* test using R. Correlations between variables were denoted by Spearman's rank-correlation coefficient (ρ).

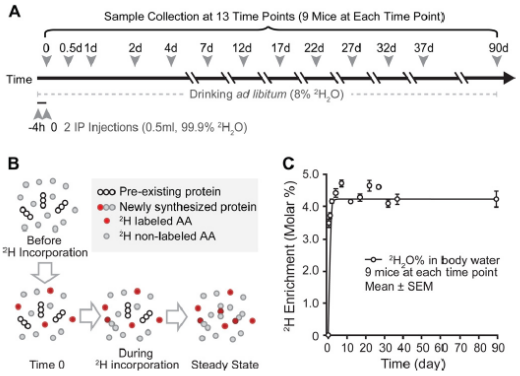

FIG. 1. **Metabolic labeling of mice using heavy water.** *A*, schematic of ^2H_2O labeling of mouse and sample collection. Twelve groups of 9 mice were given two IP injections of 99.9% ^2H_2O/saline, followed by *ad libitum* drinking of 8% ^2H_2O to maintain enrichment levels. Samples were collected at each time point of 0, 0.5, 1, 2, 4, 7, 12, 17, 22, 27, 32, 37, and 90 d of labeling. *B*, ^2H_2O labeling introduces ^2H-labeled amino acids into the precursor pool for protein synthesis. Continuous protein turnover increases the ^2H enrichment level in the protein pool until it reaches steady state. Measurement of ^2H incorporation during the labeling period provides the information about protein turnover. *C*, molar percent enrichment of ^2H in mouse serum during ^2H_2O feeding was measured via GC-MS at 13 time points. Enrichment reached 3.5% within 12 h after two IP injections of 99.9% ^2H_2O/saline and stayed at ~4.3% throughout the labeling period with 8% ^2H_2O feeding. Each data point represents an average of three biological replicates; error bar indicates S.E.

RESULTS

Precursor Enrichment in Serum during ^2H_2O Labeling—Fractional protein synthesis is calculated based on the precursor-product relationship, which states that product labeling enrichment would reach that of the precursor at steady state. To quantify the level of precursor ^2H incorporation during labeling, the serum of mice was sampled at all experimental time points. As water quickly equilibrates throughout the body and permeates cellular compartments, water in the serum serves as a proxy for ^2H incorporation in all organs. GC-MS experiments measured the molar percentage of ^2H in serum water, which rapidly reached 3.5% within 12 h following two IP injections of 99.9% ^2H_2O (Fig. 1*C*). Throughout the labeling period, *ad libitum* feeding of 8% ^2H_2O maintained ^2H enrichment at ~4.3% (Fig. 1*C*). The speed and stability of ^2H

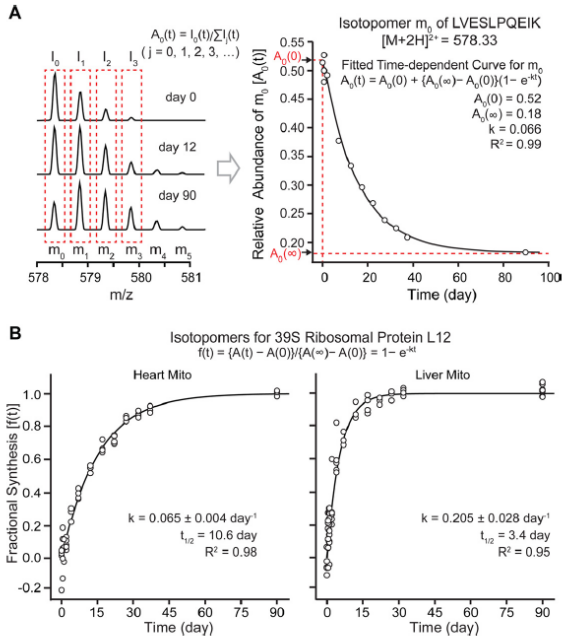

FIG. 2. **Extracting protein turnover rates from the temporal profile of mass isotopomer distribution.** *A*, the profile of the relative abundances for mass isotopomers of LVESLPQEIK ($[M+2H]^{2+}$ = 578.33 *m/z*) from mitochondrial 39S ribosomal protein L12 as a function of labeling time. ^2H_2O labeling for 90 d resulted in a decrease in the normalized peak intensity of m_0 (I_0) and appearances of extra higher mass isotopomer peaks of m_4 and m_5. The values for $A_0(0) = 0.52$, $A_0(\infty) = 0.18$, and $k = 0.066\ d^{-1}$ for m_0 of the peptide were obtained by fitting to an exponential curve ($R^2 = 0.99$) and then transformed into fractional synthesis $f(t)$ with the following equation: $f(t) = \{A(t) - A(0)\}/\{A(\infty) - A(0)\}$. Although the fitting also provides information on the rate constant for protein turnover (k), this parameter is neglected at this stage because our method determines the k value at the peptide level, not at the mass isotopomer level. *B*, the protein turnover rate was determined by fitting the fractional syntheses of mass isotopomers of a protein throughout the labeling period into an exponential curve. Individual data points represent the mass isotopomers of peptide ions belonging to mitochondrial 39S ribosomal protein L12 at the 13 labeling time points. The turnover rates for this protein in the heart and the liver are 0.065 ± 0.004 d^{-1} ($R^2 = 0.98$) and 0.205 ± 0.028 d^{-1} ($R^2 = 0.95$), respectively.

incorporation in our experiment support the calculation of fractional synthesis from constant precursor enrichment.

Time Evolution of Mass Isotopomer Abundance Distribution of ^2H-labeled Peptides—Mass isotopomer distributions of peptide ions change over time as ^2H is introduced from the precursor pool into the protein pool through protein turnover. Fig. 2*A* displays the temporal profile (0 to 90 d) of mass isotopomer distributions for a given tryptic peptide LVESLPQEIK, $[M+2H]^{2+}$ = 578.33 *m/z*, from the mitochondrial 39S ribosomal protein L12 (MRPL12). Prior to ^2H_2O labeling (0 d), the first mass isotopomer (m_0) gave the most intense peak. When the labeling time reached 12 d, the peak intensity of m_0 became comparable to that of m_1, and one new feature corresponding to m_4 was observed. After 90 d of labeling, m_0 became the third most intense mass isotopomer, and the high-mass isotopomer peak m_5 appeared. In summary, ^2H_2O labeling resulted in anticipated changes in isotopomer peak intensity that allowed protein fractional synthesis to be calculated. Accordingly, we proceeded with the proteome scale characterization of protein turnover from the heart and liver mitochondria isolated from the same animals.

The intensities of mass isotopomers were quantified using computational software developed to integrate the areas under the peak in the XIC and then normalized by the intensity of all isotopomers in a particular peptide ion to determine its relative abundance (Equation 1). For every mass isotopomer with quantification data at five or more time points, the relative abundances from all time points were fitted to an exponential decay equation (Fig. 2*A*). For a particular mass isotopomer, multiple normalized peak intensities might exist as a result of the detection of the identical peptides in multiple gel bands, different charge states, or the oxidized forms. Identical isotopomers from multiple gel bands were combined but were otherwise fitted independently. The fitting is extrapolated to yield the normalized abundance of the mass isotopomer at its initial ($A(0)$) and steady ($A(\infty)$) states.

In summary, we have applied two distinct criteria for peptide selections. The first is concerned with the protein

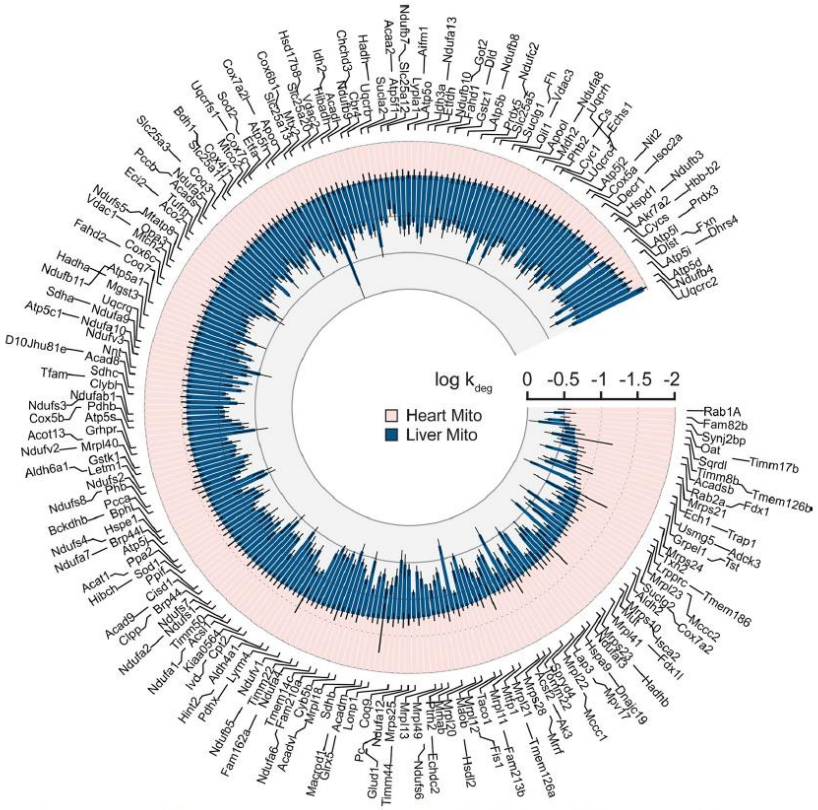

FIG. 3. **Analyses of turnover rates of mitochondrial proteins identified in both heart and liver.** The cardiac k_{deg} values (*red*) are plotted in ascending order on a logarithmic scale and paired with the corresponding hepatic k_{deg} values from the same protein (*blue*). Among the 242 proteins analyzed in both organs, only 3 had smaller turnover rates in the liver than in the heart. Error bars represent S.E.

identification, for which Scaffold was used to validate and filter peptides based on their confidence levels. The second addresses the precision of curve fitting by using an R^2 threshold filter. Mass isotopomers that met these two criteria (see detailed descriptions in the "Experimental Procedures" section) were accepted for protein turnover rate calculations.

Rates of Protein Turnover in Cardiac and Hepatic Mitochondria—From the fitted $A(0)$ and $A(\infty)$ values, all isotopomer data of a protein were transformed into protein fractional synthesis using Equation 3. For m_o at some early time points, experimentally measured $A(t)$ could be larger than the computationally determined $A(0)$ because of the fitting error, which leads to a negative fractional synthesis value. We found that filtering by R^2 value at this point excluded unquantifiable isotopomers and improved the accuracy of turnover rate calculation without significantly impacting the number of analyzed proteins. Fig. 2*B* shows an example of fractional synthesis time evolution from the mitochondrial 39S ribosomal protein L12. The fractional synthesis data were fitted to an exponential curve to yield the protein turnover rate k. The 39S ribosomal protein L12 turns over at a rate of 0.065 ± 0.004 d^{-1} ($R^2 = 0.98$) in the heart, but turnover is almost three times faster in the liver, at 0.205 ± 0.028 d^{-1} ($R^2 = 0.95$) (Fig. 2*B*). Such differences in turnover rates were generally observed between mitochondrial proteins in the heart and in the liver; the median turnover rate was about four times higher in the liver than in the heart (0.040 d^{-1} *versus* 0.16 d^{-1}). With the exception of three proteins (MRPS24, RAB1A, and SYNJ2BP), all 242 commonly analyzed proteins demonstrated slower turnover (*i.e.* longer half-life) in cardiac mitochondria (Fig. 3). In total, we deduced the turnover of 314 proteins in cardiac mitochondria and 386 in hepatic mitochondria, of which 458 are distinct. This study captured mitochondrial proteins in all major functional categories, spanning 5 orders of magnitude in protein abundance (see supplemental Fig. S3). The fractional synthesis curves of

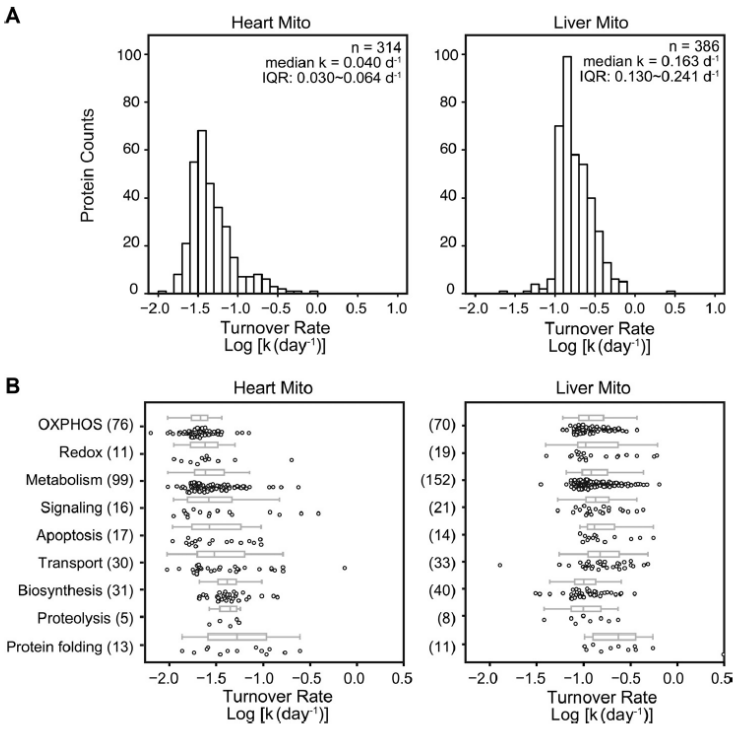

FIG. 4. **Distributions of protein turnover rates and their correlations with functions.** *A*, histograms of protein turnover rates in heart and liver mitochondria. Proteins in the heart have slower turnover rates than those in the liver (median $k = 0.042\ d^{-1}$ *versus* $0.163\ d^{-1}$). *B*, the measured turnover rates of murine mitochondrial proteins against their Gene Ontology categories. Boxes: interquartile range and median; whiskers: data range up to 1.5 interquartile ranges. The numbers of analyzed proteins in the category are presented in parentheses.

all proteins are in supplemental Figs. S1 and S2. All kinetic data are listed in supplemental Table S1.

Fig. 4*A* shows the distribution of turnover rates in the analyzed proteins in the liver and the heart. The analyzed protein kinetics ranged over 2.4 orders of magnitude in total and spanned 1.8 and 2.2 orders of magnitude in the heart and the liver, respectively. Between the 5th and 95th percentiles, protein turnover rates differed by 7.9-fold in the heart and 4.3-fold in the liver. To determine whether the observed turnover rates correlated with biological functions, we categorized the observed cardiac and hepatic mitochondrial proteins using Gene Ontology (Fig. 4*B*). In both tissues, proteins associated with protein folding showed relatively faster turnover, whereas those related to redox turned over rather slowly. In contrast, proteins involved with biosynthesis and proteolysis displayed disparate turnover between the two tissues. Biosynthesis proteins had fast turnover in the heart but not in the liver. However, significant overlaps in turnover rates were observed among the functional categories in both the liver and the heart.

DISCUSSION

We demonstrated a novel strategy utilizing ^2H_2O labeling to examine the kinetics of mitochondrial proteins in mouse heart and liver on a large scale. Our computational approach, created in-house, automated the characterization of fractional protein synthesis and deduced protein half-life without steady-state isotopomer abundance information. With this integrated platform of MS and informatics, we successfully obtained the turnover rates of 458 proteins in mouse cardiac and hepatic mitochondria.

Data Analysis—A recent investigation by Price and coworkers (18) further elevated the utilities of the ^2H_2O labeling method in evaluating protein turnovers. In their elegantly designed study, $A(\infty)$ was determined from the precursor enrichment and the theoretical number of ^2H incorporation into a peptide, derived from its sequence and established labeling sites for each amino acid. In our approach, the plateau ^2H enrichment in the peptide was computationally deduced from the experimental data points. In addition, all data processing was fully automated, which enabled us to overcome the limitations in throughput.

In analyzing our large-scale set of data points, we considered the following when addressing the experimental errors, which can be contributed by multiple sources. Firstly, the experimental error is directly linked to experimental conditions, including the reliability of the peak area measurement, the separation of overlapped chromatographic peaks, spec-

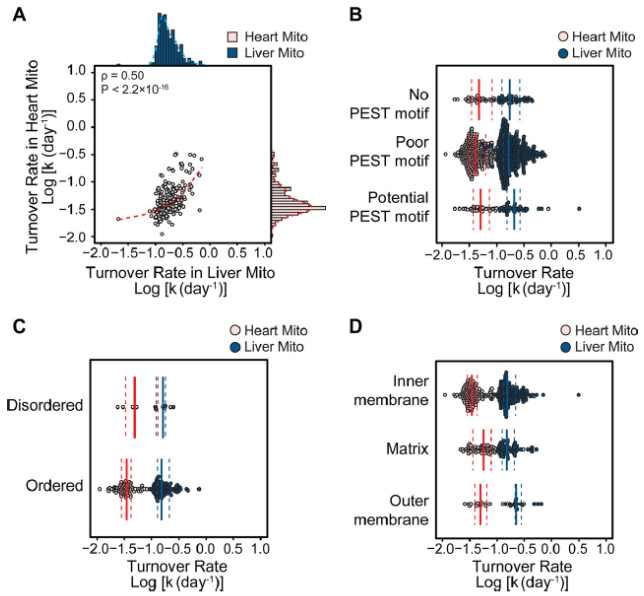

FIG. 5. **Factors affecting mitochondrial protein turnover.** *A*, protein turnover rates in the heart and the liver were significantly correlated (Spearman's $\rho = 0.50$). *B*, PEST motifs and *C*, intrinsic protein sequence disorders were not indicative of protein turnover rates. *D*, comparison between submitochondrial locations revealed that median turnover is higher in the outer membrane than in the inner membrane. The solid and dotted lines in *B*, *C*, and *D* denote the median and the interquartile range, respectively.

tral accuracy, and absolute peak intensities. Secondly, our study makes the assumption of first-order kinetics in our curve fitting to extract the kinetic information; under the scenario in which this kinetics is forced, a larger error will result. Ostensibly, the first-order kinetics model that we used in our study does not hold homogeneously for all experimental data. In other words, proteins whose turnover deviated from first-order kinetics would be fitted with a larger error. Thirdly, we filtered out redundant peptides from known protein isoforms to ensure that only unique peptides were selected for individual proteins, and to avoid ambiguity in the protein kinetics calculation. However, peptides shared by either undocumented or undiscovered isoforms might remain, subsequently causing an increased error formation in data processing.

Extensive fractionation and enrichment procedures were conducted to yield functionally viable mitochondria (19). The majority of the detected proteins are classically established mitochondria proteins. However, some identified proteins may be classified as mitochondria-associated proteins, whereas some nonmitochondrial contaminants inevitably remain in a mitochondrial isolation. Because of our stringent criteria in filtering both protein identification and turnover data, common contaminant proteins (*e.g.* keratin) were automatically expunged from the final kinetic data. We surmised that among the 458 analyzed proteins, 1 protein represented a highly likely nonmitochondrial contaminant (hemoglobin subunit beta-2 (HBB-B2)). Incidentally, our approach detected almost identical turnover rates ($k = 0.021$ d^{-1}) for only HBB-B2 in liver and heart mitochondria, which suggests the shared blood origin of the HBB-B2 protein from the two independent experiments. These data independently validate the reproducibility of our technology platform.

Rules Governing Turnover Rate of Proteins—Other metabolic labeling studies suggest that protein turnover rates differ across mammalian organs (20, 21). Our results demonstrate that such tissue-specific differences are preserved in the mitochondrial proteome (Fig. 3), supporting the hypothesis that intragenomic differences in organ phenotypes directly constrain mitochondrial protein dynamics. The turnover rates cannot be explained by liver cell turnover, as mouse liver DNA has a half-life exceeding 300 d (22).

We observed good correlation between protein turnover rates in the heart and in the liver (Spearman's $\rho = 0.50$, $p < 2.2 \times 10^{-16}$) (Fig. 5*A*), suggesting that the determined distribution of protein turnover is robust. However, the correlations are not without exceptions, which indicates additional layers of regulatory mechanisms. Several models were proposed in the literature to explain the diversity in turnover rates, either within mitochondria or across the whole cell. We further investigated whether some of these intrinsic protein properties might account for the turnover rates in our large-scale dataset. The presence of the PEST motif (23) and intrinsic protein

sequence disorder (24) have been proposed as determinants of protein kinetics. We found no proteome-wide evidence of distinct turnover for both features in either organ (Mann-Whitney *U* test, $p > 0.05$) (Figs. 5*B* and 5*C*), corroborating a recent report (25). Our data support previous observations that proteins on the outer mitochondrial membrane turn over faster than those on the inner membrane (Mann-Whitney *U* test, heart: $p = 5.55 \times 10^{-3}$; liver: $p = 5.21 \times 10^{-4}$) (Fig. 5*D*), suggesting possibilities of greater accessibility to extramitochondrial degradation mechanisms (26). A minimal inverse correlation was observed between half-life and protein abundance in both the heart ($\rho = -0.46$ and $p < 2.2 \times 10^{-16}$) and the liver ($\rho = -0.19$, $p = 7.95 \times 10^{-3}$) (supplemental Fig. S3), whereas no significant correlation was observed between turnover rate and protein molecular weight, isoelectric point, or hydrophobicity (supplemental Fig. S3). Taken together, these data argue that protein kinetics, similar to abundance, is a selectable trait of the proteome subject to cellular regulations.

Turnover of Multiprotein Complexes—As mentioned above, protein turnover rates within mitochondrial types are quite variable. The subunits of multiprotein complexes have been suggested to have coordinated turnover (20), but notable exceptions also have been reported (25, 27). In our experiments, subunits of well-defined protein complexes displayed variable kinetics, but particular members of intermediate subcomplexes may turn over together in a tighter fashion. For instance, in the respiratory chain complex I, assembly factors turned over considerably faster than the protein complex median. In the heart, NDUFAF2 and NDUFAF3 had $k = 0.053$ and 0.078 d^{-1}, compared with the median complex I value of 0.036 ± 0.007 d^{-1}. The assembly factor proteins are integral to complex I topogenesis but dissociate from the mature complex. In contrast, the core subunits of the Q subcomplex (NDUFS2, NDUFS3, NDUFS7, and NDUFS8) turned over similarly (heart: $k = 0.039$ d^{-1}, 0.036 d^{-1}, 0.042 d^{-1}, 0.039 d^{-1}). We suggest that subunits with faster turnover might be more frequently exposed to or have existed as free monomers because of assembly sequence or topology (supplemental Table S1). Under this scenario, turnover rates are influenced by the stability of the association with the final assembly, whereas in the synchronized complex model, all constitutive subunits have similar turnover kinetics. We further examined the data on the subunit NDUFA9, which has a relatively fast turnover among all subunits only in the liver ($k = 0.27$ d^{-1}), but not in the heart ($k = 0.035$ d^{-1}). In complex I biogenesis, the Q subcomplex first assembles before NDUFA9 associates with the mitochondrial-encoded ND1 to initiate the assembly of the next intermediate (28). ND1 has a considerably lower abundance in the liver than in the heart relative to other subunits, a scenario consistent with increased surplus NDUFA9 free subunits. Likewise, the NDUFA4 and NDUFS7 subunits have above-median turnover in both organs (NDUFA4: heart, $k = 0.047$ d^{-1}, liver, $k = 0.30$ d^{-1}; NDUFS7: heart, $k = 0.042$ d^{-1}, liver, $k = 0.028$ d^{-1}) and are incorporated only after stable intermediates are formed (28). Future investigations on protein kinetics are required in order to determine in-depth mechanistic insights on complex assembly.

Protein Turnover in Mitochondria—It is known that autophagy can degrade whole mitochondria when induced (29) and act as a synchronizing mechanism for protein kinetics inside the organelle. Indeed, the overall range of mitochondrial protein turnover rates we observed is much narrower than that reported for the cellular proteome. Nevertheless, the observation that individual mitochondrial protein turnover rates span at least an order of magnitude within an organ suggests that individual mitochondria cannot be simplistically assumed to turn over only as single units. In theory, the assumption of steady-state protein abundance in inferring turnover from synthesis may be transiently offset by bouts of occasional mitophagy and remains valid over the labeling period. However, because we measured protein turnover from isolated mitochondria, we reason that given the observed variability in synthesis rates, at any moment each mitochondrion contains some proteins that have been more recently synthesized than others. If mitophagy were predominant in the process of mitochondrial protein removal, then many mitochondria in the cell would be missing critical components. As this circumstance is unlikely, a mechanism is necessary to allow mitochondria with new and old proteins to preserve homeostasis under mitophagy. Mitochondrial proteins may be synthesized in excess in the cytosol at variable rates before entering the mitochondria simultaneously. Alternatively, a sorting mechanism prior to autophagy could exist such that some protein species would be preferentially recycled during fusion-fission cycles. Given that evidence of either possibility remains scarce, we posit that it is likely that individual substrate proteolysis plays significant roles in mitochondrial dynamics. The asynchronous degradation of mitochondrial proteins is attested to by the multiple protease complexes inside mitochondria. Under this model, measuring total organellar protein synthesis as a proxy for homeostasis would be an inadequate means of capturing the details of mitochondrial protein turnover. Our findings underscore the significance of obtaining a proteome dynamics map at individual protein resolution in uncovering signatures of protein quality control dysfunctions, such as in aging and metabolic perturbation studies.

In conclusion, we demonstrated the first mitochondrial proteome-wide study of *in vivo* protein dynamics. The experimental platforms tailored to the analysis of changes in mass isotopomer distribution enabled us to determine the turnover rates of 458 murine mitochondrial proteins, spanning over 2 orders of magnitude in half-life. Mitochondrial protein turnover displayed both organ-specific differences and interprotein heterogeneity, and subcellular fractionation ensured that the protein kinetics were free from interference by cytosolic pre-

cursors. We envision our kinetic data will help elucidate the mechanisms of mitochondrial homeostasis. Our methodology has wide applications in the characterization of protein kinetics and temporal proteome changes in mammalian systems. The safety and economy of ^2H_2O labeling also make it practical for use in measuring human protein dynamics in clinical studies.

* This study was supported in part by National Institutes of Health awards (NIH-R37–63901 and NHLBI-HHSN-268201000035C) to Dr. Peipei Ping and by the AHA predoctoral fellowship award (12PRE11610024) to Edward Lau.

[S] This article contains supplemental Figs. S1 to S3 and Table S1.

¶ To whom correspondence should be addressed: Peipei Ping, PhD, FISHR, FAHA, Professor and Director, Departments of Physiology and Medicine/Cardiology, NHLBI Proteomics Center at UCLA, UCLA School of Medicine, Los Angeles, CA 90095. Tel.: 310–267-5624; E-mail: pping@mednet.ucla.edu.

‡ These authors contributed equally to this work.

REFERENCES

1. Calvo, S. E., and Mootha, V. K. (2010) The mitochondrial proteome and human disease. *Annu. Rev. Genom. Hum. Genet.* **11,** 25–44
2. Balaban, R. S., Nemoto, S., and Finkel, T. (2005) Mitochondria, oxidants, and aging. *Cell* **120,** 483–495
3. Abel, E. D., and Doenst, T. (2011) Mitochondrial adaptations to physiological vs. pathological cardiac hypertrophy. *Cardiovasc. Res.* **90,** 234–242
4. Tatsuta, T., and Langer, T. (2008) Quality control of mitochondria: protection against neurodegeneration and ageing. *EMBO J.* **27,** 306–314
5. Beynon, R. J., and Pratt, J. M. (2005) Metabolic labeling of proteins for proteomics. *Mol. Cell. Proteomics* **4,** 857–872
6. Dufner, D., and Previs, S. F. (2003) Measuring *in vivo* metabolism using heavy water. *Curr. Opin. Clin. Nutr.* **6,** 511–517
7. Gasier, H. G., Fluckey, J. D., and Previs, S. F. (2010) The application of ^2H_2O to measure skeletal muscle protein synthesis. *Nutr. Metab.* **7,** 31
8. Busch, R., Neese, R. A., Awada, M., Hayes, G. M., and Hellerstein, M. K. (2007) Measurement of cell proliferation by heavy water labeling. *Nat. Protoc.* **2,** 3045–3057
9. Raman, A., Schoeller, D. A., Subar, A. F., Troiano, R. P., Schatzkin, A., Harris, T., Bauer, D., Bingham, S. A., Everhart, J. E., Newman, A. B., and Tylavsky, F. A. (2004) Water turnover in 458 American adults 40–79 yr of age. *Am. J. Physiol. Renal Physiol.* **286,** F394–F401
10. Messmer, B. T., Messmer, D., Allen, S. L., Kolitz, J. E., Kudalkar, P., Cesar, D., Murphy, E. J., Koduru, P., Ferrarini, M., Zupo, S., Cutrona, G., Damle, R. N., Wasil, T., Rai, K. R., Hellerstein, M. K., and Chiorazzi, N. (2005) In vivo measurements document the dynamic cellular kinetics of chronic lymphocytic leukemia B cells. *J. Clin. Invest.* **115,** 755–764
11. Busch, R., Kim, Y. K., Neese, R. A., Schade-Serin, V., Collins, M., Awada, M., Gardner, J. L., Beysen, C., Marino, M. E., Misell, L. M., and Hellerstein, M. K. (2006) Measurement of protein turnover rates by heavy water labeling of nonessential amino acids. *Biochim. Biophys. Acta* **1760,** 730–744
12. Lindwall, G., Hsieh, E. A., Misell, L. M., Chai, C. M., Turner, S. M., and Hellerstein, M. K. (2006) Heavy water labeling of keratin as a non-invasive biomarker of skin turnover in vivo in rodents and humans. *J. Invest. Dermatol.* **126,** 841–848
13. Yuan, C. L., Sharma, N., Gilge, D. A., Stanley, W. C., Li, Y., Hatzoglou, M., and Previs, S. F. (2008) Preserved protein synthesis in the heart in response to acute fasting and chronic food restriction despite reductions in liver and skeletal muscle. *Am. J. Physiol. Endocrinol. Metab.* **295,** E216–E222
14. Dufner, D. A., Bederman, I. R., Brunengraber, D. Z., Rachdaoui, N., Ismail-Beigi, F., Siegfried, B. A., Kimball, S. R., and Previs, S. F. (2005) Using ^2H_2O to study the influence of feeding on protein synthesis: effect of isotope equilibration *in vivo* vs. in cell culture. *Am. J. Physiol. Endocrinol. Metab.* **288,** E1277–E1283
15. Xiao, G. G., Garg, M., Lim, S., Wong, D., Go, V. L., and Lee, W. N. P. (2008) Determination of protein synthesis in vivo using labeling from deuterated water and analysis of MALDI-TOF spectrum. *J. Appl. Physiol.* **104,** 828–836
16. De Riva, A., Deery, M. J., McDonald, S., Lund, T., and Busch, R. (2010) Measurement of protein synthesis using heavy water labeling and peptide mass spectrometry: discrimination between major histocompatibility complex allotypes. *Anal. Biochem.* **403,** 1–12
17. Kasumov, T., Ilchenko, S., Li, L., Rachdaoui, N., Sadygov, R. G., Willard, B., McCullough, A. J., and Previs, S. (2011) Measuring protein synthesis using metabolic ^2H labeling, high-resolution mass spectrometry, and an algorithm. *Anal. Biochem.* **412,** 47–55
18. Price, J. C., Holmes, W. E., Li, K. W., Floreani, N. A., Neese, R. A., Turner, S. M., and Hellerstein, M. K. (2012) Measurement of human plasma proteome dynamics with ^2H_2O and liquid chromatography tandem mass spectrometry. *Anal. Biochem.* **420,** 73–83
19. Zhang, J., Li, X. H., Mueller, M., Wang, Y. J., Zong, C. G., Deng, N., Vondriska, T. M., Liem, D. A., Yang, J. I., Korge, P., Honda, H., Weiss, J. N., Apweiler, R., and Ping, P. (2008) Systematic characterization of the murine mitochondrial proteome using functionally validated cardiac mitochondria. *Proteomics* **8,** 1564–1575
20. Price, J. C., Guan, S. H., Burlingame, A., Prusiner, S. B., and Ghaemmaghami, S. (2010) Analysis of proteome dynamics in the mouse brain. *Proc. Natl. Acad. Sci. U.S.A.* **107,** 14508–14513
21. Claydon, A. J., Thom, M. D., Hurst, J. L., and Beynon, R. J. (2012) Protein turnover: measurement of proteome dynamics by whole animal metabolic labelling with stable isotope labelled amino acids. *Proteomics* **12,** 1194–1206
22. Commerford, S. L., Carsten, A. L., and Cronkite, E. P. (1982) Histone turnover within non-proliferating cells. *Proc. Natl. Acad. Sci. U.S.A.* **79,** 1163–1165
23. Rogers, S., Wells, R., and Rechsteiner, M. (1986) Amino-acid-sequences common to rapidly degraded proteins—the PEST hypothesis. *Science* **234,** 364–368
24. Tompa, P., Prilusky, J., Silman, I., and Sussman, J. L. (2008) Structural disorder serves as a weak signal for intracellular protein degradation. *Proteins* **71,** 903–909
25. Doherty, M. K., Hammond, D. E., Clague, M. J., Gaskell, S. J., and Beynon, R. J. (2009) Turnover of the human proteome: determination of protein intracellular stability by dynamic SILAC. *J. Proteome Res.* **8,** 104–112
26. Lau, E., Wang, D., Zhang, J., Yu, H., Lam, M. P. Y., Liang, X., Zong, N., Kim, T.-Y., and Ping, P. (2012) Substrate- and isoform-specific proteome stability in normal and stressed cardiac mitochondria. *Circ. Res.* **110,** 1174–1178
27. Savas, J. N., Toyama, B. H., Xu, T., Yates, J. R., and Hetzer, M. W. (2012) Extremely long-lived nuclear pore proteins in the rat brain. *Science* **335,** 942
28. Janssen, R. J., Nijtmans, L. G., van den Heuvel, L. P., and Smeitink, J. A. M. (2006) Mitochondrial complex I: structure, function and pathology. *J. Inherit. Metab. Dis.* **29,** 499–515
29. Gottlieb, R. A., and Carreira, R. S. (2010) Autophagy in health and disease. 5. Mitophagy as a way of life. *Am. J. Physiol. Cell Physiol.* **299,** C203–C210

Metabolic Labeling Reveals Proteome Dynamics of Mouse Mitochondria

This online Supplemental Material contains 4 figures and 1 table.

Supplemental Figure S1. Fractional synthesis of analyzed cardiac mitochondrial proteins as a function of time follows first-order kinetics. This figure contains the individual kinetic curves for all 314 proteins analyzed in cardiac mitochondria.

Supplemental Figure S2. Fractional synthesis of analyzed hepatic mitochondrial proteins as a function of time follows first-order kinetics. This figure contains the individual kinetic curves for all 386 proteins analyzed in hepatic mitochondria.

Supplemental Figure S3. Correlation between protein turnover rates and biophysical parameters. This figure plots mitochondrial protein turnover in both organs as functions of four protein biophysical parameters: relative abundance, molecular weight, isoelectric point, and hydrophobicity.

Supplemental Figure S4. Histogram of the standard errors in the rate constants for cardiac mitochondrial proteins. This figure portrays a comparison between the errors in rate constants as determined by non-linear curve fitting and the Monte Carlo method.

Supplemental Figure S5. Mitochondrial protein turnover rates in the heart and the liver. This figure shows the protein turnover rates (*k*) of all analyzed mitochondrial proteins in the heart and the liver on linear, non-logarithmic scale.

Supplemental Table S1. Raw kinetic data determined in our mitochondrial protein turnover study using heavy water. This standalone Excel spreadsheet file contains all the raw kinetic data in this study as well as relevant information including standard errors and protein annotations.

Supplemental Table S1 can be found at:

http://www.mcponline.org/content/11/12/1586/suppl/DC1

Supplemental Fig. S1. Fractional synthesis of analyzed cardiac mitochondrial proteins as a function of time follows first-order kinetics.

The fractional syntheses of all 314 proteins analyzed in cardiac mitochondria are listed. Each data point represents the experimentally measured relative abundance of a single mass isotopomer belonging to one of the constituent peptides of the protein at a particular time point. A first-order kinetics model was fitted to the data points using non-linear least-squares to derive the rate constant *k*. The standard error of *k* was calculated stochastically using the Monte Carlo method, by assuming a distribution for the absolute value of the residuals from fitting.

24 proteins out of 314 are shown as an example.

Complete Supplemental Fig. S1 can be found at:

http://www.mcponline.org/content/suppl/2012/08/21/M112.021162.DC1/mcp.M112.021162-1.pdf

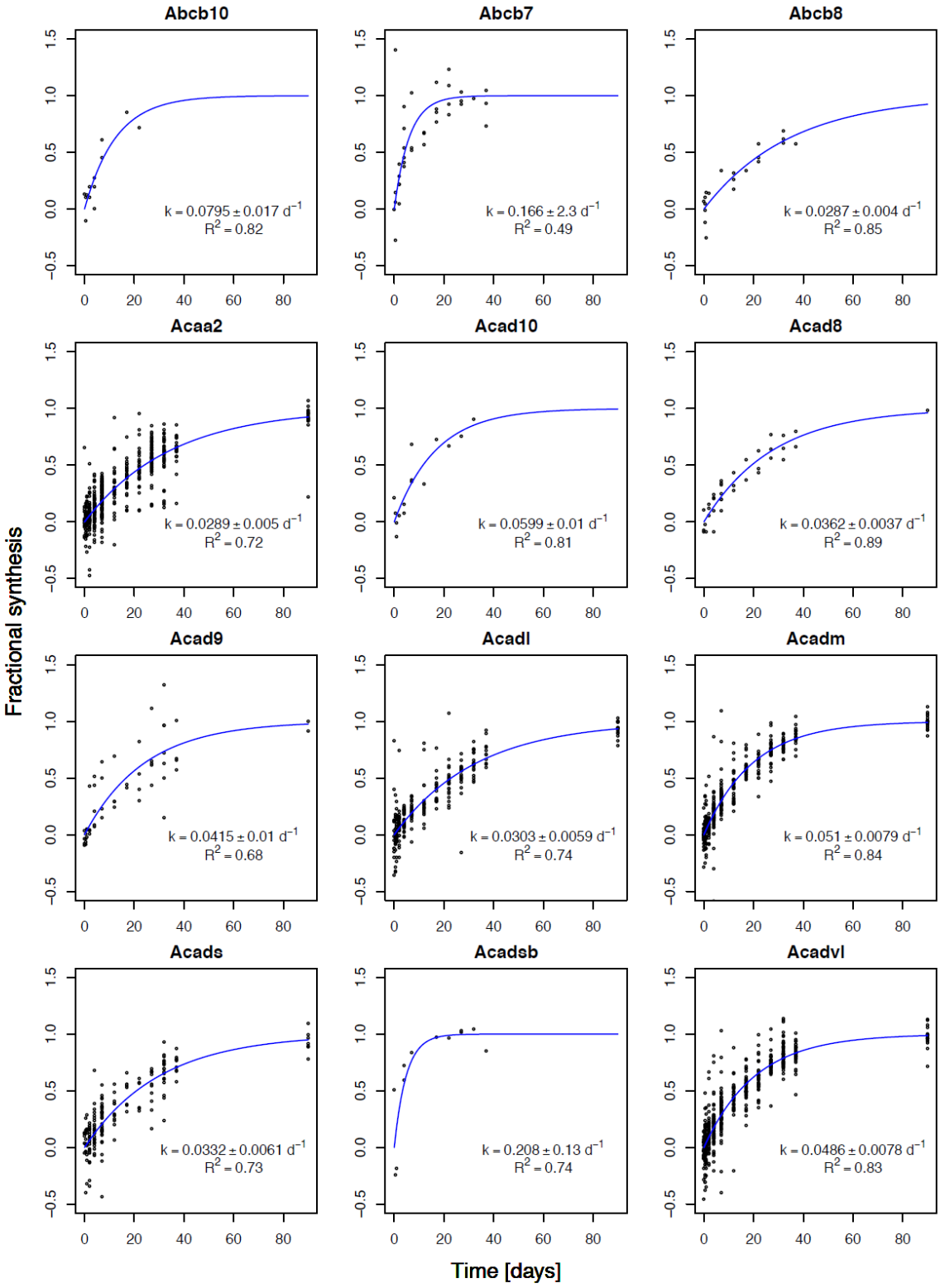
Abcb10
k = 0.0795 ± 0.017 d−1
R2 = 0.82
Abcb7
k = 0.166 ± 2.3 d−1
R2 = 0.49
Abcb8
k = 0.0287 ± 0.004 d−1
R2 = 0.85
Acaa2
k = 0.0289 ± 0.005 d−1
R2 = 0.72
Acad10
k = 0.0599 ± 0.01 d−1
R2 = 0.81
Acad8
k = 0.0362 ± 0.0037 d−1
R2 = 0.89
Acad9
k = 0.0415 ± 0.01 d−1
R2 = 0.68
Acadl
k = 0.0303 ± 0.0059 d−1
R2 = 0.74
Acadm
k = 0.051 ± 0.0079 d−1
R2 = 0.84
Acads
k = 0.0332 ± 0.0061 d−1
R2 = 0.73
Acadsb
k = 0.208 ± 0.13 d−1
R2 = 0.74
Acadvl
k = 0.0486 ± 0.0078 d−1
R2 = 0.83
Fractional synthesis
Time [days]

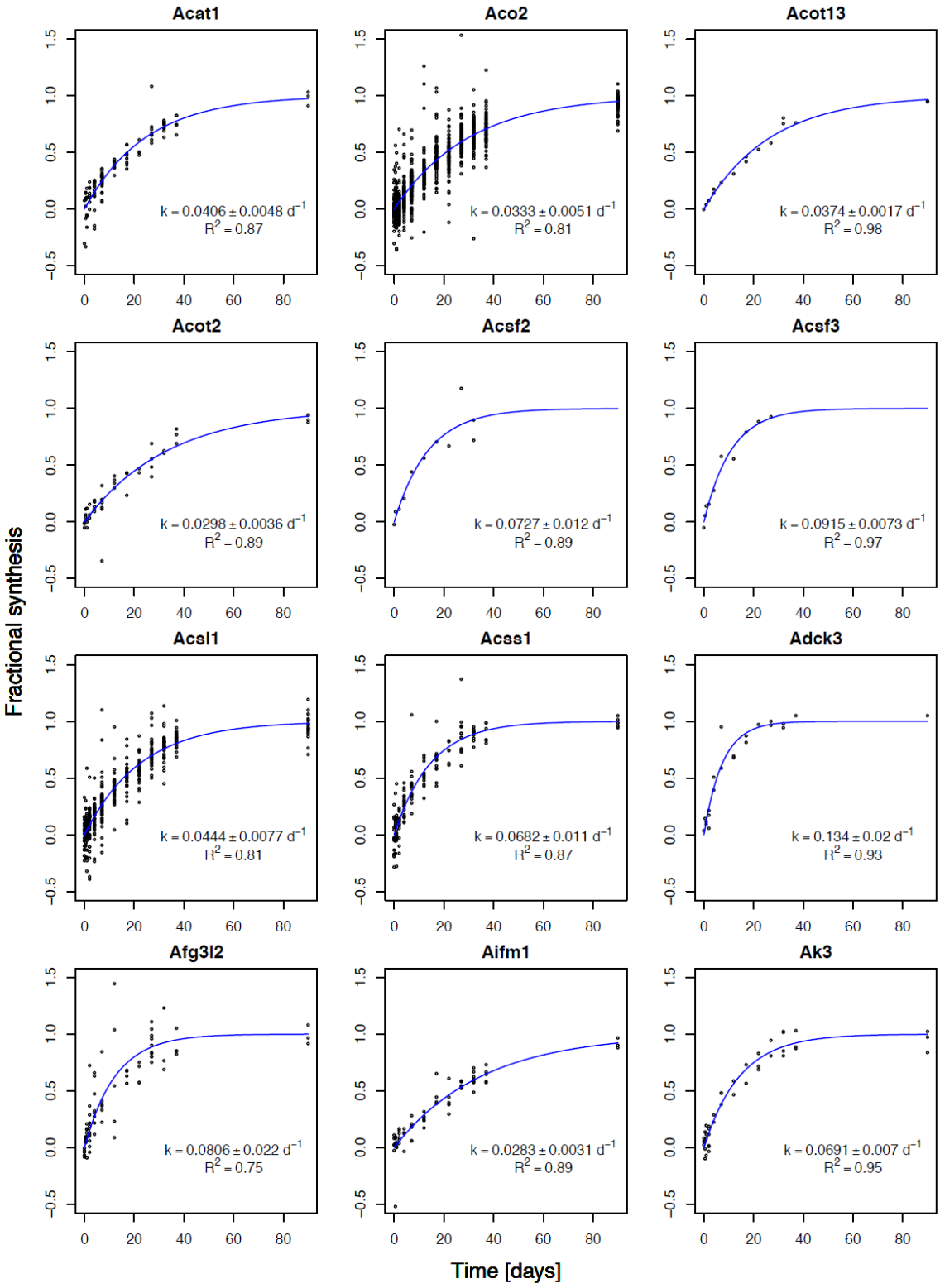
Acat1
k = 0.0406 ± 0.0048 d−1
R2 = 0.87
Aco2
k = 0.0333 ± 0.0051 d−1
R2 = 0.81
Acot13
k = 0.0374 ± 0.0017 d−1
R2 = 0.98
Acot2
k = 0.0298 ± 0.0036 d−1
R2 = 0.89
Acsf2
k = 0.0727 ± 0.012 d−1
R2 = 0.89
Acsf3
k = 0.0915 ± 0.0073 d−1
R2 = 0.97
Acsl1
k = 0.0444 ± 0.0077 d−1
R2 = 0.81
Acss1
k = 0.0682 ± 0.011 d−1
R2 = 0.87
Adck3
k = 0.134 ± 0.02 d−1
R2 = 0.93
Afg3l2
k = 0.0806 ± 0.022 d−1
R2 = 0.75
Aifm1
k = 0.0283 ± 0.0031 d−1
R2 = 0.89
Ak3
k = 0.0691 ± 0.007 d−1
R2 = 0.95
Fractional synthesis
Time [days]

Supplemental Fig. S2. Fractional synthesis of analyzed hepatic mitochondrial proteins as a function of time follows first-order kinetics.

The fractional syntheses of all 386 proteins analyzed in hepatic mitochondria are listed. Each data point represents the experimentally measured relative abundance of a single mass isotopomer belonging to one of the constituent peptides of the protein at a particular time point. A first-order kinetics model was fitted to the data points using non-linear least-squares to derive the rate constant *k*. The standard error of *k* was calculated stochastically using the Monte Carlo method, by assuming a distribution for the absolute value of the residuals from fitting.

24 proteins out of 386 are shown as an example.

Complete Supplemental Fig. S2 can be found at:

http://www.mcponline.org/content/suppl/2012/08/21/M112.021162.DC1/mcp.M112.021162-1.pdf

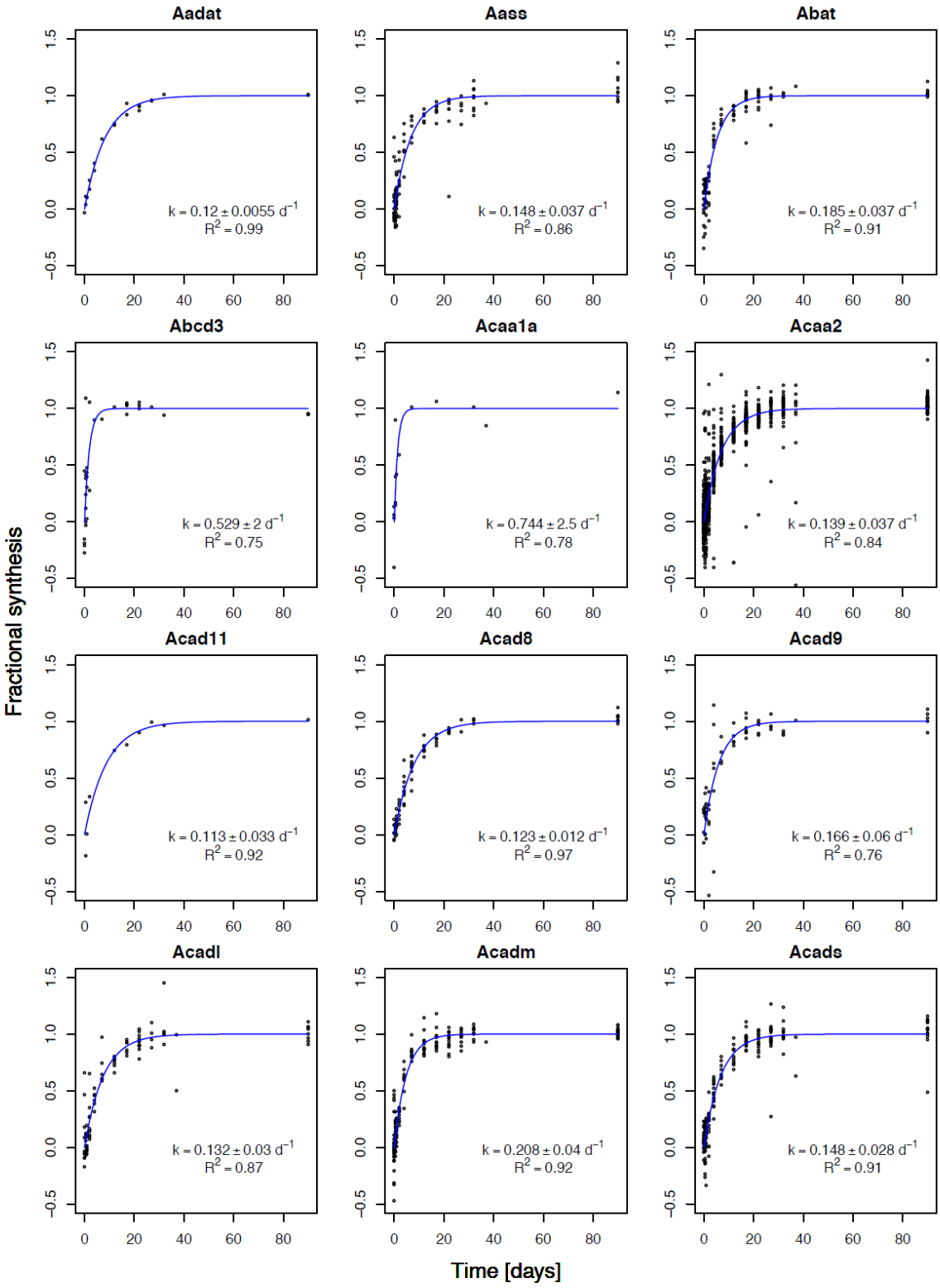
Aadat
k = 0.12 ± 0.0055 d−1
R2 = 0.99
Aass
k = 0.148 ± 0.037 d−1
R2 = 0.86
Abat
k = 0.185 ± 0.037 d−1
R2 = 0.91
Abcd3
k = 0.529 ± 2 d−1
R2 = 0.75
Acaa1a
k = 0.744 ± 2.5 d−1
R2 = 0.78
Acaa2
k = 0.139 ± 0.037 d−1
R2 = 0.84
Acad11
k = 0.113 ± 0.033 d−1
R2 = 0.92
Acad8
k = 0.123 ± 0.012 d−1
R2 = 0.97
Acad9
k = 0.166 ± 0.06 d−1
R2 = 0.76
Acadl
k = 0.132 ± 0.03 d−1
R2 = 0.87
Acadm
k = 0.208 ± 0.04 d−1
R2 = 0.92
Acads
k = 0.148 ± 0.028 d−1
R2 = 0.91
Fractional synthesis
Time [days]

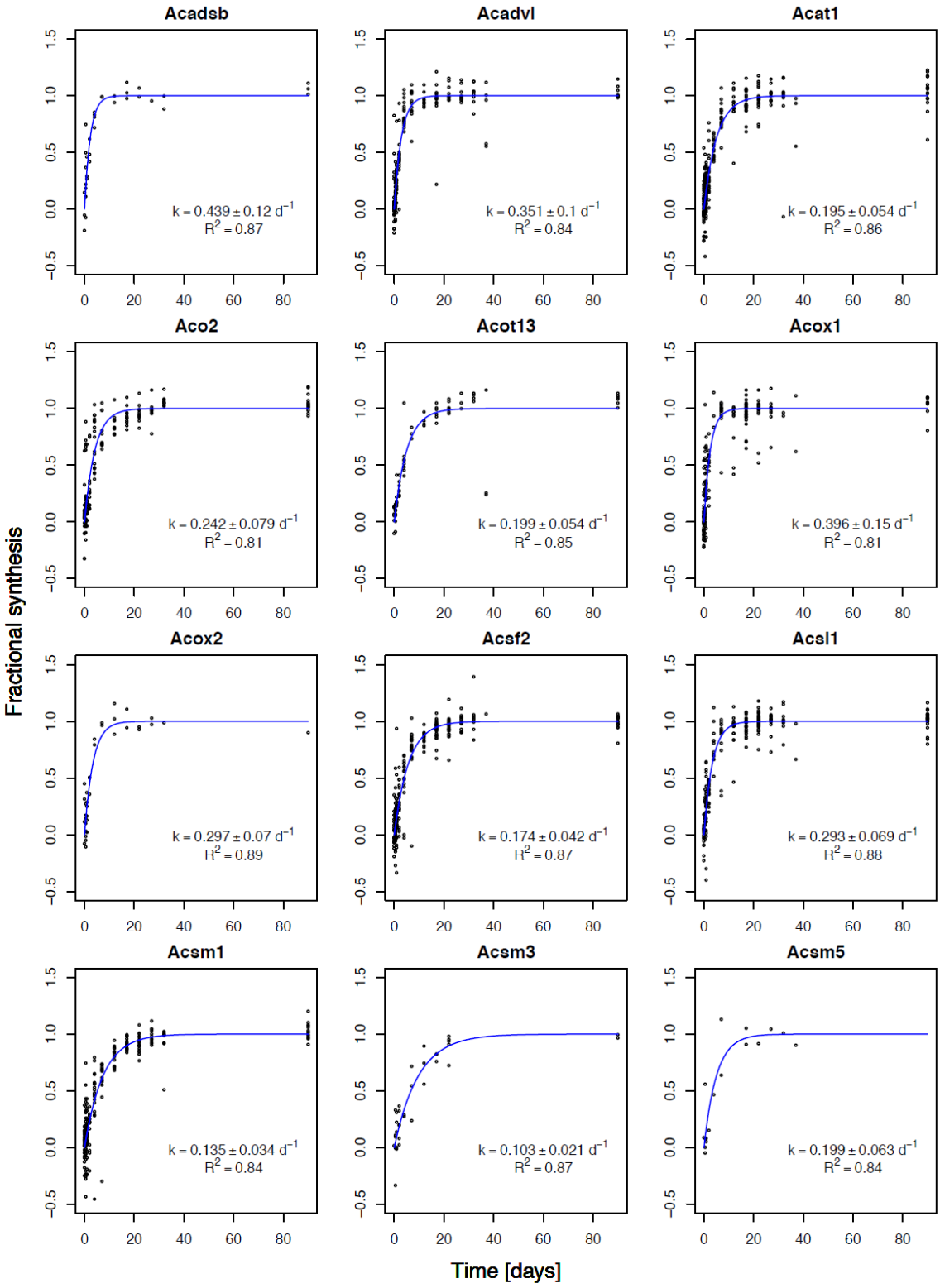
Acadsb
k = 0.439 ± 0.12 d−1
R2 = 0.87
Acadvl
k = 0.351 ± 0.1 d−1
R2 = 0.84
Acat1
k = 0.195 ± 0.054 d−1
R2 = 0.86
Aco2
k = 0.242 ± 0.079 d−1
R2 = 0.81
Acot13
k = 0.199 ± 0.054 d−1
R2 = 0.85
Acox1
k = 0.396 ± 0.15 d−1
R2 = 0.81
Acox2
k = 0.297 ± 0.07 d−1
R2 = 0.89
Acsf2
k = 0.174 ± 0.042 d−1
R2 = 0.87
Acsl1
k = 0.293 ± 0.069 d−1
R2 = 0.88
Acsm1
k = 0.135 ± 0.034 d−1
R2 = 0.84
Acsm3
k = 0.103 ± 0.021 d−1
R2 = 0.87
Acsm5
k = 0.199 ± 0.063 d−1
R2 = 0.84
Fractional synthesis
Time [days]

Supplemental Fig. S3. Correlation between protein turnover rates and biophysical parameters.

(A) A weak inverse correlation was observed between protein turnover rate and relative protein abundance (heart: ρ = -0.46, $P < 2.2 \times 10^{-16}$ and liver: ρ = -0.19, $P = 7.95 \times 10^{-3}$), suggesting abundant proteins are turned over more slowly in general. The relative abundance of a protein was determined by the summation of total chromatographic areas of the constituent peptide ion peaks divided by the areas of all identified peptide ions in the experimental dataset using Progenesis LC-MS (Ver. 4.0.4441.29989, Nonlinear Dynamics). By contrast, we observed no significant correlations in either tissue between protein turnover rates and their molecular weights (B), or their isoelectric points (C), or their hydrophobicities (D).

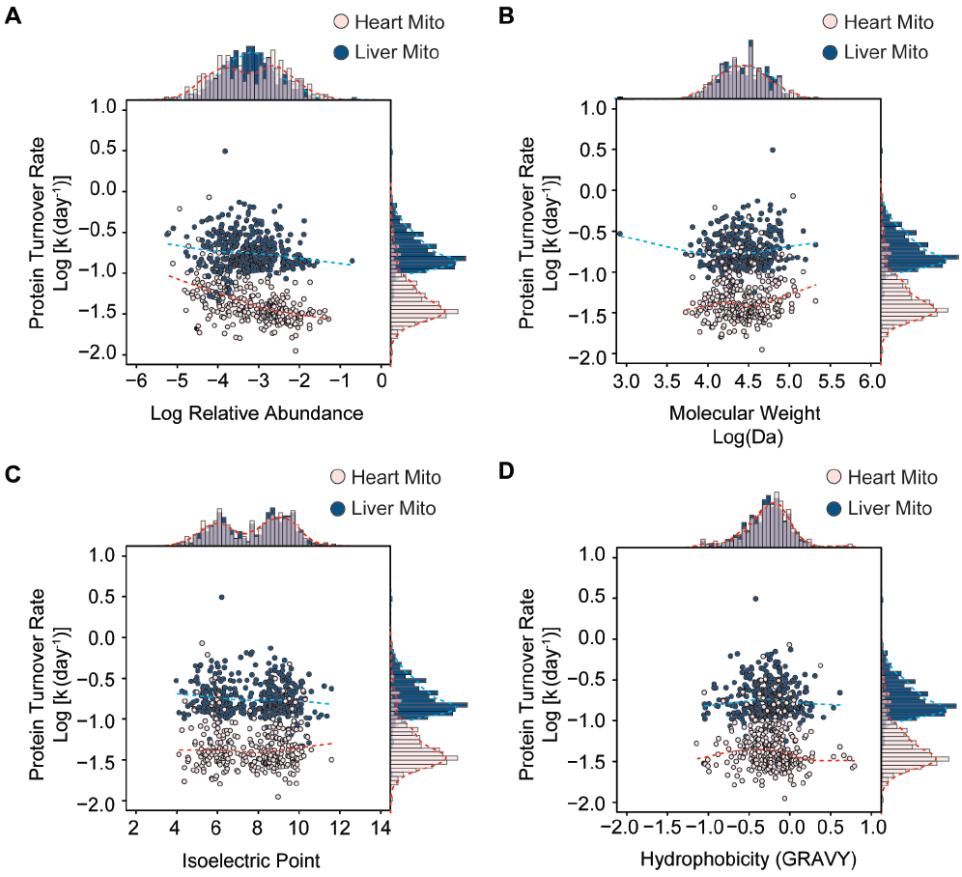

Supplemental Fig. S4. Histograms of the standard errors in the rate constants for cardiac mitochondria proteins.

The standard errors (σ_k) in the rate constants for cardiac mitochondrial protein turnover were calculated using both the Monte Carlo and the Non-linear curve fitting methods. The distributions of the standard errors are not significantly different, although the Monte Carlo method is more conservative in the estimated errors.

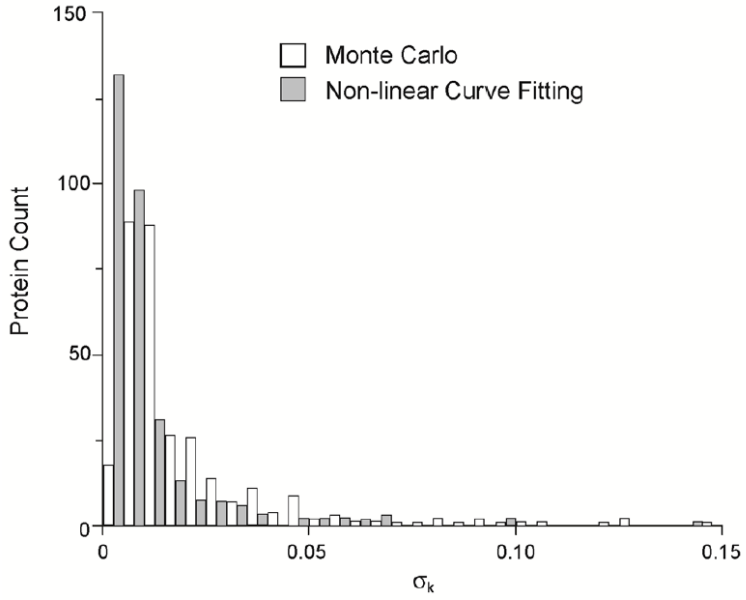

Supplemental Fig. S5. Mitochondrial protein turnover rates in the heart and the liver.

The protein turnover rates (*k*) of all analyzed murine mitochondrial proteins in the liver and in the heart are displayed on linear, non-logarithmic scale based on protein functional categories. The median turnover rates in the heart and the liver were 0.04 and 0.163 d^{-1}, respectively. The number in the parenthesis represents the total number of proteins belonging to a functional category. Cardiac and hepatic mitochondrial proteins are indicated in red and blue dots, respectively.

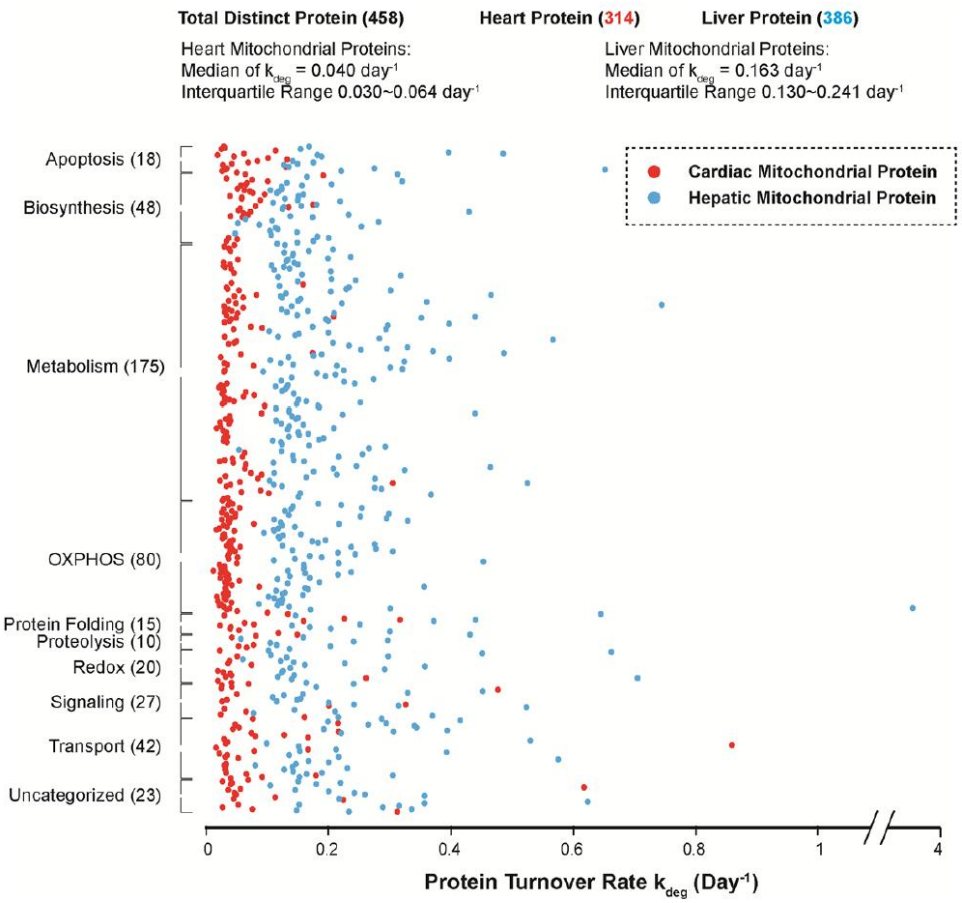

CHAPTER 4

Sexual Dimorphisms in HSP72-mediated Control of Mitochondrial Function and Insulin Sensitivity

4.1 Introduction

Insulin resistance is a defining feature of the metabolic syndrome and is an early underpinning involved in the pathogenesis of type 2 diabetes mellitus (T2DM). Insulin resistance is characterized by diminished insulin action in peripheral tissues including skeletal muscle, liver, and adipose tissue[1-4]. The onset and severity of T2DM has been correlated with age, genetics, and sex[5]. Since men and women diverge in susceptibility to insulin resistance and T2DM, with men showing a higher prevalence of insulin resistance and T2DM vs age-matched premenopausal women[6-8], it is important to understand the mechanisms underlying sexual dimorphisms in metabolism and disease susceptibility. Understanding the biology underlying sex differences related to metabolic disease pathobiology will aid in the development of novel sex-specific therapeutic interventions for diseases including T2DM.

While the precise molecular mechanisms involved in the etiology of insulin resistance are not fully understood, many agree that inflammation and stress kinase activation impair insulin signal transduction[9-14]. The primary cellular defense against metabolic and inflammatory insult is the rapid synthesis of a family of chaperone proteins (heat shock proteins, HSPs) by the induction of heat shock transcription factor 1 (HSF1). Impaired heat shock protein response to cellular stress is thought to underlie chronic disease susceptibility[15-18], and this notion is supported by the observation that expression of the inducible HSP isoform, HSP72, is significantly diminished in obese

patients with T2DM, while conversely, expression levels are elevated in healthy endurance trained individuals[19-24].

Previous evidence reveals that an impaired HSP response to cellular stress underlies insulin resistance and T2DM[15-18]. We have shown that HSP72, a protein chaperone that facilitates the proper folding of newly translated and misfolded proteins, is associated with the maintenance of insulin sensitivity. Reduced protein abundance of HSP72 promotes dysfunctional mitochondria and insulin resistance in rodents and is associated with metabolic dysfunction in humans[20-22]. HSP72 is the most highly induced HSP in response to cellular stress and chronic endurance exercise[20], however its precise role in regulating metabolic homeostasis and insulin action is incompletely understood. We have previously shown that HSP72 translocates to depolarized mitochondria and regulates the E3 ubiquitin ligase Parkin, a protein involved in mitochondrial quality control[20]. Male mice with an HSP72 knockout mutation (HSP72 KO) exhibit reduced fatty acid oxidation, increased reactive oxygen species (ROS) production, and impaired insulin action[20]. This phenotype occurred at least in part as a consequence of accumulation of dysfunctional hyperfused mitochondria and impaired Parkin action in skeletal muscle[25-29]. In the absence of HSP72, Parkin accumulates in the cytosol and fails to translocate to mitochondria to promote mitophagy. We attributed the increase in adiposity of HSP72 KO mice to reduced oxidative metabolism in skeletal muscle. In contrast, in animals with muscle-specific overexpression of HSP72, we observed protection against genetic- and diet-induced obesity and insulin resistance[22]. Although strong correlations between

HSP72 expression, adiposity, and insulin sensitivity are well-established[19-22], these observations have only been shown in men and male rodents. Therefore, to improve our understanding of the effect of sex on HSP72 expression and metabolic homeostasis, we experimentally reduced HSP72 in female mice and cells by genetic means to determine whether HSP72 serves a similar role in regulating metabolism between the sexes. In contrast to male HSP72 KO mice, herein we show that female HSP72 KO mice are lean, glucose tolerant, and have enhanced insulin sensitivity. Moreover, although a similar elevation of muscle Parkin was observed in female and male HSP72 KO mice, females were protected against metabolic dysfunction that we surmise is a consequence of impaired mitophagy in male KO animals. In female HSP72 KO mice, we observed increased ERα expression and mitochondrial fission signaling. We show increased muscle oxidative function paralleled by enhanced insulin sensitivity even under the basal, normal chow-fed condition. Thus, our findings suggest a novel sex-specific role for HSP72 in the regulation of skeletal muscle mitochondrial function and insulin action. Our data support the notion that sex is an important biological variable of important consideration when testing and validating molecular targets of therapeutic potential.

4.2 Research Design and Methods

Animals

Female wild-type (WT) and HSP72 KO (global null mutation of Hspa1a/Hspa1b genes; Mutant Mouse Regional Resource Center Repository; University of California, Davis). WT and KO animals were confirmed to be of pure C57BL/6 background (The Jackson Laboratory). Ten cohorts of HSP72 KO mice were bred at the University of California, Los Angeles (UCLA) and used for *in vivo* and *ex vivo* investigation. All procedures were performed in accordance with the Guide for Care and Use of Laboratory Animals of the National Institutes of Health and were approved by the Animal Subjects Committee of UCLA. Animals were studied in the 6-h fasted condition unless otherwise specified, for example fed or starved (24 h).

Leupeptin Treatment Studies

To assess whether Parkin protein is degraded by the lysosome under basal conditions, 6-h fasted WT mice were treated for 1 h with leupeptin (L2884, Sigma-Aldrich; 40 mg/kg; intraperitoneal injection) to inhibit lysosomal proteases. Quadricep and soleus muscles were harvested for LC3B immunoblot analyses.

Circulating Factors, Glucose Tolerance, and Ambulatory Movement

The circulating factors insulin, leptin, resistin (Multiplex, Millipore), and adiponectin were analyzed in the blood of 6-h fasted 8-, 20-, 28-week-old mice. Intraperitoneal glucose tolerance tests (GTTs; 1 g/kg dextrose) were performed on the 6-h fasted mice[30, 31]. Mice from a separate cohort were acclimated to their metabolic chambers (Columbus Instruments) for the initial 24 hours, and their ambulatory movement was recorded for 48 hours.

Hyperinsulinemic-Euglycemic Clamp Studies

At 28 weeks of age, dual catheters were surgically placed in the right jugular vein. 3 days post surgery, glucose clamp studies were performed as previously described[30-32].

Muscle Fatty Acid Oxidation and Esterification

Fatty acid oxidation and esterification assays were performed on isolated soleus muscle; detailed methodology previous described in[33].

Primary Skeletal Muscle Cells

Primary skeletal muscle myoblasts were isolated from WT and HSP72 KO mice at 8–12 weeks of age, as previously described[34]. Myoblasts were cultured to confluence then differentiated to myotubes in Dulbecco's modified Eagle's medium (DMEM)/5% horse serum for 5–7 days prior to experimentation.

Cell Culture and Treatments

C2C12 myoblasts (ATCC) were maintained and proliferated in DMEM/10% FBS and differentiated in DMEM/2% horse serum.

Insulin-Stimulated 2-Deoxyglucose Uptake Into Myocytes

Glucose uptake was performed on cultured skeletal muscle cell in 12-well culture plates using the 2-deoxyglucose method in[32].

Fatty Acid Oxidation and Esterification in Cultured Muscle Cells

Fatty acid oxidation and esterification in cultured skeletal muscle cells were performed in six-well culture plates, as previously described[32].

Ex Vivo Soleus Muscle Strip Glucose Uptake

Whole muscle ex vivo glucose uptake was analyzed with 2-deoxyglucose, with minor changes to that described previously[32, 35].

Mitochondria Isolations

Two separate techniques were used to isolate mitochondria from WT and HSP72 KO skeletal muscle: 1) a Dounce homogenizer and the Mitochondria Isolation Kit for Cultured Cells (Thermo Scientific) and 2) by percoll density method[36]. Quadriceps were washed in ice-cold PBS. A Dounce homogenizer (25 strokes) broke up the tissue and fragments of the cell were pelleted at 800g for 10 min at 4°C. Subsequently, mitochondria in the supernatant were pelleted at 12,000g for 15 min at 4°C and washed twice with isolation buffer.

Mitochondrial Respiration from Isolated Mitochondria

Mitochondrial respiration (oxygen consumption) from mitochondria isolated from skeletal muscle was assessed using an XF96 Extracellular Flux Analyzer (Seahorse Biosciences). Crude mitochondrial isolations were prepared to maintain high mitochondrial respiratory function. Mitochondrial respiration was measured using an

XF96 Extracellular Flux Analyzer. Skeletal muscle were loaded in the XF96 microplate at 4.5-6 µg/well for Complex I-driven respiration (pyruvate and malate) and 2.5-4 µg/well for Complex II-driven respiration (succinate and rotenone) in 20 µl of respective substrates and mitochondrial assay solution (MAS) per well. The plate was centrifuged 2,400 g for 5 minutes at 4°C before 130µl of MAS was carefully added per well and the plates were incubated at 37°C for 5 min. MAS buffer contained 70mM sucrose, 220mM mannitol, 5mM KH_2PO_4, 5mM MgCl2, 2mM HEPES, 1mM EGTA, 0.1% BSA fatty acid-free (pH 7.2 adjusted with KOH) and substrates were used at concentrations of: 5mM pyruvate, 5 mM malate, 5 mM succinate, and 2µM rotenone. Mitochondria were loaded into the XF96 instrument and the first oxygen consumption measure was taken with substrates only (State 2) prior to the injection of 2mM ADP to induce State 3 respiration. Additional injections included 3µM oligomycin from Port B for State 4o, 4µM FCCP from Port C to measure uncoupled respiration, and Antimycin A at 4µM from Port D to inhibit mitochondrial oxygen consumption. All analyzed oxygen consumption data are normalized to µg protein loaded per well (pmoles O2/min/µg protein).

Muscle Fiber Respiration

Muscle fibers were separated and permeabilized with saponin. Muscle fibers of similar masses were placed in an Oroboros Oxygraph-2k (Oroboros Instruments). Substrates added to assess respiration included malate, octanoylcarnitate, ADP, Cytochrome C, pyruvate, glutamate, succinate, CCCP, rotenone, and Antimycin A. Samples with impaired mitochondrial membrane integrity (using a +10% increase threshold in respiration after cytochrome c addition) were excluded.

Mass Spectrometry (MS) and Data Analyses

Mitochondria were isolated using the above isolation procedure. Mitochondrial pellets were resuspended in lysis buffer (0.5% sodium deoxycholate, 12mM sodium lauroyl sarcosine, and 50mM triethylammonium bicarbonate) prior to in-solution trypic digestion. Stable-isotopic dimethyl labeling of the peptides was utilized to provide relative quantitation between male and female proteomes. The samples were fractionated via strong cation exchange (SCX) chromatography for global proteomic analysis. Peptides were injected onto a laser-pulled nanobore C18 column with 1.8 um beads and resolved using a 3 hour gradient optimized on a hybrid quadrupole-Orbitrap mass spectrometer in dd-MS2 mode. The raw data were analyzed in Proteome Discoverer 2.1, which provided measurements of abundance for the identified peptides. Uniprot[37] was used to convert MS IDs to protein IDs. Biological information of individual proteins was extrapolated from gene ontology (GO) biological processes and molecular functions annotations. The polarHistogram function in R, a software for statistical computing and graphics, was used to illustrate proteins significantly changed between the genotypes in a polar histogram. Data was also run through g:Profiler[38] and PANTHER[39] for functional profiling of the mitochondrial proteome.

Electron Microscopy

Fresh soleus tissue was harvested and placed in 2% glutaraldehyde in PBS for 2 hours at room temperature and then at 4°C overnight. Fixed tissues were washed and post-fixed the following day in a solution of 1% OsO4 for 2 hours. Tissues were dehydrated,

embedded in pure epon 812, and cured (60°C for 48 hours). Muscle longitudinal sections of 60 nm thickness were cut using an ultramicrotome (RMC MTX). The tissue sections were double stained in 8% uranyl acetate for 25 min at 60°C and lead citrate for 3 min at room temperature. A 100CX JEOL electron microscope was used to examine the stained slices.

Immunoprecipitation and Immunoblot Analysis

Mouse tissues and cell cultures for immunoblotting were homogenized in RIPA lysis buffer containing protease and phosphatase inhibitors before being clarified and resolved by SDS-PAGE. Proteins for immunoprecipitations were solubilized in RIPA containing deoxycholate, 1% glycerol, and protease inhibitors by rotation at 4°C for 1 h, then cell debris were pelleted for 10 min at 5,000g. Total protein was measured, and 500 µg of sample was incubated with antibody (HSP72, Enzo Life Sciences) overnight then immobilized on Pierce™ Protein A/G Magnetic Beads (Thermo Scientific) for 2 h at 4°C prior to washing 3× in RIPA buffer. Proteins were resolved by SDS-PAGE. All samples for Western blotting were transferred to polyvinylidene fluoride membranes and probed with the following antibodies: HSP72 (Stressgen), ERα exon III MC-20 (Santa Cruz), glyceraldehyde-3-phosphate dehydrogenase (Millipore), p62 (ProGen), phosphatase and tensin homolog–induced putative kinase 1 (PINK1; Cayman Chemicals), DJ-1/Park7 (R&D Systems), Mfn2 (Abcam), porin/voltage-dependent anion channel (MitoSciences), Ubiquitin-FK2 (Enzo Life Sciences), HA-mouse (Covance), V5 (Invitrogen), DNAJB2 (Protein Tech Group), and cABL (BD Pharmingen). The following antibodies were all from Cell Signaling Technologies: pSer473-Akt (#9271), Parkin

(#2132 & #4211), pan-actin, LC3B, Beclin1, LAMP1, HSP60, HSP90, and HA-rabbit. Densitometric analyses were performed using BioRad Chemidoc Quantity One image software.

Muscle Lipid Intermediates and Lipidomics Analyses

Triacylglycerol, diacylglycerol, and ceramides were extracted from the quadriceps muscle (n = 6 per genotype) and quantified as previously described[40-42]. Lipidomic analyses were performed by the Baker IDI Lipidomics Core on quadriceps homogenized in 300 µl PBS buffer, pH 7.47 according to previous methods, with modifications[43].

RNA Extraction, cDNA, and Quantitative RT-PCR

RNA from tissues and cells was extracted using RNeasy columns as per manufacturer's instructions (Qiagen). cDNA was synthesized from 1 µg of total RNA using SuperScript II as per manufacturer's instructions (Invitrogen). qPCR was performed on 20 ng cDNA on a BioRad MyiQ PCR Detection System using SyBR Green chemistry and analyzed using iQ5 Software (BioRad version 2.1) as previously described[32].

Statistics

Values presented are expressed as means ± SEM. Statistical analyses were performed using Student t tests as well as one- and two-way ANOVA with Tukey's post hoc comparison for identification of significance within and between groups where appropriate (SPSS graduate pack, Chicago, IL). Significance was set a priori at $p < 0.05$.

4.3 Results

HSP72 Regulates Insulin Action in a Sexually Dimorphic Manner

A global null mutation of Hspa1a/Hspa1b genes was used to create a HSP72 KO mouse and was compared to WT female littermates under basal normal chow-fed conditions. In contrast to observations in male HSP72 KO mice[20], female HSP72 KO mice demonstrated lower total body weight (**Figure 2A**), and reduced white adipose tissue (WAT), and liver mass compared to age-matched (8.5-10 months old) wild-type (WT) female mice (**Figure 2B**). This phenotype was recapitulated in aged (12.5-15 months old) female mice (**Figure 2C-D**). Since we observed a difference in body weight between the genotypes, we chose to perform glucose tolerance testing on weight-matched animals. Enhanced glucose tolerance was observed in female KO vs. WT mice (**Figure 3A**. In parallel to improved glucose tolerance in female KO animals, insulin signal transduction, phosphorylation of GSK-3, a key regulator of glycogen synthesis, and at Akt^{Ser473}, a critical component of the insulin signaling pathway involved in glucose import, was enhanced in female KO mice (**Figure 3B**). Enhanced insulin action was confirmed by the gold standard method for assessment of whole body insulin sensitivity, the hyperinsulinemic-euglycemic clamp. Female KO mice showed enhanced insulin sensitivity compared to female WT mice (**Figure 3C**).

HSP72 Is Critical for Mitochondrial Morphology, Parkin Regulation, and Autophagic Signaling

The role of HSP72 in mitochondrial function and health is well-studied[15, 44-46]. However, these molecular phenotypes have been observed only in male model systems. To investigate the sex-specific relationship between HSP72 and metabolism, we first assessed parameters of mitochondrial health. We have previously identified HSP72 as critical in regulating Parkin action. Although Parkin protein expression was similarly elevated in male and female KO mice (**Figure 4A**), we found that Parkin was incapable of mitochondrial translocation and mitophagic turnover in muscle in male mice. In contrast to the male KO animals, in female HSP72 KOs, Parkin was observed on the outer mitochondrial membrane of damaged organelles thus indicating the maintenance of Parkin functionality in females despite the loss of HSP72 (**Figure 4B**). Protein expression of mitochondrial fission factor (MFF) and mitochondrial fission 1 protein (FIS1), proteins involved in mitochondrial fission, were higher in female HSP72 KO mice compared with WT. While total dynamin-related protein 1 (Drp1), a key GTPase involved in of mitochondrial division, was reduced in the KO female animals compared to WT, phosphorylation of the inhibitory site, serine 637, of Drp1 was also significantly reduced in KO vs. WT (**Figure 4C**). Of interest, although Drp1 protein levels were identical between the groups, mRNA levels for the gene encoding Drp1, *dnm1l*, was significantly increased in female KO skeletal muscle (**Figure 4D**). Protein levels for fusion components (mitofusin 2, Mfn2) were also reduced in the KOs, supporting an enhanced mitochondrial fission phenotype (**Figure 4E**). We assessed mitochondrial

number using a surrogate marker, mtDNA abundance, between female WT and KO mice. Interestingly, qPCR revealed that mtDNA abundance was reduced in muscle of female KO animals (**Figure 4F**). This reduction was further confirmed by the sensitive method Digital Droplet PCR. Electron micrographs (EMs) of female KO mouse muscle showed mitochondria of significantly smaller area and perimeter vs. WT, compared to the enlarged, tubulated, and highly fused mitochondria observed in male HSP72 KO skeletal muscle vs. WT (**Figure 5**). Interestingly, mtDNA abundance was decreased in female KO mice, as were TFAM and PGC1α protein levels (**Figure 6A-B**). Furthermore, mRNA expression of Nrf1, Polg1, and Polrmt was reduced in the female KO skeletal muscle vs. WT (**Figure 6C**). Together, these data suggest that mitochondrial biogenesis is reduced in HSP72 KO females compared with WT. We assessed autophagic flux using leupeptin, and observed increased accumulation of LC3I and LC3II in female KO mice over WT (**Figure 6D**). These data reflect increased autophagic flux in KO compared to WT females and this is in sharp contrast to our findings for male animals. Enhanced fission dynamics and autophagic flux is associated with improved fatty acid oxidation[47] and diminished ROS production[48, 49] since fission is hypothesized to improve mitochondrial bioenergetic efficiency[50] and promote the elimination of dysfunctional mitochondria[51].

Furthermore, to determine the mechanisms underlying improved mitochondrial function, we took a large-scale approach of the mitochondrial proteome and identified changes in individual mitochondrial proteins and their expression levels to provide insight into the remodeling changes in the female WT and KO skeletal muscle mitochondrial proteome

(**Figure 7**). Our proteomic analysis confirmed a decrease in the relative protein abundance of Mfn2 in female KO mice compared to WT mice (**Supplemental Figure 1**). Of interest, only 3 out of the 67 significantly changed proteins were higher expressed in the female KOs: 1) 3-Hydroxybutyrate Dehydrogenase 1(Bdh1) which is a mitochondrial enzyme involved in fatty acid catabolism, 2) Family With Sequence Similarity 162 Member A (Fam162a) is involved in apoptosis, cytochrome c release, and caspase activation, and 3) Nudix Hydrolase 8 (Nudt8) which mediates hydrolysis of nucleoside diphosphate derivatives. Functional analysis using PANTHER[39] revealed that proteins significantly changed between the basal female WT and KO skeletal muscle mitochondria profile were enriched in catalytic activity, binding, structural molecule activity, and antioxidant activity GO molecular function processes. Furthermore, the three highest PANTHER[39] pathways these significant proteins were predominantly involved in were Insulin/IGF pathway-protein kinase B signaling cascade, PI3 kinase pathway, and Gonadotropin-releasing hormone receptor pathway.

HSP72 KO Enhances Compensatory Molecular Mechanisms in Females

Our laboratory has previously shown that in addition to regulating mitochondrial functionality, HSP72 chaperones the estrogen receptor α (ERα) and controls its protein expression in skeletal muscle[52]. We find that the abundance of ERα is elevated in females compared with males, is the predominant receptor expressed in skeletal muscle, and is highly associated with insulin sensitivity[52]. Next, we examined the relationship between HSP72, ERα, mitochondrial health, and metabolism. Work from

our laboratory and others[52, 53] has established that the loss of ERα in both female and male whole-body and muscle-specific KO (MERKO) mouse results in an accumulation of lipids, tissue inflammation, and insulin resistance in skeletal muscle. Interestingly, female and male ERαKO and MERKO skeletal muscle mitochondria exhibited a dysmorphic, hyperfused phenotype and had impaired respiration[52, 53]. To complement these studies, we cultured C2C12 myotubes, a mouse myoblast cell line, with the ERα-selective agonist propyl pyrazole triol (PPT) and showed augmented fission signaling (**Figure 8A**). Together, these data suggest that ERα expression is not only integral in maintaining metabolic homeostasis, but also mitochondrial morphology and functionality. We assessed ERα expression in the female HSP72 WT and KO mice and found that female KO mice have both elevated ERα protein and Esr1 (**Figure 8B**) mRNA levels. In contrast, ERα protein levels were identical between male WT and KO mice (**Figure 8C**).

4.4 Discussion

Sex-specific Regulation of Mitochondrial Dynamics

Proper mitochondrial function is required to maintain metabolic homeostasis and cellular energetic capacity. There is evidence that males and females differ in the regulation of mitochondrial processes. Females possess a higher mitochondrial content and antioxidant activity[54-56]. However, the sex-specific mechanisms that contribute to

mitochondrial dysfunction and insulin resistance in men and women remain unclear. Therefore, determining the underlying differential mechanisms of insulin resistance in men and women will aid in the current understanding of metabolic dysfunction and facilitate the development of novel sex-specific interventions to combat metabolic syndrome.

Previous studies show that imbalanced mitochondrial fission-fusion dynamics promotes the onset of insulin resistance[20, 57-59], impairs mitochondrial bioenergetic capacity, and mitochondrial quality control[51]. The ablation of key fusion and fission proteins, including Mfn2 and Drp1, leads to insulin resistance[60-62]. Mfn2 is an outer mitochondrial membrane protein that mediates mitochondrial fusion and is a target of the E3 ubiquitin ligase Parkin, a protein involved in mitochondrial quality control[21]. Drp1 is a cytosolic GTPase recruited to the mitochondrial outer membrane where it oligomerizes to form high order mitochondrial ribbons around the mitochondrion. Drp1 interacts with pro-fission proteins including mitochondrial fission protein 1 (Fis1) and mitochondrial fission factor (Mff) on the outer mitochondrial membrane to drive the division of a mitochondrion to two daughter organelles[57, 63]. Disrupting the fission and fusion signaling machinery led to obesity and insulin resistance; for example, our laboratory and others have shown that chronic mitochondrial hyperfusion is correlated with metabolic dysfunction[54-56]. These observations highlight the importance of mitochondrial fission-fusion dynamics in maintaining insulin sensitivity.

Sex-specific Regulation of Mitochondrial Dynamics

Recently our laboratory found an important role for HSP72 in skeletal muscle mitochondrial dynamics. We observed that HSP72 translocates to depolarized mitochondria and regulates the functionality of the E3 ubiquitin ligase Parkin. Male HSP72 KO mice exhibited reduced fatty acid oxidation, increased reactive oxygen species (ROS) production, and impaired muscle insulin action[21]. The impairment in muscle oxidative function was paralleled by increased WAT mass in male KO mice. Metabolic dysfunction occurred as a consequence of the accumulation of dysfunctional hyperfused mitochondria and impaired mitophagic flux due to impaired Parkin action[25-29]. In the absence of HSP72, Parkin accumulated in the cytosol (impaired protein autoregulation) and failed to translocate to depolarized mitochondria to induce mitophagy.

Interestingly, although we observed a similar increase in Parkin protein in the cytosol in both HSP72 KO male and female animals, KO female mice showed improved insulin sensitivity and oxidative function compared with WT mice, thus a sex-specific effect of HSP72 in the control of oxidative function and insulin action was observed by our laboratory. The mechanisms underlying these differences in metabolism between males and females) remain largely unknown. However work in collaboration with Jake Lusis[64-68] shows that estrogens contribute markedly to the genetic architecture of insulin sensitivity with females showing enhanced muscle insulin sensitivity over males. Therefore, sex-specific strategies may be delineated to combat diseases in which differing mechanisms contribute to disease pathobiology in women compared with men.

This notion is reinforced by our findings indicating that the loss of HSP72, promotes opposing sex-specific metabolic alterations. In sharp contrast to male HSP72 KO mice that show an obese, insulin resistance phenotype compared to WT males, female HSP72 KO animals relative to WT exhibit reduced adiposity and heightened insulin sensitivity. We have previously shown that HSP72 is a chaperone of ERα and controls its protein expression in skeletal muscle[52]. Herein, we show that reduced HSP72 expression in female mice increases skeletal muscle ERα action which we hypothesize underlies sexually dimorphic outcomes related to mitochondrial function and insulin action. While a striking accumulation of cytosolic Parkin was noted in both male and female HSP72 KO mouse skeletal muscle, the remaining molecular phenotypes differed between the sexes. Specifically, in female KO mice compared to their WT counterparts, we observed elevated ERα levels, the predominant estrogen receptor in skeletal muscle that we have previously shown to be involved in the maintenance of mitochondria and metabolic health[52, 53].

The Absence of HSP72 Increases ERα Expression Levels and Fission Signaling

Two principal forms of ER have been identified to date, ERα and ERβ, encoded by separate genes - *Esr1* and *Esr2*, although ERα is more highly expressed than ERβ in insulin-sensitive tissues. Our lab has previously shown that ERα is a critical transcription factor in the maintenance of whole body insulin action and protection against tissue inflammation in both female[53] and male mice[52].

We have demonstrated in C2C12 myotubes that treatment with propyl pyrazole triol (PPT), an ERα-selective agonist, induces mitochondrial fission signaling and mtDNA replication by Polg1. Thus, ERα appears to be a driving factor for mitochondrial division and mtDNA replication. With this in mind and since mitochondrial morphology was altered with the loss of HSP72 in male mouse skeletal muscle, we turned our attention to the morphology of skeletal muscle mitochondria in female HSP72 KO. Electron micrographs of the skeletal muscle mitochondrial confirmed that the both the area and perimeter of mitochondria in female KO mice were smaller compared to female WT mice. In line with findings from EM analyses, we determined that fission signaling and the expression of fission-related proteins were elevated in muscle of female HSP72 KO animals.

We next focused on identifying how ERα interacts with mitochondria to promote fission. Though this mechanism is not fully elucidated, an ERα IP suggests that ERα interacts with mitochondrial inner membrane fusion regulators OPA1 and OMA1 (**Supplemental Figure 2**). Enhanced fission is thought to improve fatty acid oxidation and uncoupling and reduce ROS production. It is also theorized to improve quality control as a way to more rapidly eliminate damaged mitochondria and maintain a healthy population of mitochondria. Elevated fission signaling paired with an increase in autophagic flux seen in the female KO skeletal muscle suggests an increase in the turnover of damaged mitochondria. Together with decreased mitochondrial biogenesis signaling, this could lead to decreased mtDNA copy number as seen in the female KOs, indicating that there could be fewer mitochondria in the female KOs. These remaining mitochondria,

however, have enhanced efficiency; respiration measured in individual permeabilized muscle fibers using an Oroboros Oxygraph-2k (Oroboros Instruments) show that the female KOs are able to respond to cellular stressors comparatively to WT female mice (**Supplemental Figure 3A**). Isolated mitochondria respiration assessed with a Seahorse XF96 also recapitulated these findings (**Supplemental Figure 3B**). This is in stark contrast to male KO primary myotubes which had reduced oxygen consumption (basal and maximal respiration rates) compared to those from WT mice[20]. Collectively, our findings suggest that the induction of ERα and enhanced mitochondrial fission and autophagy likely underlie improvements in the health of the mitochondrial network in female mice.

Since ERα is highly expressed in female skeletal muscle, and HSP72 is a chaperone of ERα that controls its protein turnover, we hypothesize that ERα may underlie protection of mitochondrial function and insulin action that we observe in female HSP72 KO mice. Our data support the notion that increased ERα contributes to compensatory alterations in metabolic function and the prevention of obesity and insulin resistance in females.

Conclusion

Mitochondria are key organelles in regulating metabolism and energy expenditure, mitochondrial dysfunction has been associated with the development of insulin resistance in glucoregulatory tissues[52]. Our laboratory has recently shown that HSP72 is critical for the maintenance of for mitochondrial function, cellular metabolism, and

insulin action. Importantly, HSP72 protein levels are markedly reduced in muscle from obese and diabetic patients. In male mice, we have consistently shown that HSP72 is directly correlated with insulin sensitivity and inversely correlated with adiposity. In contrast, herein we provide evidence that these relationships for HSP72 are sex-specific. Considering that small molecule drugs are in development for targeting HSP72 to enhance insulin sensitivity, it is imperative that we understand the role of sex in regulating metabolism and insulin so that therapeutic strategies are equally as efficacious in males and females.

4.5 Acknowledgements

The authors appreciate the generosity of and informative discussions with Alexander van der Bliek (UCLA), and Peter Tontonoz (UCLA) for specialized reagents. The authors thank the Advanced Light Microscopy/Spectroscopy facility at UCSD and Sushil Mahata for assistance with electron microscopy studies on mouse muscle.

4.6 Author Contributions

A.J.L carried out many of the in vitro and ex vivo experiments, performed animal and tissues studies, and wrote the initial manuscript. Z.Z. and T.M.M. assisted in conducting and expression analyses and performed in vitro experiments. B.R.R., K.C., and K.W.

assisted in performing genotyping of the HSP72 KO mice and assisted in performing animal and tissues studies. D.M. assisted in mass spectrometry and statistical data analyses. D.C.H. assisted in performing in vivo phenotyping of the HSP72 KO mice and contributed to the final drafting of the manuscript. L.S. and L.V. assisted in conducting oxygen consumption studies in isolated mitochondria. J.P.W. and W.C. assisted in mass spectrometric identification of the mitochondrial proteome. J.W. provided advice and technical consultation and contributed to the final drafting of the manuscript. K.S. and S.S. assisted in assessing individual permeabilized muscle fiber respiration using the Oroboros. K.R. and O.S.S. assisted in conducting oxygen consumption studies in isolated mitochondria and contributed to the final drafting of the manuscript. M.A.F. provided advice and technical consultation and contributed to the final drafting of the manuscript. A.L.H. designed the studies, performed *in vivo* phenotyping of the HSP72 KO mice, performed animal and tissues studies, supervised the project, and contributed to the manuscript during all stages of drafting. A.L.H. is the guarantor of this work and, as such, had full access to all the data in the study and takes responsibility for the integrity of the data and the accuracy of the data analysis.

Conflict of Interest:

No other potential conflicts of interest relevant to this article were reported.

Funding:

This work was supported in part by the NIH DK-078760 and UCSD–UCLA DRC Mouse Phenotyping Core DK-063491 to A.L.H, and by the National Health and Medical

Research Council of Australia (Project Grant 1004441) to M.A.F., a Senior Principal Research Fellow of the National Health and Medical Research Council of Australia. A.J.L was supported by the NIH T32 Neuroendocrinology, Sex Differences, and Reproduction Training Grant (5T32HD007228), the NIH T32 Center for Duchenne Muscular Dystrophy Training Grant (T32AR065972), the NIH T32 Molecular, Cellular, and Integrative Physiology Training Grant (T32GM065823), the 2014 Jennifer S. Buchwald Graduate Fellowship in Physiology (UCLA Department of Physiology), and the American College of Sports Medicine - NASA Space Physiology Research Grant. Z.Z. was supported by UCLA Claude Pepper Older Americans Independence Center funded by the National Institute of Aging (5P30AG028748), NIH/NCATS UCLA CTSI Grant Number UL1TR000124, and UCLA Center for Duchenne Muscular Dystrophy-NIH NIAMS U54 AR052646 Wellstone Center of Excellence Training Fellowship. T.M. was supported by the NIH Kirschstein-NRSA predoctoral fellowship (F31DK108657) from NIDDK, Carl V. Gisolfi Memorial Research grant from the American College of Sports Medicine, and a predoctoral graduate student award from the Dornsife College at the University of Southern Califronia. L.V. and K.R. are supported in part by the National Institutes of Health (HL28481), and the Seahorse XF24 Instrument is supported by a shared instrument grant from the National Institutes of Health National Center for Research Resources (S10RR026744).

4.7 Figures

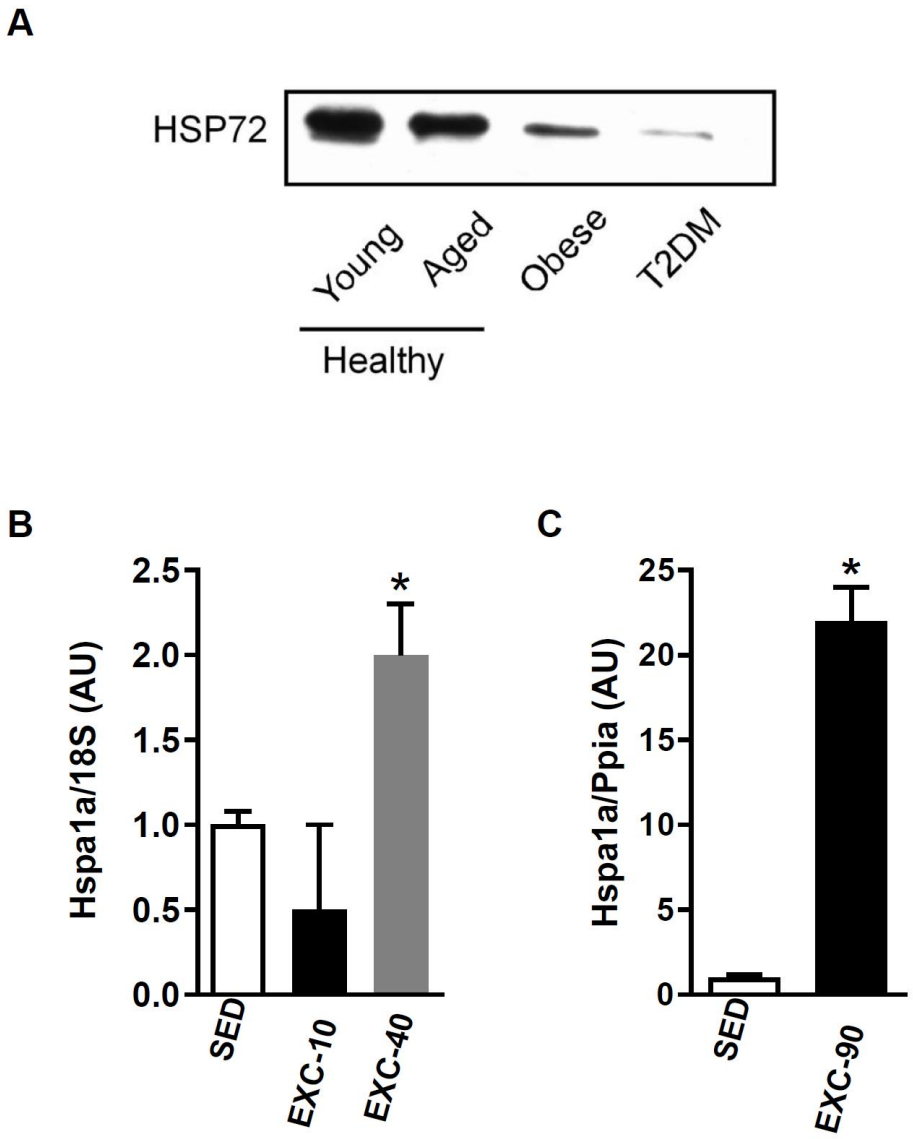

Figure 1: Clinical Rationale for Targeting HSP72. A) Skeletal muscle HSP72 protein levels are markedly reduced in obese and type 2 diabetic (T2DM) individuals compared with young and aged healthy individuals. Muscle HSP72 mRNA expression is elevated in humans after 40 minutes of cycling (B) and in mice after 90 minutes of treadmill exercise (C). Values are means ± SEM. *, significance, $p<0.05$.

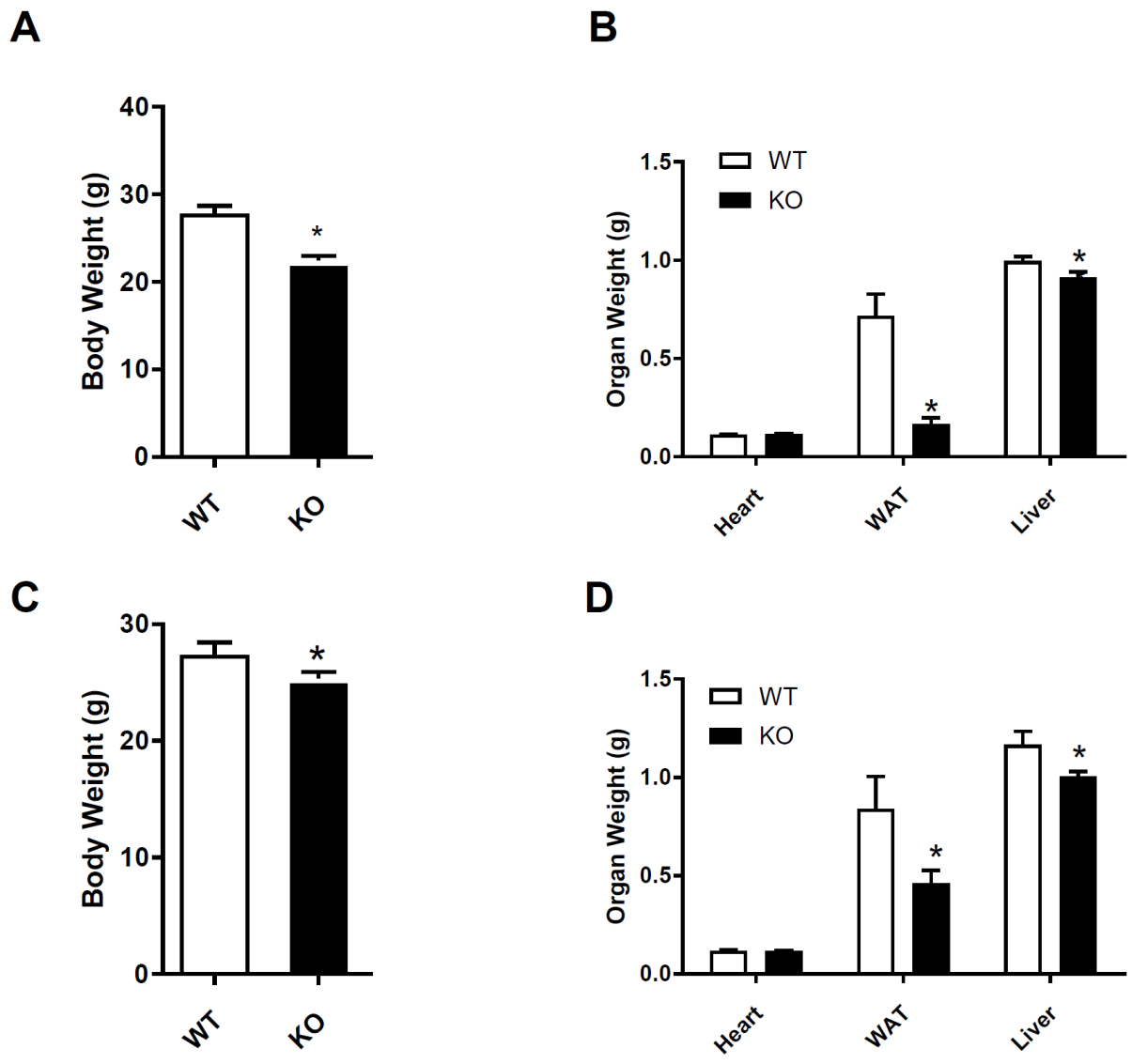

Figure 2: **The Effects of Aging on Body and Organ Weights for Female HSP72 WT and KO Mice.** A) Female 8-10 month KO mice (n=22 mice/genotype) weighed less than their WT counterparts (n=17 mice/genotype). B) White adipose tissue (WAT) and liver mass was reduced in female KO mice compared to WT. Heart mass was used as a control. C-D). The same phenotypes were reflected in aged 13-14 month female KO (n=9 mice/genotype) mice compared to WT controls (n=5 mice/genotype). Values are means ± SEM. *, significance, $p<0.05$.

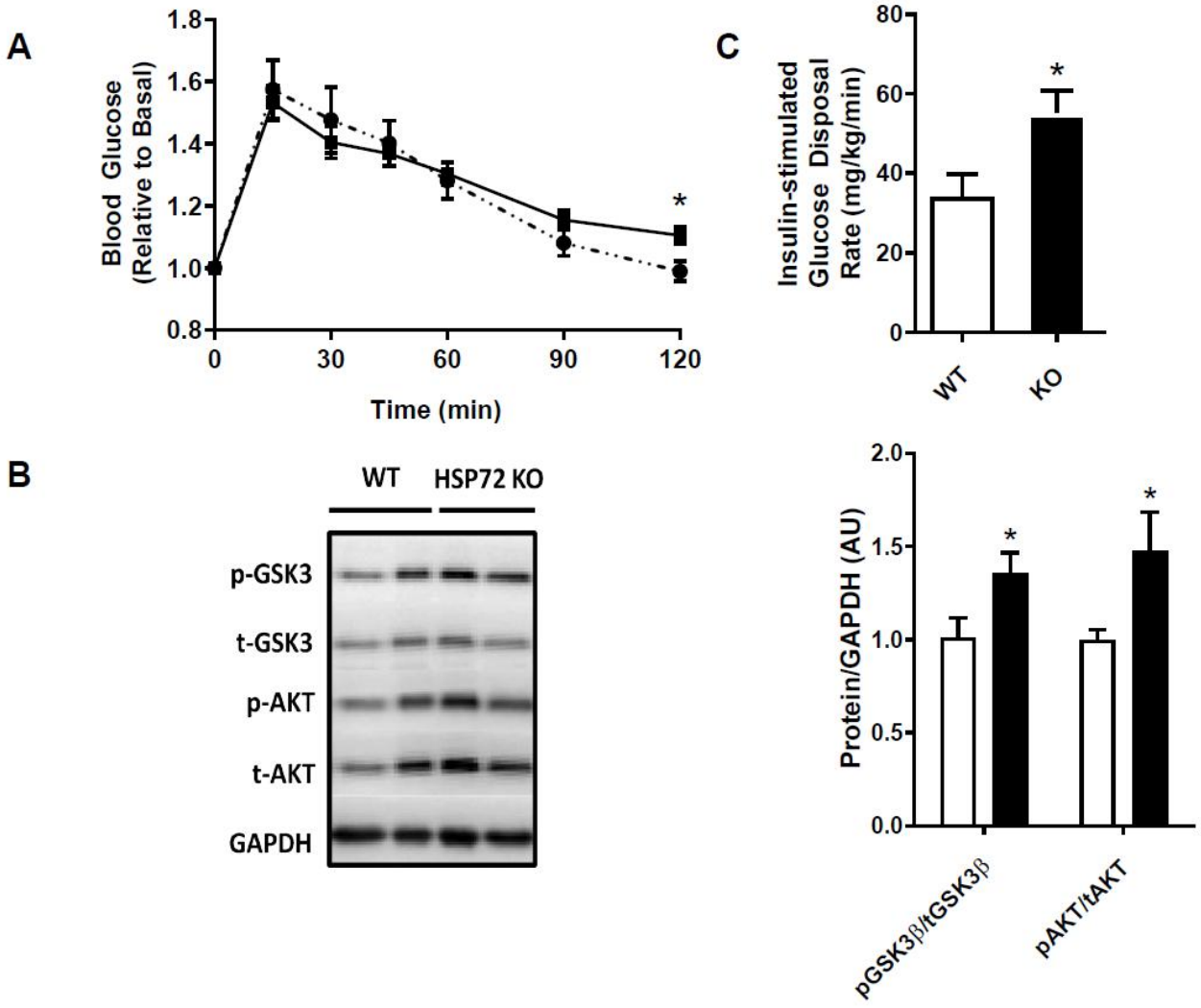

Figure 3: **Glucose Tolerance in Female HSP72 KO Mice.** A) Glucose tolerance is enhanced in KO (closed squares) vs WT (open circles) (n=11-13 mice/genotype). B) Representative immunoblots and densitometry of insulin signaling in muscle of WT and HSP72 KO female mice (n=6 mice/genotype). C) Insulin-stimulated glucose disposal rate is enhanced in female KO vs. WT and mice (n=8 mice/genotype).

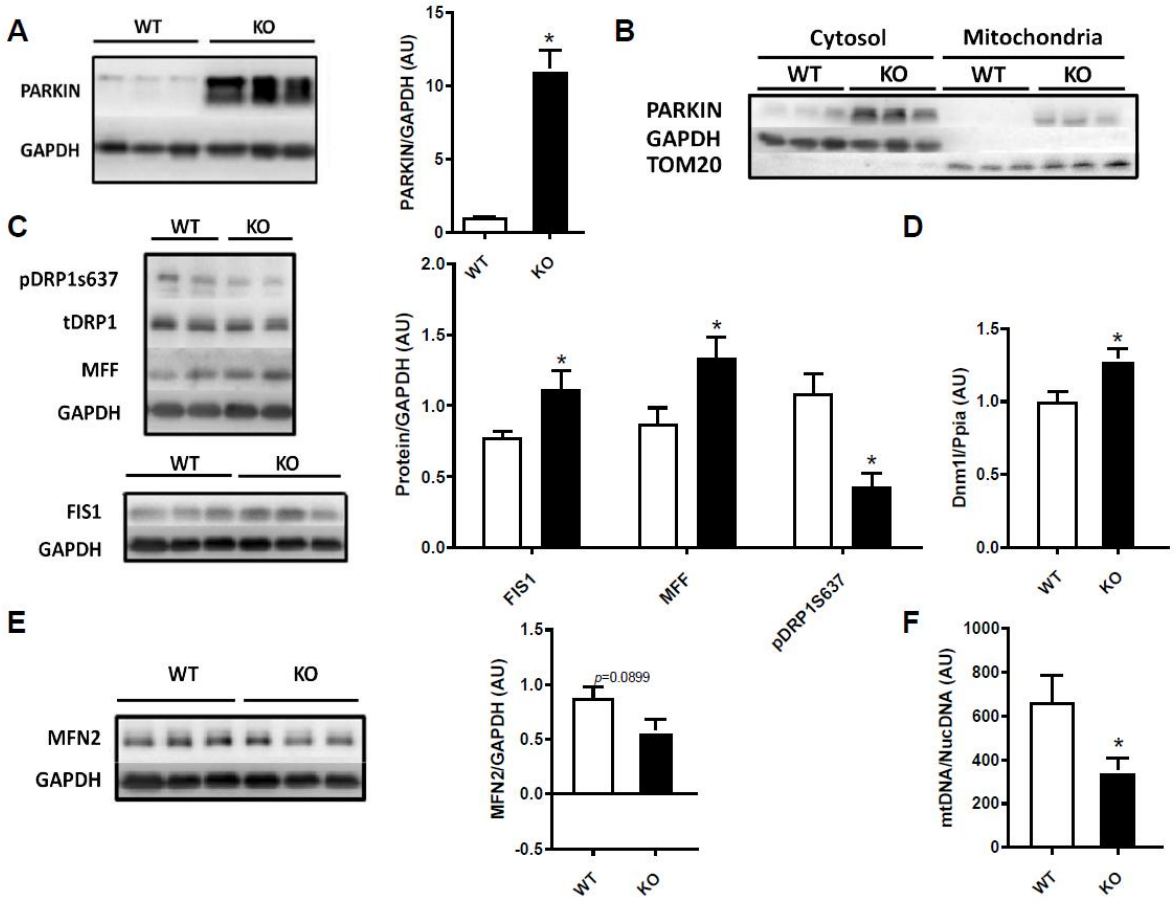

Figure 4: Mitochondrial Fission Signaling in Muscle of HSP72 KO Female Mice. A) Parkin protein expression levels were elevated in muscle from female HSP72 KO mice compared to WT (n=6 mice/genotype). B) Parkin protein localization was found in both the cytosol and mitochondrial fraction of female KO skeletal muscle (n=6 mice/genotype). C) Fission signaling in skeletal muscle of female HSP72 KO mice was increased compared to WT (n=5-6 mice/genotype). D) Muscle Drp1 (dnm1l) expression levels were elevated in KO female mice (n=7-8 mice/genotype). E) Mfn2 protein expression was reduced in female KO mice compared to WT controls (n=5-6 mice/genotype). F) Mitochondrial DNA (mtDNA) copy number was reduced in female

HSP72 KO mice (D) (n=7 mice/genotype). Values are means ± SEM. *, significance, $p<0.05$ between genotypes.

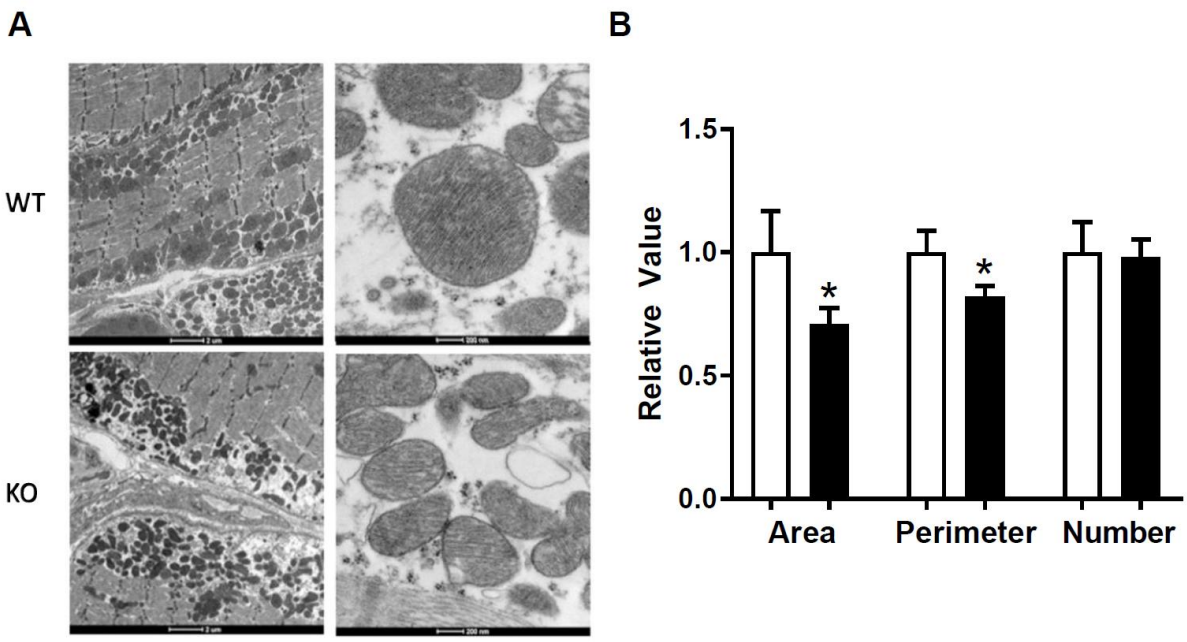

Figure 5: **Smaller and Fragmented Muscle Mitochondria in HSP72 KO Females.** A) Electron micrographs of soleus muscle show smaller, fragmented mitochondria in HSP72 KO (bottom panels) females compared to WT (top panels), n=2 mice/genotype. B) Although muscle mitochondrial number was identical between the genotypes, relative mitochondrial area and perimeter were significantly reduced in HSP72 KO females. Values are means ± SEM. *, significance, $p<0.05$ between genotypes.

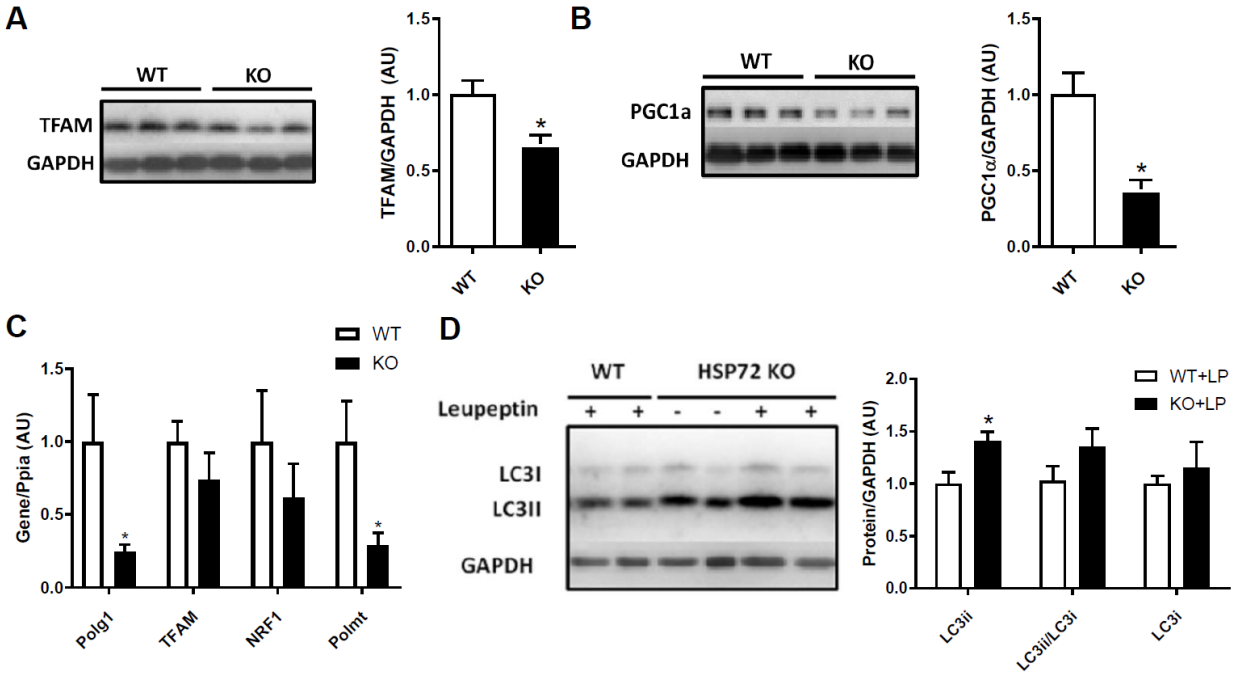

Figure 6: **Mitochondrial Biogenesis and Autophagy Signaling in Female HSP72 WT and KO Skeletal Muscle.** Representative immunoblots of TFAM (A) and PGC1α (B) protein levels in WT and KO female mice (n=6 mice/genotype). C) Expression of mitochondrial biogenesis genes from quadriceps of WT and KO female mice (n=7-8 mice/genotype). D) Markers of autophagy were increased in HSP72 female KO mice compared to WT mice following leupeptin, an autophagy inhibitor, treatment. Values are means ± SEM. *, significance, $p<0.05$, between genotypes.

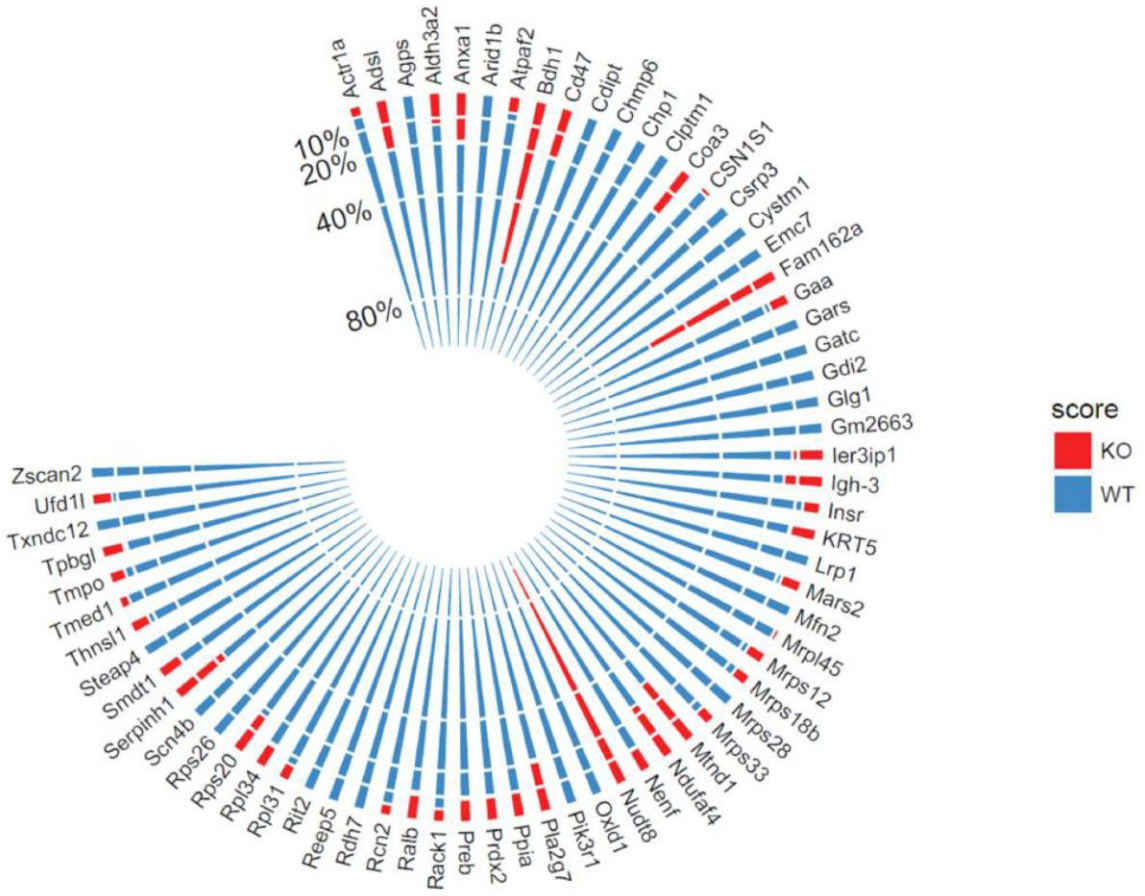

Figure 7: Muscle Mitochondrial Proteomic Profile in Female HSP72 WT and KO Mice. Muscle mitochondrial proteins in female HSP72 WT and KO mice under basal conditions (n = 6/genotype). This clearly shows that there are marked changes in female HSP72 WT and KO skeletal muscle mitochondria. Bars are fold change. Blue = WT. Red = KO. All proteins shown had a significance of $p < 0.05$.

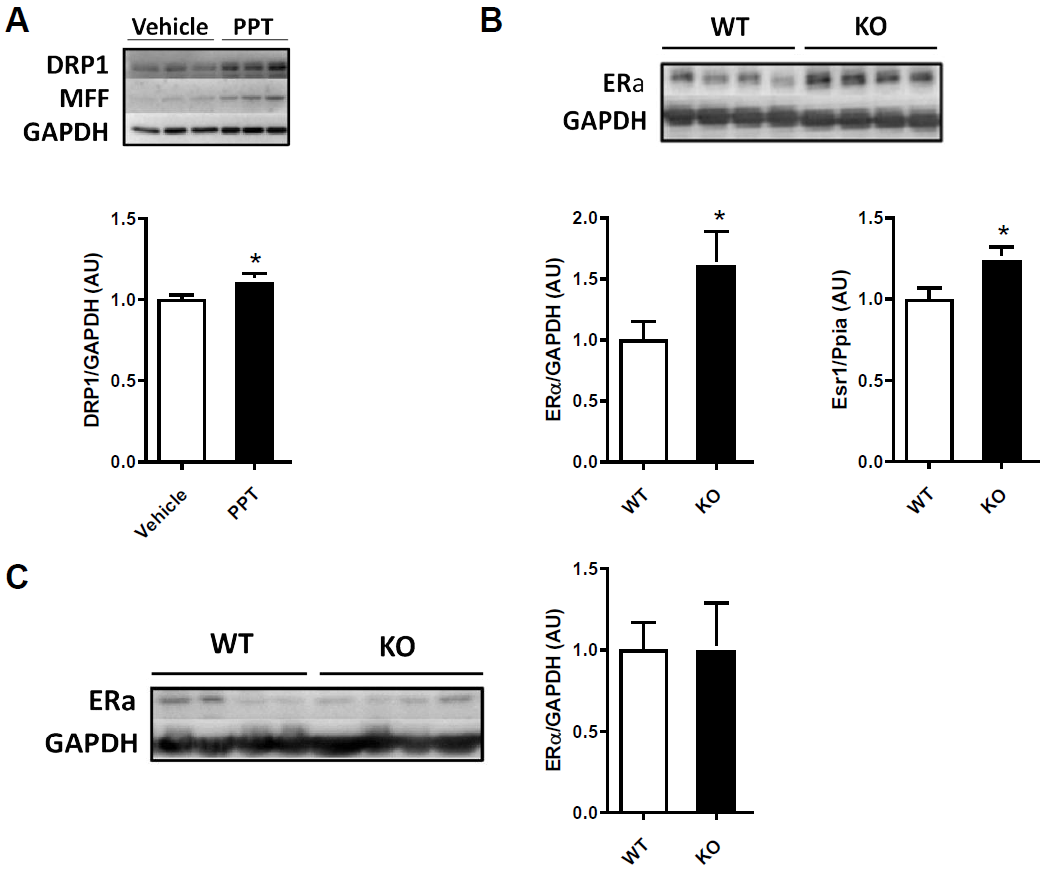

Figure 8: **ERα Expression Levels in Muscle of HSP72 KO Female Mice.** A) C2C12 myotubes treated with a vehicle or the ERα-selective agonist, propyl pyrazole triol (PPT) had increased fission signaling. Muscle ERα protein (B; left) and mRNA (B; right) expression was elevated in HSP72 KO female mice compared to WT (n=6-8 mice/genotype). C) No change was observed for muscle ERα protein levels between male WT and KO mice (n=6 mice/genotype). Values are means ± SEM. *, significance, $p<0.05$, between genotypes.

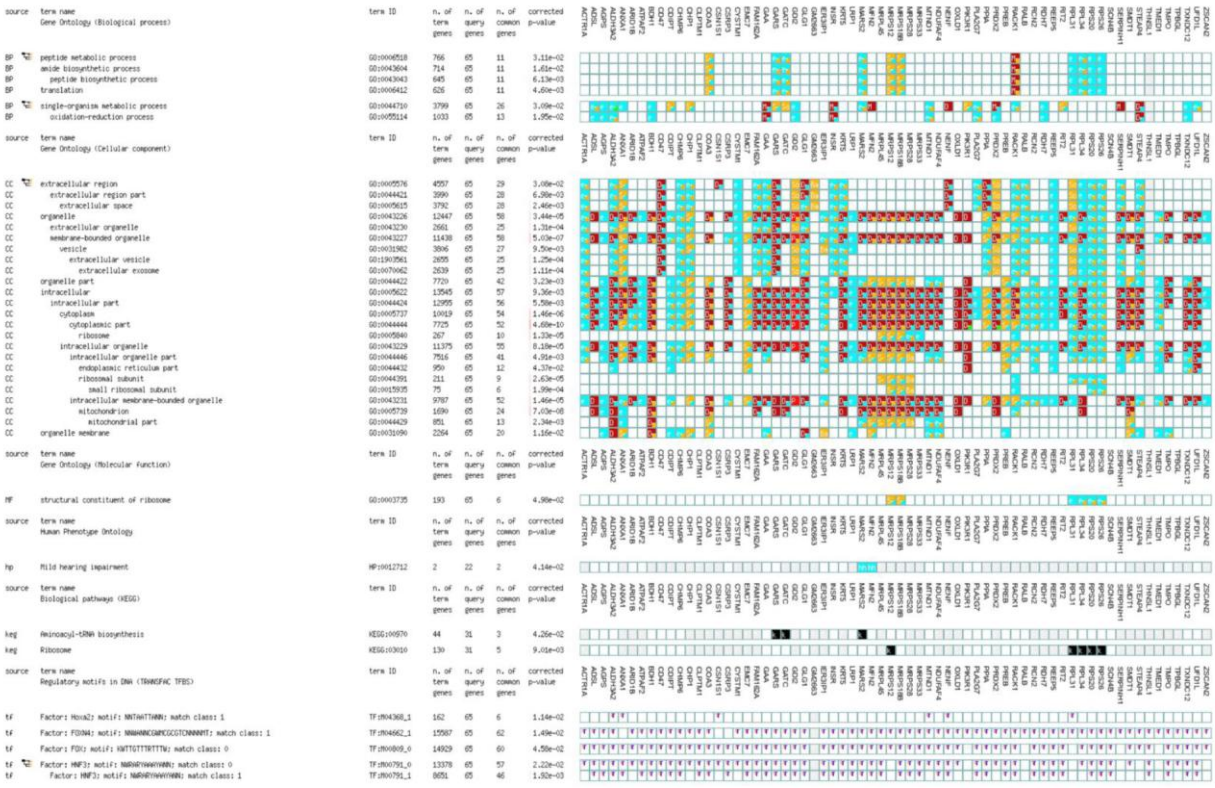

Supplemental Figure 1: **Bioinformatics Analysis of the Female HSP72 WT and KO Mitochondrial Proteome.** A functional analysis using g:Profiler shows translation as the top biological process and cytoplasm as the top cellular component based on a significance, $p<0.05$. Aminoacyl-tRNA biosynthesis was the top biology pathway (KEGG).

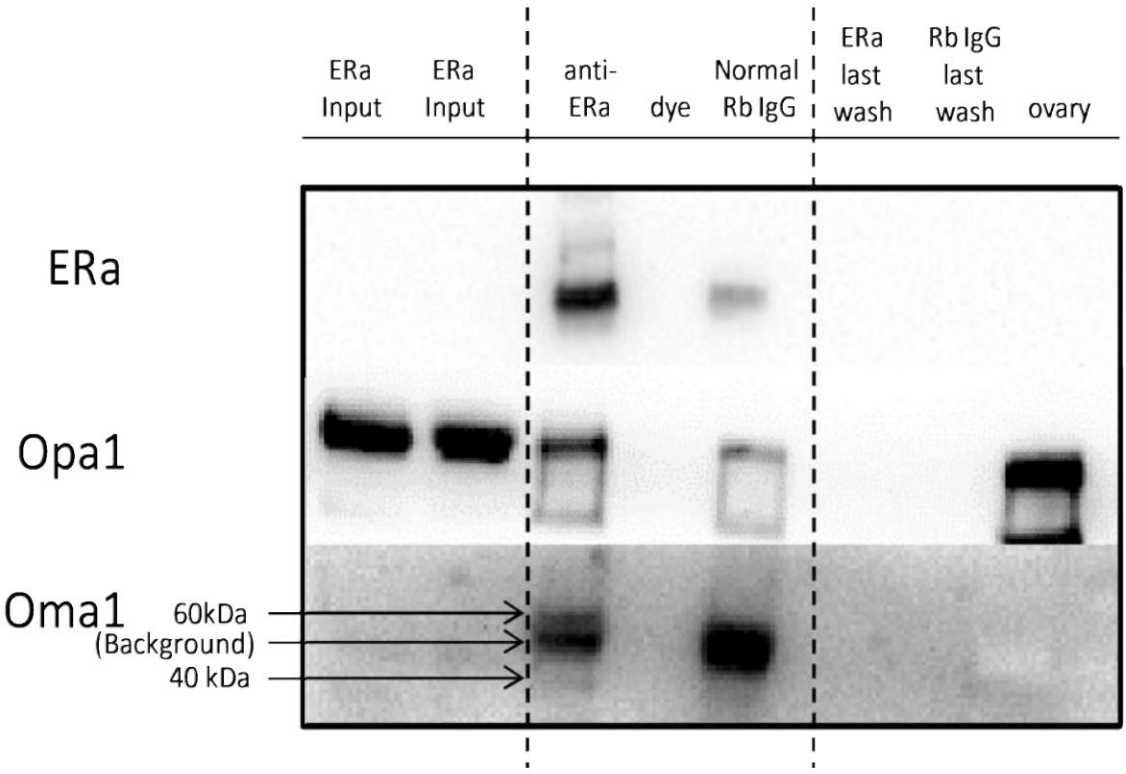

Supplemental Figure 2: **ERα Binding to Mitochondrial Fusion Proteins.** After IP of skeletal muscle with an ERα antibody or normal rabbit (Rb) IgG, immunoblotting with the ERα antibody verified that ERα present in the input was recovered in the bound material. Fusion proteins Opa1 and Oma1 were found in higher abundance in the anti-ERα bound material. For the comparison, a positive control for ERα, ovary, was shown.

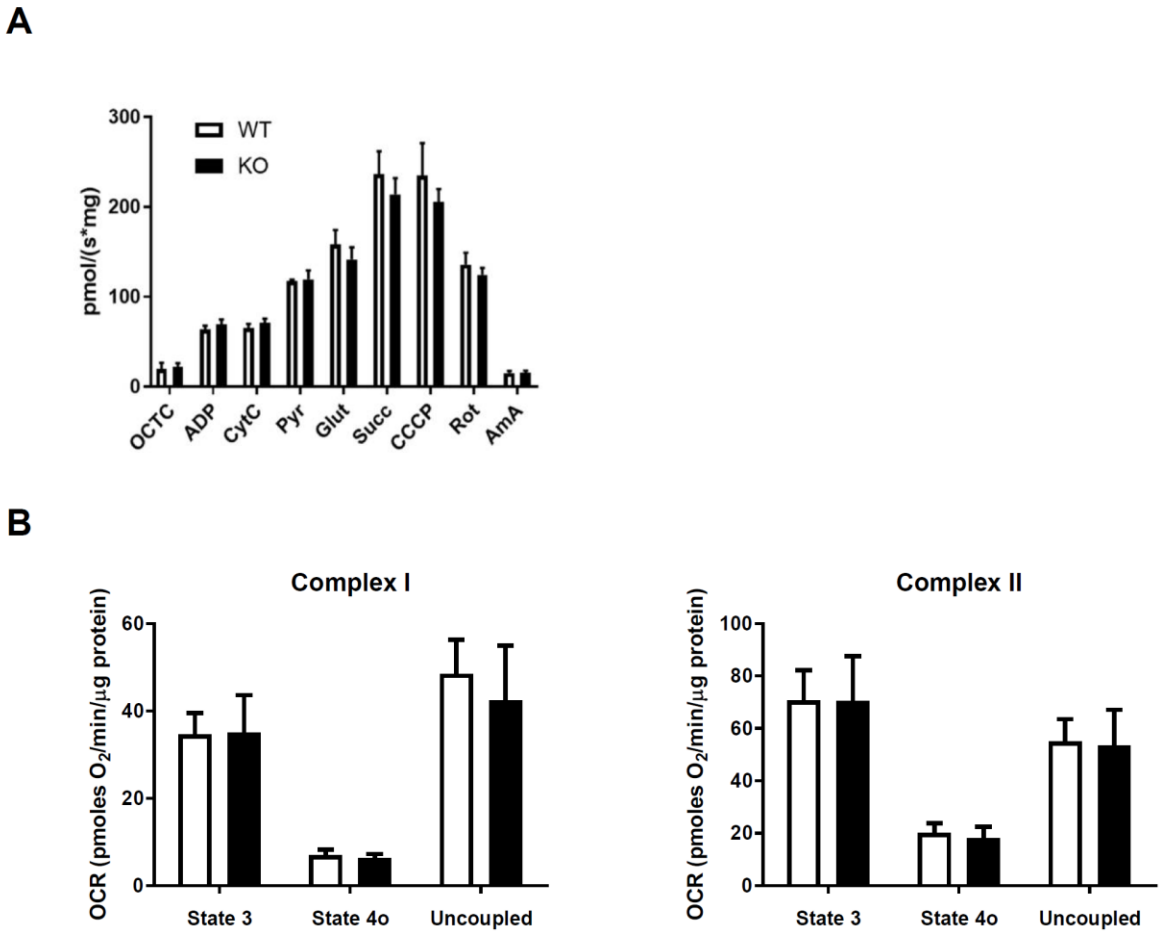

Supplemental Figure 3: **Mitochondrial Respiration in Female HSP72 WT and KO Mice.** A) Respiration from individual permeabilized muscle fibers was measured using an Oroboros Oxygraph-2k (Oroboros Instruments). Mitochondrial membrane integrity was assessed using a +10% increase threshold in respiration after CytC addition. OCTC, Octanoylcarnitate. ADP, Adenosine diphosphate. CytC, Cytochrome C. Pyr, Pyruvate. Glut, Glutamate. Succ, Succinate. CCCP, Carbonyl cyanide m-chlorophenyl hydrazone. Rot, Rotenone. AntA, Antimycin A. B) Quantification of oxygen consumption rates (OCR) drive by Complex I (*left*) and Complex II (*right*) in skeletal muscle

mitochondria isolated from WT and KO female mice. State 3 quantifies respiration linked to maximal ATP synthesis, State 4o, induced with oligomycin (ATP Synthase inhibitor), determines proton leak, and uncoupled respiration quantifies maximal electron transport chain activity induced by the chemical uncoupler, FCCP. There were no statistically significant changes in any respiratory parameter with pyruvate and malate (Complex I) or succinate and rotenone (Complex II). Values are means ± SEM. *, significance, $p<0.05$, between genotypes.

4.8 References

1. DeFronzo, R.A. and D. Tripathy, *Skeletal muscle insulin resistance is the primary defect in type 2 diabetes.* Diabetes Care, 2009. **32 Suppl 2**: p. S157-63.

2. Kido, Y., et al., *Tissue-specific insulin resistance in mice with mutations in the insulin receptor, IRS-1, and IRS-2.* J Clin Invest, 2000. **105**(2): p. 199-205.

3. Petersen, K.F., et al., *The role of skeletal muscle insulin resistance in the pathogenesis of the metabolic syndrome.* Proc Natl Acad Sci U S A, 2007. **104**(31): p. 12587-94.

4. Shoelson, S.E., J. Lee, and A.B. Goldfine, *Inflammation and insulin resistance.* J Clin Invest, 2006. **116**(7): p. 1793-801.

5. Association, A.D. *Statistics About Diabetes*. 2014; Available from: http://www.diabetes.org/diabetes-basics/statistics/.

6. Geer, E.B. and W. Shen, *Gender differences in insulin resistance, body composition, and energy balance.* Gend Med, 2009. **6 Suppl 1**: p. 60-75.

7. Shi, H., R.J. Seeley, and D.J. Clegg, *Sexual differences in the control of energy homeostasis.* Front Neuroendocrinol, 2009. **30**(3): p. 396-404.

8. Parks, B.W., et al., *Genetic architecture of insulin resistance in the mouse.* Cell Metab, 2015. **21**(2): p. 334-347.

9. Tanti, J.F. and J. Jager, *Cellular mechanisms of insulin resistance: role of stress-regulated serine kinases and insulin receptor substrates (IRS) serine phosphorylation.* Curr Opin Pharmacol, 2009. **9**(6): p. 753-62.

10. Dokken, B.B., et al., *Oxidative stress-induced insulin resistance in rat skeletal muscle: role of glycogen synthase kinase-3.* Am J Physiol Endocrinol Metab, 2008. **294**(3): p. E615-21.

11. Draznin, B., *Molecular mechanisms of insulin resistance: serine phosphorylation of insulin receptor substrate-1 and increased expression of p85alpha: the two sides of a coin.* Diabetes, 2006. **55**(8): p. 2392-7.

12. Aguirre, V., et al., *The c-Jun NH(2)-terminal kinase promotes insulin resistance during association with insulin receptor substrate-1 and phosphorylation of Ser(307).* J Biol Chem, 2000. **275**(12): p. 9047-54.

13. Olefsky, J.M. and C.K. Glass, *Macrophages, inflammation, and insulin resistance.* Annu Rev Physiol, 2010. **72**: p. 219-46.

14. de Luca, C. and J.M. Olefsky, *Inflammation and insulin resistance.* FEBS Lett, 2008. **582**(1): p. 97-105.

15. Henstridge, D.C., M. Whitham, and M.A. Febbraio, *Chaperoning to the metabolic party: The emerging therapeutic role of heat-shock proteins in obesity and type 2 diabetes.* Mol Metab, 2014. **3**(8): p. 781-93.

16. Padmalayam, I., *The heat shock response: its role in pathogenesis of type 2 diabetes and its complications, and implications for therapeutic intervention.* Discov Med, 2014. **18**(97): p. 29-39.

17. Hooper, P.L. and P.L. Hooper, *Inflammation, heat shock proteins, and type 2 diabetes.* Cell Stress Chaperones, 2009. **14**(2): p. 113-5.

18. Tiss, A., et al., *Immunohistochemical profiling of the heat shock response in obese non-diabetic subjects revealed impaired expression of heat shock proteins in the adipose tissue.* Lipids Health Dis, 2014. **13**: p. 106.

19. Kurucz, I., et al., *Decreased expression of heat shock protein 72 in skeletal muscle of patients with type 2 diabetes correlates with insulin resistance.* Diabetes, 2002. **51**(4): p. 1102-9.

20. Drew, B.G., et al., *HSP72 is a mitochondrial stress sensor critical for Parkin action, oxidative metabolism, and insulin sensitivity in skeletal muscle.* Diabetes, 2014. **63**(5): p. 1488-505.

21. Henstridge, D.C., et al., *Activating HSP72 in rodent skeletal muscle increases mitochondrial number and oxidative capacity and decreases insulin resistance.* Diabetes, 2014. **63**(6): p. 1881-94.

22. Chung, J., et al., *HSP72 protects against obesity-induced insulin resistance.* Proc Natl Acad Sci U S A, 2008. **105**(5): p. 1739-44.

23. Rodrigues-Krause, J., et al., *Divergence of intracellular and extracellular HSP72 in type 2 diabetes: does fat matter?* Cell Stress Chaperones, 2012. **17**(3): p. 293-302.

24. Bruce, C.R., et al., *Intramuscular heat shock protein 72 and heme oxygenase-1 mRNA are reduced in patients with type 2 diabetes: evidence that insulin resistance is associated with a disturbed antioxidant defense mechanism.* Diabetes, 2003. **52**(9): p. 2338-45.

25. Jin, S.M. and R.J. Youle, *PINK1- and Parkin-mediated mitophagy at a glance.* J Cell Sci, 2012. **125**(Pt 4): p. 795-9.

26. Chen, H., et al., *Mitochondrial fusion is required for mtDNA stability in skeletal muscle and tolerance of mtDNA mutations.* Cell, 2010. **141**(2): p. 280-9.

27. Seo, A.Y., et al., *New insights into the role of mitochondria in aging: mitochondrial dynamics and more.* J Cell Sci, 2010. **123**(Pt 15): p. 2533-42.

28. Joseph, A.M., et al., *Dysregulation of mitochondrial quality control processes contribute to sarcopenia in a mouse model of premature aging.* PLoS One, 2013. **8**(7): p. e69327.

29. Safdar, A., et al., *Endurance exercise rescues progeroid aging and induces systemic mitochondrial rejuvenation in mtDNA mutator mice.* Proc Natl Acad Sci U S A, 2011. **108**(10): p. 4135-40.

30. Hevener, A.L., et al., *Muscle-specific Pparg deletion causes insulin resistance.* Nat Med, 2003. **9**(12): p. 1491-7.

31. Hevener, A.L., et al., *Macrophage PPAR gamma is required for normal skeletal muscle and hepatic insulin sensitivity and full antidiabetic effects of thiazolidinediones.* J Clin Invest, 2007. **117**(6): p. 1658-69.

32. Ribas, V., et al., *Myeloid-specific estrogen receptor alpha deficiency impairs metabolic homeostasis and accelerates atherosclerotic lesion development.* Proc Natl Acad Sci U S A, 2011. **108**(39): p. 16457-62.

33. Bruce, C.R., et al., *Overexpression of carnitine palmitoyltransferase-1 in skeletal muscle is sufficient to enhance fatty acid oxidation and improve high-fat diet-induced insulin resistance.* Diabetes, 2009. **58**(3): p. 550-8.

34. Henstridge, D.C., et al., *The effect of the nitric oxide donor sodium nitroprusside on glucose uptake in human primary skeletal muscle cells.* Nitric Oxide, 2009. **21**(2): p. 126-31.

35. McCurdy, C.E. and G.D. Cartee, *Akt2 is essential for the full effect of calorie restriction on insulin-stimulated glucose uptake in skeletal muscle.* Diabetes, 2005. **54**(5): p. 1349-56.

36. Taylor, S.W., et al., *Characterization of the human heart mitochondrial proteome.* Nat Biotechnol, 2003. **21**(3): p. 281-6.

37. The UniProt, C., *UniProt: the universal protein knowledgebase.* Nucleic Acids Res, 2017. **45**(D1): p. D158-D169.

38. Reimand, J., et al., *g:Profiler--a web-based toolset for functional profiling of gene lists from large-scale experiments.* Nucleic Acids Res, 2007. **35**(Web Server issue): p. W193-200.

39. Mi, H., A. Muruganujan, and P.D. Thomas, *PANTHER in 2013: modeling the evolution of gene function, and other gene attributes, in the context of phylogenetic trees.* Nucleic Acids Res, 2013. **41**(Database issue): p. D377-86.

40. Allred, J.B. and D.G. Guy, *Determination of Coenzyme a and Acetyl Coa in Tissue Extracts.* Analytical Biochemistry, 1969. **29**(2): p. 293-&.

41. Preiss, J., et al., *Quantitative measurement of sn-1,2-diacylglycerols present in platelets, hepatocytes, and ras- and sis-transformed normal rat kidney cells.* J Biol Chem, 1986. **261**(19): p. 8597-600.

42. Frayn, K.N. and P.F. Maycock, *Skeletal muscle triacylglycerol in the rat: methods for sampling and measurement, and studies of biological variability.* J Lipid Res, 1980. **21**(1): p. 139-44.

43. Matthews, V.B., et al., *Interleukin-6-deficient mice develop hepatic inflammation and systemic insulin resistance.* Diabetologia, 2010. **53**(11): p. 2431-41.

44. Volobouеva, L.A., et al., *Overexpression of mitochondrial Hsp70/Hsp75 protects astrocytes against ischemic injury in vitro.* J Cereb Blood Flow Metab, 2008. **28**(5): p. 1009-16.

45. Kavazis, A.N., et al., *Short-term exercise training protects against doxorubicin-induced cardiac mitochondrial damage independent of HSP72.* Am J Physiol Heart Circ Physiol, 2010. **299**(5): p. H1515-24.

46. Knowlton, A.A. and D.H. Korzick, *Estrogen and the female heart.* Mol Cell Endocrinol, 2014. **389**(1-2): p. 31-9.

47. Salabei, J.K. and B.G. Hill, *Mitochondrial fission induced by platelet-derived growth factor regulates vascular smooth muscle cell bioenergetics and cell proliferation.* Redox Biol, 2013. **1**: p. 542-51.

48. Javadov, S. and A.V. Kuznetsov, *Mitochondria: the cell powerhouse and nexus of stress.* Front Physiol, 2013. **4**: p. 207.

49. Hagenbuchner, J. and M.J. Ausserlechner, *Mitochondria and FOXO3: breath or die.* Front Physiol, 2013. **4**: p. 147.

50. Liesa, M. and O.S. Shirihai, *Mitochondrial dynamics in the regulation of nutrient utilization and energy expenditure.* Cell Metab, 2013. **17**(4): p. 491-506.

51. Twig, G., B. Hyde, and O.S. Shirihai, *Mitochondrial fusion, fission and autophagy as a quality control axis: the bioenergetic view.* Biochim Biophys Acta, 2008. **1777**(9): p. 1092-7.

52. Ribas, V., et al., *Impaired oxidative metabolism and inflammation are associated with insulin resistance in ERalpha-deficient mice.* Am J Physiol Endocrinol Metab, 2010. **298**(2): p. E304-19.

53. Ribas, V., et al., *Skeletal muscle action of estrogen receptor alpha is critical for the maintenance of mitochondrial function and metabolic homeostasis in females.* Sci Transl Med, 2016. **8**(334): p. 334ra54.

54. Borras, C., et al., *Direct antioxidant and protective effect of estradiol on isolated mitochondria.* Biochim Biophys Acta, 2010. **1802**(1): p. 205-11.

55. Vina, J., et al., *Why females live longer than males? Importance of the upregulation of longevity-associated genes by oestrogenic compounds.* FEBS Lett, 2005. **579**(12): p. 2541-5.

56. Vina, J., et al., *Role of mitochondrial oxidative stress to explain the different longevity between genders: protective effect of estrogens.* Free Radic Res, 2006. **40**(12): p. 1359-65.

57. Jheng, H.F., et al., *Mitochondrial fission contributes to mitochondrial dysfunction and insulin resistance in skeletal muscle.* Mol Cell Biol, 2012. **32**(2): p. 309-19.

58. Kim, J.A., Y. Wei, and J.R. Sowers, *Role of mitochondrial dysfunction in insulin resistance.* Circ Res, 2008. **102**(4): p. 401-14.

59. Joseph, A.M., et al., *Mitochondrial dysregulation in the pathogenesis of diabetes: potential for mitochondrial biogenesis-mediated interventions.* Exp Diabetes Res, 2012. **2012**: p. 642038.

60. Montgomery, M.K. and N. Turner, *Mitochondrial dysfunction and insulin resistance: an update.* Endocr Connect, 2015. **4**(1): p. R1-R15.

61. Zorzano, A., et al., *Mitofusin 2 as a driver that controls energy metabolism and insulin signaling.* Antioxid Redox Signal, 2015. **22**(12): p. 1020-31.

62. Westermeier, F., et al., *Defective insulin signaling and mitochondrial dynamics in diabetic cardiomyopathy.* Biochim Biophys Acta, 2015. **1853**(5): p. 1113-8.

63. Watanabe, T., et al., *Roles of mitochondrial fragmentation and reactive oxygen species in mitochondrial dysfunction and myocardial insulin resistance.* Exp Cell Res, 2014. **323**(2): p. 314-25.

64. Arnold, A.P. and A.J. Lusis, *Understanding the sexome: measuring and reporting sex differences in gene systems.* Endocrinology, 2012. **153**(6): p. 2551-5.

65. Arnold, A.P., A. van Nas, and A.J. Lusis, *Systems biology asks new questions about sex differences.* Trends Endocrinol Metab, 2009. **20**(10): p. 471-6.

66. Lusis, A.J., A.D. Attie, and K. Reue, *Metabolic syndrome: from epidemiology to systems biology.* Nat Rev Genet, 2008. **9**(11): p. 819-30.

67. Wang, S., et al., *Genetic and genomic analysis of a fat mass trait with complex inheritance reveals marked sex specificity.* PLoS Genet, 2006. **2**(2): p. e15.

68. Yang, X., et al., *Tissue-specific expression and regulation of sexually dimorphic genes in mice.* Genome Res, 2006. **16**(8): p. 995-1004.

CHAPTER 5

Conclusion and Future Direction

5.1 Proteomic Profiling of Mitochondria Reveals Inter- and Intra-species Heterogeneity From Both Expressional and Functional Perspectives

Contextualization of mitochondrial proteins to their biological pathways and their corresponding linkages to clinical phenotypes affords great opportunities to advance our understanding regarding the fundamentals of mitochondrial diseases. Proteomics investigations in the past 15 years have paved a foundation for future studies to establish a comprehensive mitochondrial proteome map. Several challenges remain. At the technology front, these include the identification of proteins in low abundance, proteins that are associated with mitochondria, or proteins with unique biochemical features. Future tasks detailing comprehensive and quantitative characterization of the mitochondrial protein PTMs are also daunting. In the biology arena, functional information regarding individual components within many mitochondrial subproteomes is far from completion. Characterization of these proteins may lead to the discovery of novel mitochondrial functions, of which we are not yet aware. Integrating MS strategies with other approaches such as computational biology, protein arrays, and biochemical analyses will facilitate the advancement and completion of a mitochondrial proteome knowledgebase. The ultimate goal of mitochondrial proteome research is to bridge the knowledge gap between mitochondrial compositions and their functionalities, therefore providing potential diagnostic and prognostic targets for mitochondrial-associated diseases.

Herein, we characterized the mitochondrial proteomic profile in great detail and presented rigorous evidence for organ- and organism-specific mitochondrial identity[1]. We analyze the mitochondrial proteome from four different model systems including two cardiac mitochondrial proteomes from distinct genomes (mouse heart vs human heart) as well as two unique organ systems from the same genome (mouse heart vs mouse liver), and a metazoan our-group (drosophila). Assessment of mitochondrial protein abundance and their biochemical properties reflected core mitochondrial functionalities specific to each host milieu. Compared to published reports on the mitochondrial proteome at the time[2-6], we identified the largest mitochondria proteomic pool to date. Our study of the proteome−function correlation confirms previous observations of mitochondrial biology and contributes new evidence of the expediency of diagnosing mitochondrial disease through proteomic parameters. Furthermore, correlational analyses suggest that mitochondrial proteome design is primarily driven by cellular environment. This investigation bridges the knowledge gap between molecular compositions and their accompanying functions, which ultimately aids in the translation of mitochondrial proteomics data to a contextualized understanding of complex mitochondrial biology as well as allows for the acquisition of a prospective source for not only the diagnosis of mitochondrial pathologies but also the procurement of mitochondrial therapeutic targets.

5.2 Metabolic Heavy Water Labeling of Mitochondrial Proteins Demonstrates Individualized Protein Turnover Rates

The maintenance of a healthy network of mitochondria hinges upon the delicate homeostasis between protein synthesis and degradation, known as the turnover of proteins. Imbalances in mitochondrial turnover and quality control have been associated with many diseases. It is well-known that mitochondria are degraded in a whole organelle fashion through mitochondrial autophagy (mitophagy). However, it was not known how the process of mitochondrial dynamics was regulated in different cellular contexts. Furthermore, up to this point, the majority of quantitative proteomics was dictated by steady-state measurements which served as fragmentary snapshots of the mitochondrial proteome.

To analyze mitochondrial dynamics *in vivo*, we used a deuterium (^2H_2O; heavy water) labeling strategy to study individual protein turnover in mouse heart and mouse liver[7] – two organs that contained large quantities of mitochondria, but differed in cellular composition and function. We saw that individual mitochondrial turnover rates spanned at least an order of magnitude within an organ. This was conceptually significant because it suggests that individual mitochondria cannot be assumed to turn over as single units. Instead, it is likely that mitochondrial proteins are synthesized at variable rates in the cytosol and enter mitochondria, resulting in mitochondria with old and new proteins to preserve homeostasis under mitophagy. Our findings underscore the significance of obtaining a proteome dynamics map at individual protein resolution in uncovering signatures of protein quality control dysfunctions, such as in aging and metabolic perturbation studies.

In conclusion, we demonstrated the first mitochondrial proteome-wide study of *in vivo* protein dynamics. Our designed experimental platforms enabled us to calculate the turnover rates of 458 murine mitochondrial proteins, ranging over 2 orders of magnitude in half-life[7]. Mitochondrial protein turnover displayed both organ-specific differences and interprotein heterogeneity, and subcellular fractionation ensured that the protein kinetics were free from interference by cytosolic pre-cursors. Our methodology has wide applications in the characterization of protein kinetics and temporal proteome changes in mammalian systems and clinical studies.

5.3 HSP72 is a Sex-specific Regulator of Insulin Sensitivity and Mitochondrial Dynamics

The exact involvement of mitochondria in the onset of insulin resistance and metabolic dysfunction remains a controversial subject. This issue is one worth investigating, as evidence suggests a causal role for the dysfunction of these organelles in the pathological response to metabolic syndrome in animal models. As cellular stress adaptation is essential for the maintenance of metabolic homeostasis, heat shock proteins (HSPs) are induced in response to stress. We see that expression levels of a specific HSP, HSP72, are reduced in obese and diabetic human muscle[8], and increased following exercise training. Moreover, we have shown that the induction of HSP72 is critical for the protection against genetic- and diet-induced obesity and insulin

resistance in rodents[9]. Our laboratory has shown that HSP72 is a mitochondrial stress sensor linking mitochondrial function and cellular metabolism with insulin action[10]. We have shown that HSP72 overexpression promotes enhanced mitochondrial function and we have identified HSP72 as a binding partner of the mitochondrial quality control protein, Parkin. HSP72 deletion impaired Parkin turnover and action, resulting in the retention of enlarged, dysmorphic mitochondria with reduced respiratory capacity. As a consequence, KO mice accumulated lipid in muscle and became insulin resistant and glucose intolerant over time compared with control animals. These findings suggest that the HSP72-Parkin axis links mitochondrial health with insulin sensitivity; however, these studies were performed exclusively in males.

Despite similar impairment in Parkin turnover between male and female KOs, in contrast to males, female KOs remained insulin sensitive and glucose tolerant. Interestingly, ERα was elevated in muscle from female HSP72 KO mice and this observation was paralleled by enhanced mitochondrial fission signaling (↑Fis1 and MFF) and a reduction in mitochondrial size. We have demonstrated previously that ERα is critical for mitochondrial function and muscle insulin action; therefore, since HSP72 binds ERα to regulate its protein turnover, we hypothesized that induction of ERα may compensate for a loss of HSP72 and thus, preserve metabolic homeostasis in female KO mice. Overall, our findings suggest that sex may control the impact of HSP72 in regulating mitochondrial health and insulin sensitivity. Our research provides the important foundation for the rational design of novel therapeutic strategies that can be used to combat metabolic-related diseases in women.

5.4 References

1. Lotz, C., et al., *Characterization, design, and function of the mitochondrial proteome: from organs to organisms.* J Proteome Res, 2014. **13**(2): p. 433-46.

2. Zhang, J., et al., *Systematic characterization of the murine mitochondrial proteome using functionally validated cardiac mitochondria.* Proteomics, 2008. **8**(8): p. 1564-75.

3. Pagliarini, D.J., et al., *A mitochondrial protein compendium elucidates complex I disease biology.* Cell, 2008. **134**(1): p. 112-23.

4. Kislinger, T., et al., *Global survey of organ and organelle protein expression in mouse: combined proteomic and transcriptomic profiling.* Cell, 2006. **125**(1): p. 173-86.

5. Forner, F., et al., *Quantitative proteomic comparison of rat mitochondria from muscle, heart, and liver.* Mol Cell Proteomics, 2006. **5**(4): p. 608-19.

6. Taylor, S.W., et al., *Characterization of the human heart mitochondrial proteome.* Nat Biotechnol, 2003. **21**(3): p. 281-6.

7. Kim, T.Y., et al., *Metabolic labeling reveals proteome dynamics of mouse mitochondria.* Mol Cell Proteomics, 2012. **11**(12): p. 1586-94.

8. Kurucz, I., et al., *Decreased expression of heat shock protein 72 in skeletal muscle of patients with type 2 diabetes correlates with insulin resistance.* Diabetes, 2002. **51**(4): p. 1102-9.

9. Henstridge, D.C., et al., *Activating HSP72 in rodent skeletal muscle increases mitochondrial number and oxidative capacity and decreases insulin resistance.* Diabetes, 2014. **63**(6): p. 1881-94.

10. Drew, B.G., et al., *HSP72 is a mitochondrial stress sensor critical for Parkin action, oxidative metabolism, and insulin sensitivity in skeletal muscle.* Diabetes, 2014. **63**(5): p. 1488-505.